MONASH University

REAL-TIME WIRELESS AMBULATORY GAIT MONITORING SYSTEM INCORPORATING ONLINE PERIODICAL GAIT EVALUATIONS

DARWIN GOUWANDA

Bachelor of Engineering (Mechatronics) (Hons)

Monash University

A thesis submitted in the fulfillment of the requirement for degree of

Doctor of Philosophy

Faculty of Engineering

Monash University

January 2011

Statement of Authorship

The thesis contains no material which has been accepted for the award of any other degree or diploma in any university or other institute of tertiary education. I affirm that, to the best of my knowledge, the thesis contains no material previously published or written by another person, except where due reference is made in the text of the thesis

Darwin Gouwanda

Date: 18 January 2011

Copyright Notices

CONTENTS

ABSTRACT

Human gait analysis studies the coordination of human lower extremity in providing propulsion to move forward while maintaining the body balance, with one foot in contact with the ground at all time. Hence, gait analysis plays an important role in clinical settings and rehabilitations. It is widely performed to identify various gait disorders, to assess the functional performance of a patient's lower limb before and after a surgery or medical treatment, and to evaluate patient's rehabilitation progress. In engineering, its importance is reflected in the design and development of the prosthetic limb, Functional Electrical Stimulation (FES) system as well as the humanoid robot.

Optical motion capture system and force platform are commonly used in gait analysis to quantify human motion. However, these systems are expensive, bulky and can only capture human motion in a dedicated environment i.e. laboratory. As an alternative, this thesis developed a real-time gait monitoring system that utilizes wireless miniature gyroscopes. The miniature gyroscope is small, light-weight, and can capture human motion in both indoor and outdoor environments. More importantly, it is equipped with wireless data transmission, which offers additional benefits. Wireless gyroscope provides relatively larger movement area. It also does not obstruct the natural motion of human lower extremity.

Apart from the advantages offered by the wireless gyroscopes, this system also uses several novel methods to assist clinicians and researchers in identifying abnormal gait. These methods evaluate three main aspects of human gait. They are referred as the gait normality test, gait asymmetry analysis, and the estimation of gait dynamic stability. Gait normality test examines a person's gait relative to normal/healthy individual's gait that was established by other researchers. Parameters considered in this method are the duration of stride (T_{stride}), stance phase (T_{stance}), and swing phase (T_{swing}), and the Coefficient of Determination (CoD). Gait asymmetry analysis is an evaluation that examines the bilateral differences between the left and right limbs. Normalized Cross-Correlation (Cc_{norm}), time delay (Ts), temporal Symmetry Index (SI), and Normalized Symmetry Index (SI_{norm}) are the parameters used to define human gait asymmetry. The estimation of gait dynamic stability determines human walking stability using nonlinear time series analysis. It uses short-term (λ_S^*) and long-term maximum Lyapunov exponent (λ_L^*)

to quantify the ability of human neuromuscular locomotor system in maintaining body balance during walking.

Experimental study was also conducted to examine the overall capability of this system. This study simulated the abnormal gait by placing a load on one side of the limbs and by wearing a sandal on one foot. These methods successfully altered the inertial property of a person's lower limb, hence inducing significant differences in spatio-temporal gait parameters between the affected limb and the non-affected limb. As expected, the experimental results were satisfactory. Significant differences between normal and abnormal gait were observed in T_{stride}, T_{stance} and T_{swing}. Similar results were also found in CoD, Cc_{norm}, Ts, SI, SI_{norm}, λ_S^* and λ_L^* with $p < 0.01$. These results validated the use of these methods to simulate abnormal gait on a healthy individual. They also demonstrated the viability of this system for future clinical applications.

ACKNOWLEDGEMENT

I would like to express my gratitude to the following for their help and support, in one way or another:

- First and foremost, my supervisor, Dr. S. M. N.Arosha Senanayake for his continuous and relentless support and guidance throughout this research.
- Monash University Sunway campus, School of Engineering administrative staffs, particularly, Ms. Penny Tan, Ms. Tong Siew Peng, Ms. Deborah Cheah, Ms. Eliz Graze Mr. Panneerselvam, Mr. Paremanan, and Mr. Badmanadan for their supports.
- My friends and fellow postgraduates, Jason Leong, Alpha Agape, Yogeswaran, Oon-ee Ng, Mark Ng, Boon How Khoo, Jimmy Lim for their encouragements throughout my postgraduate study.
- My fellow Monashians for their voluntary participations in the experimental study of this thesis.
- My parents for their support and encouragement to undertake this research.
- Those who provided funds to support this research, particularly Monash University Sunway campus and the Ministry of Science, Technology and Innovation, Malaysia (Grant no. 03-02-10-SF0028 under title “Bio-inspired Robotics Devices for Sportsman Screening Service)

LIST OF PUBLICATIONS

Journal papers

D Gouwanda, SMNA Senanayake. Identifying gait asymmetry using gyroscopes – a cross-correlation and normalized symmetry index approach. Journal of Biomechanics. Paper accepted.

D Gouwanda, SMNA Senanayake. Wireless ambulatory monitoring system with online periodical gait assessment. International Journal of Biomedical Engineering and Technology. Paper accepted.

D Gouwanda, SMNA Senanayake. Periodical gait asymmetry assessment using real-time wireless gyroscopes gait monitoring system. Journal of Medical Engineering & Technology. Paper submitted

D Gouwanda, SMNA Senanayake. Wireless gyroscope gait monitoring system for dynamic stability assessment. IEEE Transaction on Mechatronics. Paper submitted.

Conference papers

D Gouwanda, SMNA Senanayake. Emerging trends of body-sensors in sports and human gait analysis. IFMBE Proceedings of 4th Kuala Lumpur International Conference on Biomedical Engineering (Biomed). 2008;21:715-718.

D Gouwanda, SMNA Senanayake. Application of hybrid multi-resolution wavelet decomposition method in detecting human walking gait events. Proceedings of International Conference of Soft Computing and Pattern Recognition (SoCPaR) 2009. 2009. p. 580-585

D Gouwanda, SMNA Senanayake. Identification of gait asymmetry using wireless gyroscopes. Proceedings of IEEE Asia-Pacific Conference on Circuits and Systems (APCCAS) 2010. 2010. p. 608-611

White paper

D Gouwanda, SMNA Senanayake. Periodical gait event detection using wireless gyroscopes. 2010 ASEAN Virtual Instrumentation Applications Contest. (Winner of best innovation in wireless technology applications).

LIST OF FIGURES

LIST OF TABLES

LIST OF ABBREVIATIONS/NOTATIONS

Description	Abbreviation/notation
Coefficient of Determination	CoD
Number of data point	n
Duration of stance phase	T_{stance}
Duration of stride	T_{stride}
Duration of swing phase	T_{swing}
Embedding dimension	d_E
Functional Electrical Stimulation system	FES
Global coordinate system	{G}
Heel-strike	HS
Hybrid Multi-resolution Wavelet Decomposition method	HMWD
Hyper Text Markup Language	HTML
Left shank angular rate	$\dot{\theta}_{Lshank}$
Left shank orientation	θ_{Lshank}
Left thigh angular rate	$\dot{\theta}_{Lthigh}$
Left thigh orientation	θ_{Lthigh}
Long-term maximum Lyapunov exponent	λ_L^*
Maximum Lyapunov exponent	λ*
Micro Electro-Mechanical System	MEMS
Mid-swing	MS
Multi-resolution Wavelet Decomposition method	MWD
Normal overground walking	Norm
Normal overground walking with 2.5 kg load on lower right shank	NormWr
Normal overground walking with 2.5 kg load on lower left shank	NormWl
Normal overground walking with a sandal on left foot	NormSl
Normal overground walking with a sandal on right foot	NormSr
Normal treadmill walking at 3 km/h	Norm3

Normal treadmill walking at 3 km/h with 2.5 kg load on lower left shank	Norm3Wl
Normal treadmill walking at 3 km/h with 2.5 kg load on lower right shank	Norm3Wr
Normal treadmill walking at 4 km/h	Norm4
Normal treadmill walking at 4 km/h with 2.5 kg load on lower left shank	Norm4Wl
Normal treadmill walking at 4 km/h with 2.5 kg load on lower right shank	Norm4Wr
Normal treadmill walking at 5 km/h	Norm5
Normal treadmill walking at 5 km/h with 2.5 kg load on lower left shank	Norm5Wl
Normal treadmill walking at 5 km/h with 2.5 kg load on lower right shank	Norm5Wr
Normalized Cross-correlation	Cc_{norm}
Normalized Symmetry Index	SI_{norm}
Number of gait cycle	m
Peak detection algorithm	PD
Ratio of stance phase	R_{stance}
Ratio of swing phase	R_{swing}
Region of Interest	RoI
Right shank angular rate	$\dot{\theta}_{Rshank}$
Right shank orientation	θ_{Rshank}
Right thigh angular rate	$\dot{\theta}_{Rthigh}$
Right thigh orientation	θ_{Rthigh}
Sampling time	Δt
Shank angular rate	$\dot{\theta}_{shank}$
Shank orientation	θ_{shank}
Sensor local coordinate system	{S}
Short-term maximum Lyapunov exponent	λ_S^*
State-space time delay	τ
Symmetry Index	SI
Symmetry index of duration of stance phase	SI_{stance}
Symmetry index of duration of stride	SI_{stride}

Symmetry index of duration of swing phase	SI_{swing}
Thigh angular rate	$\dot{\theta}_{thigh}$
Thigh orientation	θ_{thigh}
Time	t
Time delay	Ts
Toe-off	TO
Total number of data point in one gait cycle	N
Total number of gait cycle	M
Valley detection algorithm	VD

Chapter 1

INTRODUCTION

1.1 Human Gait

Walking is the most common and most important human movement [1]. It is human body's natural means of moving from one location to another. Although it may seem trivial, walking is a complex and repetitive process that requires the coordination of both human lower limbs to provide support and propulsion, with at least one foot in contact with the ground at all times [2]-[3]. This repetitive process is generally referred as gait cycle. Perry defines a gait cycle as an action that flows smoothly to the next action; there is no specific starting point or ending point [2]. Hence any events can be selected as the starting point. However, since the moment of floor contact is the most readily defined event, this action is normally described as the start of a gait cycle in various literatures. This action is commonly regarded as 'Heel-strike' or 'Initial Contact'. For consistency, this action is regarded as 'Heel-strike' in this thesis. One gait cycle for a limb starts from one heel-strike and ends at subsequent heel-strike.

One gait cycle is divided into two main phases: stance phase and swing phase [2]-[3]. Stance phase is defined as the period which the foot is on the ground and it begins with heel-strike. Stance phase is subdivided into four periods: loading response, mid-stance, terminal stance, and pre-swing. Loading response is the period where both feet are on the ground and body weight is transferred from one limb to another. Mid-stance is the period where body weight passes over one limb while the other limb is in swinging motion. Terminal stance begins when one heel rises above the ground while the other heel touches

the ground. Pre-swing begins when both feet are briefly on the ground and the body weight is supported by both limbs.

On the other hand, swing phase is defined as the period which the foot is in the air and it begins with toe-off. It is further divided into three periods: initial swing, mid-swing and terminal swing. Initial swing occurs when one foot leaves the ground and starts to swing forward. Mid-swing occurs when the foot completely leaves the ground. Terminal swing is the period when the foot is about to hit the ground and to start subsequent gait cycle. The gross normal distribution of the stance phase is 60% of the gait cycle and the swing phase is 40% of the gait cycle [2]-[3]. Apart from gait phases and gait periods, one gait cycle is characterized into seven different events: heel-strike, opposite toe-off, heel-rise, opposite heel-strike, toe-off, feet adjacent and tibia vertical. A complete illustration of one gait cycle is presented in Figure 1.1.

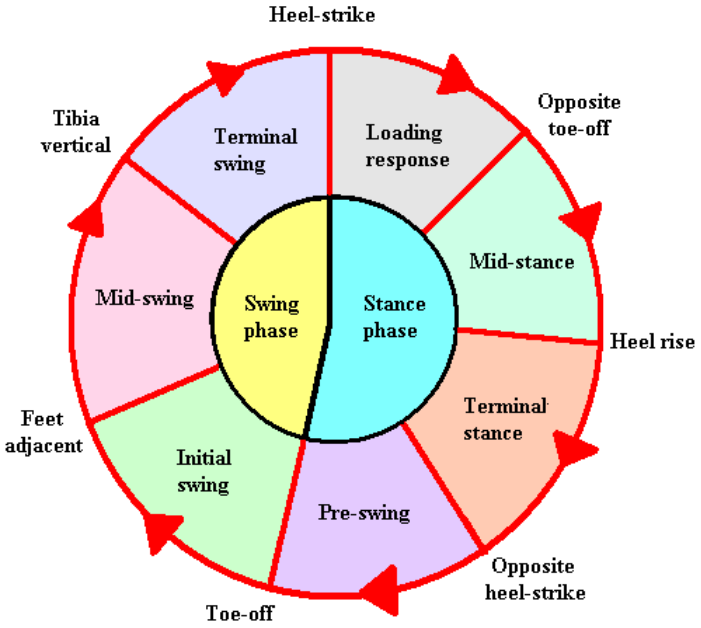

Figure 1.1 A complete illustration of human gait cycle adopted from [2].

Acute injury to one of the limbs or other pathological conditions such as functional deformity of the muscle and ligament, muscle weakness, sensory loss, pain and impaired motor control can disrupt the gait cycle [2]. They can alter the timing of the gait events and restrict the movement of the lower extremity. Patients with cerebral palsy [4]-[7], hemiplegic [8]-[11], amputation [11]-[13], osteoarthritis [14]-[15] and Parkinson disease [16]-[17] and patients who have undergone major surgery on the lower extremity, such as

hip or knee arthoplasty [18]-[19] have these symptoms. In most cases, patients unconsciously perform various compensatory mechanisms that may introduce stresses/pains to other parts of the body [2]-[3], [20].

Identifying patients' conditions and tracking their rehabilitation progress have become one of the primary functionalities of gait analysis. An increasing number of clinicians is selecting proper treatments for their patients based on gait analysis results [21]. For this reason, technology and knowledge related to gait analysis in clinical applications have significantly improved over the past 25 years [22]. Besides that, gait analysis is also used to design and to develop orthotic and prosthetic devices and Functional Electrical Stimulation (FES) systems, to study human movement in sports, and to study human musculoskeletal function in various activities i.e. running, walking and jumping [22].

At present, gait analysis is commonly conducted in a laboratory using optical motion capture system. This system uses several cameras to capture human motion in a 3-D space through reflective markers placed on human body. Despite being a gold standard in gait analysis, this system is expensive, bulky and difficult to operate [22]. Moreover, it is only capable of capturing limited number of consecutive gait cycles, which may not completely represent a person's gait [23]. Lastly, it only confines to a dedicated space i.e. laboratory [24]-[25].

With the recent developments of the miniature sensor technology, inertial sensors such as accelerometer, gyroscope and magnetometer are widely considered to be simpler and inexpensive alternatives to capture human motion. However, inertial sensors generally suffer from one major drawback. Inertial sensor has to be physically wired to a workstation to measure and record human motion. Hence, it may restrict subject's movements and the experiment may only be conducted in laboratory environment. In order to overcome this limitation, wireless technology is embedded into the sensor. Wireless technology enables the sensor to capture human motion for a long period of time in both indoor and outdoor environments. [24]-[31]. Hence, wireless inertial sensor is suitable for long term real-time ambulatory monitoring purposes.

1.2 Research Statement

In view of the merits offered by miniature inertial sensor, this research aimed to design and develop a new real-time motion capture system that can measure human motion during walking and provide immediate and comprehensive examination of a person's walking condition. This system was developed using wireless gyroscope as the main sensing device to capture human lower extremity in real-time. This system was also designed to be used in various clinical settings and rehabilitations thus it offers several computational methods that can directly assist clinicians, biomechanists and researchers to obtain better understanding of the overall functionality of human lower extremity. These computational methods were developed to examine several aspects of human gait, which include:

- *Gait events identification*

  Identifying gait events is the first step of gait analysis. Identifying gait events, particularly heel-strike and toe-off allows the estimation of temporal gait parameters and allows the gait data to be segmented on stride-to-stride basis. This thesis aimed to develop an algorithm that could automatically identify gait events using data measured by miniature sensors. This algorithm has to be robust and does not involve complex computations so that it can identify human gait events in various walking conditions and it can be implemented as one of the online data processes.

- *Gait normality test*

  Determining the normality of a person's gait is another important aspect of gait analysis. Experts in human movement science can determine patient's pathological conditions based on patient's spatio-temporal gait parameters, such as duration of stride, stance phase, swing phase and the orientation of the lower extremity during certain gait phases. Using real-time data captured by miniature sensors, this thesis aimed to provide comprehensive information on a person's spatio-temporal gait parameters when a person is walking on a treadmill or on the ground. This thesis also aimed to develop a method that can provide discrete measure that can differentiate normal and abnormal gait. More importantly, this method has to be able to perform necessary computations in a relatively short period of time so that it can be implemented as one of the online data processes.

- *Gait asymmetry*

  Gait asymmetry is another important gait characteristic. Gait of a healthy individual is fairly symmetrical with acceptable deviations. Symmetrical gait offers a stable and

adaptive gait, minimizes energy expenditure and minimizes the risk of fall. This thesis aimed to develop computational methods that were robust and practical, which could be easily implemented in various clinical applications while overcoming limitations posed by current methods.

- *Gait dynamic stability*

  Gait dynamic stability presented in this thesis aimed to examine the stability of human body segments i.e. thigh and shank during walking. This thesis adopted tools available in nonlinear dynamical system theory, particularly the Lyapunov exponent. In gait analysis, the maximum Lyapunov exponent corresponds to the ability of human neuromuscular locomotor system in maintaining walking stability.

To achieve above objectives, this thesis attempted to

- Perform an extensive study to determine the right wireless miniature sensor that can capture human lower extremity motion in real-time
- Create an interactive and user-friendly hardware/software co-design system that allows the real-time data streaming and data visualization
- Develop and optimize a computational method which is able to identify various important spatio-temporal gait parameters derived from the sensors outputs.
- Develop and optimize computational methods which can differentiate normal and abnormal gait i.e. the gait normality test, gait asymmetry analysis and the estimation of gait dynamic stability.
- Optimize the overall system architecture to facilitate periodical and immediate gait evaluation results without interrupting the real-time data streaming and data recording.
- Conduct an experimental study to examine the performances of the system.
- Conduct necessary statistical analysis to validate the experimental results and to examine the efficacy of the system in identifying gait abnormalities.
- Establish normative data for the gait monitoring system that uses gyroscope as its main sensing device and for the new computational methods introduced in this thesis.

1.3 Dissertation Outline

As the first step, an extensive research on human gait analysis was conducted. The focus of this research was to investigate several aspects of the current gait analysis including the merits and drawbacks of the instruments, the usefulness of gait analysis in

clinical applications, and the efficacy of the methods used to identify abnormalities in human gait. These aspects were later considered as the major factors that shape the system framework. Details of this research are discussed in Chapter 2.

This thesis produced a gait monitoring system that uses five inertial sensors to capture human lower extremity motion in real-time. Movements captured by the system are periodically examined to determine a person's walking condition. Additionally, it also records measurement data into a spreadsheet file for future reference. Whenever necessary, this file can be uploaded to the system to re-examine his/her gait. Detailed descriptions of the overall hardware/software co-design system architecture are presented in Chapter 3.

Interactive and user-friendly software was developed to accommodate the wireless data transmissions and data processing. It provides several functionalities that segment the measurement data on stride-to-stride basis, perform periodical gait evaluations, and present the outcomes qualitatively and quantitatively. The complete software architecture of the system is described in Chapter 4.

Several computational methods were implemented in the system to process and transform the measurement data to valuable information. Among them are the Hybrid Multi-resolution Wavelet Decomposition method, the computations of temporal gait parameters, the estimation and evaluation of the lower extremity motion in each gait cycle, and the computation of gait asymmetry index. These methods are discussed in further details in Chapter 5.

An experimental study was conducted to assess the overall performances of the system. In this study, participants were requested to walk on a treadmill and on the ground. Abnormal gait was simulated to examine the effectiveness of the online gait normality test, online gait asymmetry analysis, and offline gait dynamic stability analysis. Experimental setup and its results are presented in Chapter 6 and Chapter 7 respectively. Discussion on the system capabilities and the significances of the computational methods used to determine gait normality, gait asymmetry and gait dynamic stability are discussed in Chapter 8.

Conclusion of this thesis is drawn in Chapter 9 together with its possibilities for future research.

Chapter 2

BACKGROUND

This chapter describes the prior research conducted in clinical applications and biomechanics in order to provide a better understanding on why a real-time gait monitoring system equipped with periodical gait evaluation was designed and developed in this thesis. It also discusses the merits and demerits of existing methods used to examine a person's walking condition and to identify and track rehabilitation progress of patients with pathologic gait. Lastly, it briefly justifies how the developed system addresses those drawbacks and achieves exceptional outcomes out of this thesis.

2.1 Motion Capture System

Research and development in human motion analysis has been growing rapidly over these few decades. This growth does not only involve medical branches, but computing technology and engineering science too [32]. Human motion analysis possesses vast potential applications including clinical rehabilitation of patients with stroke or spinal cord injuries, and patients with walking disabilities and knee problems [33]-[41]. Besides that, it is also widely used in sports training to identify the faulty movements in various sports events i.e. golf, swimming, and running [33]-[46].

Human motions are mainly captured using optical and magnetic technologies. However, these technologies are expensive and only restricted to laboratory environment. Due to these reasons and the advances in MEMS (Micro Electro-Mechanical System) technology, inertial sensors, such as accelerometer, gyroscope, magnetometer, have been widely

considered as an alternative solution to capture human motion in various activities [47]. Following subsection describes the main characteristics of the conventional technologies i.e. optical motion capture system and magnetic tracking system and the main attributes of the inertial sensor.

2.1.1 Optical Motion Capture System

Optical motion capture system uses active or passive reflective markers placed on various body segments and Charge Coupled Device (CCD) cameras to capture a person's movement within the field of view. The merits of this system are that it has minimal impact on the natural motion of a person and it also allows the movement to be captured without the need to tether the data acquisition device. However, this system is expensive, requires high-speed processing devices and is only able to capture human motion within the field of view of the cameras in a dedicated space i.e. laboratory [39],[48].

Figure 2.1 Vicon F-series cameras for motion analysis [48].

2.1.2 Magnetic Tracking System

Magnetic tracking system utilizes magnetic sensors that are attached on various body segments to measure the strength of magnetic pulses generated by a transmitter. It uses more than 11 magnetic sensors to acquire full body motion in a 3-D space [32]. The merits of this system are that it is able to overcome the line of sight restriction and it runs on battery supply, hence making it is suitable for body mounting and ambulatory measurement. However, magnetic sensors are sensitive to nearby ferromagnetic materials that can distort the signal and lead to less accurate readings [1],[32],[49]. Due to this reason, this system is not a preferred tool for research in sports and gait analysis [1].

Figure 2.2 MotionStar Wireless 2 from Ascension Technologies, Inc. [50].

2.1.3 Miniature Body-mounted Sensor – Inertial Sensor

Due to rapid growth of MEMS technology, communication system and transmission, inertial sensors have been used to measure the kinematic parameters of human motion in both indoor and outdoor activities. These inertial sensors generally include accelerometer, gyroscope, magnetometer and their combinations. Inertial sensor offers a convenient and practical way to capture human motion. Its miniature size and light-weight will not encumber human movement. Moreover, it can be easily mounted on a human body hence increasing its adaptability and flexibility.

Roetenberg et al. attached tri-axial accelerometer, gyroscope and magnetometer on subjects' upper arm, back and thigh to acquire kinematic parameters of their motions in a 3-D space [49]. To validate their research outcomes, a test was conducted against an optical motion capture system. Test results indicated that their system can reach accuracy about 5 mm for position and 3 degrees for orientation measurements. The accuracy of their system might deteriorate when movements with high velocities occurred. Nevertheless, their findings proved the efficacy of the inertial sensors for human gait analysis.

Aminian et al. proposed the use of miniature gyroscopes to estimate spatio-temporal parameters in walking [51]. Gyroscopes were attached with a rubber band to right thigh, right shank and left shank to measure the angular rate parallel to the mediolateral axis (on the sagittal plane). They used wavelet analysis to identify heel-strike and toe-off events in every gait cycle and used a simple mechanical model to derive the stride length and walking velocity. Their research outcomes indicated that miniature gyroscope can be a promising tool for human gait analysis.

Plamondon et al. developed a hybrid system composed of two inertial sensors which each consists of accelerometer, magnetometer and gyroscope to measure the movement of human trunk [38]. Their research also used additional source of information: a potentiometer to measure the relative rotation between the inertial sensors to validate their system. Experimental results showed that the root mean square error of their system was generally below 3^o for the flexion and lateral bending axes and less than 6^o for the torsion axis.

Jasiewicz et al. combined a gyroscope with two bi-axial accelerometers to define the gait events of normal and spinal cord injured persons [40]. For validation, they placed pressure-sensitive foot switches on their subject's feet. Their experiments showed a promising result. Inertial sensors were as accurate as the foot switches in estimating the time of heel-strike and toe-off in both normal and spinal-cord injured individuals.

From the literatures published so far, it is evident that inertial sensor offers a great prospect ahead in acquiring human motion in both indoor and outdoor environment. Moreover, it is relatively cheaper and less sophisticated. It also does not restrict the data acquisition process to laboratory environment. A summary of the main characteristics of the inertial sensors compared to conventional motion capture technologies is presented in Table 2.1. For these reasons, this research initiated its first step and proposed a wireless gait monitoring system that is solely based on the measurement data obtained from wireless inertial sensor.

Table 2.1 Comparison of various motion capture technologies

Description	**Optical motion capture system**	**Magnetic tracking system**	**Miniature Body-mounted sensor**
Complexity/ sophistication	High	Medium	Low
Method	Reflective markers and CCD cameras	Magnetic sensors	Inertial sensors
Reliability/ accuracy	High	High	Depends on the computational method
Implementation	Difficult	Medium	Easy
Mobility	Low	Medium	Low
Environment	Indoor	Indoor	Indoor and outdoor
Main application	Human gait analysis and sports science	3-D animation	Human gait analysis and sports science

2.2 Gait Event Identification

Gait event identification is essential in human motion analysis. Heel-strike and toe-off represent the start of stance phase and the start of swing phase respectively. These two events are widely used to measure and segment other definable gait events, and to aid the analysis of gait and the development of gait assisted devices [27],[52]-[54]. In several clinical settings, gait event identification is used to evaluate treatments for patients with pathologic gait and cerebral palsy, to assess the functional performance of a patient's lower limb after treatment or surgery, such as hip or knee arthroplasty, to refine proper alignment and fit of eternal prosthesis or orthesis and to asses fall risk of elderly person. Due to these reasons, many tools and methodologies have been proposed and developed to identify gait events.

One of the earliest tools to identify gait events is the microswitch shoe developed by Winter, et al. [55]. In their approach, two microswitches were placed on the heel area and three microswitches were placed on the sole area of the shoe. Despite of its simplicity, microswitch shoe successfully identified various gait events i.e. heel-strike, flat-foot, heel-rise, opposite heel-strike and toe-off. However, due to advances in engineering and computing, this microswitch shoe does not seem to be a feasible tool for gait event identification anymore as there are more accurate and more sophisticated tools available now.

Vetlink, et al. developed orthopaedic shoes equipped with six degrees of freedom force sensors to identify the gait events and to obtain various kinematic and kinetic parameters such as ground reaction force and center of pressure [56]. Comparing to the conventional force plate, it achieved reasonably accurate readings with root mean square difference of the ground reaction force is equal to 15±2 N and root mean square difference of the center of pressure is equal to 2.9±0.4 mm.

Catalfamo, et al. used F-scan in-shoe measurement system to identify heel-strike and toe-off in walking [57]. They proposed a new area detection method, which uses the loaded area during the gait cycle to identify gait events. This approach produced reliable and accurate results with absolute mean differences between their method and F-scan in-built algorithm were equal to 42±11 ms for heel-strike and 37±11 ms for toe-off.

Ghoussayni et al. placed reflective markers on human feet to detect four major gait events: heel-strike, heel-rise, toe-contact and toe-off and three intervals i.e. heel contact to toe-contact, toe-contact to heel-rise, heel-rise to toe-off [58]. They calculated velocities of these markers on the sagittal plane using empirically set thresholds to determine four gait events. These thresholds were determined visually by inspecting two barefoot and two shod trials for two randomly selected subjects. Their research outcomes indicated that four major gait events could be automatically derived using kinematic data alone with acceptable error of 16.7 ms. This error is comparable to findings published by other researchers [57], [134]-[136].

As the research in human motion capture system advances, inertial sensors attract attentions of biomechanists, clinicians, and physiotherapists, as discussed in Chapter 2.1.3. Besides Aminian et al. and Jasiewicz et al., Mansfield and Lyons also used miniature body-mounted sensor, particularly, accelerometer to identify gait events in hemiplegic patients who used FES system [59]. They placed an accelerometer on the patient's trunk to detect the heel contact events on both legs based on the examination of the anterior-posterior horizontal acceleration signal. For validation, foot-switches were placed on the sole of one foot to record the heel-strike and heel-off times. Their research concluded that accelerometer was a valid tool to identify the occurrences of heel-strike during FES assisted walking.

Sabatini et al. constructed an inertial sensor that consisted of one bi-axial accelerometer and one uni-axial gyroscope to estimate spatio-temporal gait parameters [22]. Inertial sensor was attached to the instep of the foot. This sensor was combined with gait phase segmentation procedure to obtain the occurrences of heel-strike and toe-off, and to determine the duration of stride, swing phase and stance phase. Even though it was only tested during treadmill walking, it appeared to be a promising measuring device for various applications in rehabilitation, sports medicine, and health monitoring.

A clear indication that can be extracted from above literatures is that identification of gait events is important in gait analysis and clinical rehabilitation. Kinematic and/or kinetic parameterscan be used to extract the timing information of various gait events such as heel-strike, toe-off, heel-rise, and opposite heel-strike. It is also evident that a miniature body-mounted sensor can be a valid and reliable tool to identify these events.

2.3 Discrimination of the Normal and Abnormal Gaits

Gait analysis is the study of the biomechanics of human movement aimed at quantifying factors governing the functionality of human lower extremity [60]. This study may involve analysis of the orientation of the lower extremity, muscle activities, analysis of human body balance, study on the oxygen consumption and the interaction between many neuromuscular and structural element of the locomotor system including the brain, spinal cord, nerves, joints and skeletons [60]. Gait analysis is commonly conducted by clinicians, biomechanists and researchers for detection of gait disorder, identification of body balance factors, assessment of clinical gait intervention and rehabilitations. In engineering, human gait plays important role in the design and development of prostheses and controllers used in exoskeletons and robotics [61].

A conventional gait analysis involves a gait laboratory, optical motion capture system, force platforms, and a high-end workstation. In this laboratory, human walking motion is measured and recorded using optical motion capture system and force platforms. For most clinicians and therapists, interpretation of the gait data can be difficult due to its high complexity. This complexity arises from high data dimensionality and volume, non-linear data dependencies and non-unique correlations, as described in [60]-[62].

To conveniently interpret human gait data and to identify the deviations of abnormal gait from normal movement patterns, various parameterization techniques and waveform classifiers have been employed by clinicians and researchers [63]. Parameterization techniques use a fraction of available kinematics and kinetics parameters by extracting the instantaneous values of their amplitude and time. Romei, et al. proposed Normalcy Index (NI) to quantify the amount of deviation in a subject's gait [6]. NI involves 16 kinematic parameters i.e. time to toe-off, walking speed, cadence, mean pelvic tilt, range of pelvic tilt, mean pelvic rotation, minimum hip flexion, range of hip flexion, peak abduction in swing phase, mean hip rotation in stance phase, knee flexion at initial contact, time of peak flexion, range of knee flexion, peak dorsiflexion in stance phase, peak dorsiflexion in swing phase, and mean foot progression angle in stance. In their study, they found that NI was robust enough to categorize pathological gait of idiopathic toe-walkers and patients with cerebral palsy.

Regardless of its viability in several clinical applications, parameterization techniques are not practical. It is difficult to identify the required peaks and valleys. Moreover, the

variables used in these techniques are seldom justified [64]. Lastly, they do not provide information regarding the waveform patterns of the variables [63].

With the intention to overcome the drawbacks of the parameterization techniques, waveform classifiers were proposed by several researchers [63]. These methods include use of Principal Component Analysis (PCA) [11],[65], neural network [64]-[66], and other pattern recognition techniques [67]-[68]. Schutte, et al. used PCA to derive a set of 16 independent variables from 16 selected gait variables [11]. Some of the variables include walking speed, cadence, mean pelvic tilt, mean pelvic rotation, minimum hip flexion, knee flexion, peak dorxiflexion and mean foot progression. Using the variables derived from PCA, they proposed a normalcy index that measured the distance between the variables describing patient's gait and variables of a normal and healthy person. As a result, their normalcy index was able to classify Type I, Type II, Type III, and Type IV hemiplegic patients.

Tingley, et al. applied PCA to angular rotation of hip, knee and ankle during a complete gait cycle [65]. Data reduction using PCA was achieved by locating the primary directions of the kinematic parameters from the mean behavior. Variations from the mean were then calculated to obtain one-dimensional index that classified a child's gait as normal, unusual or abnormal. The merit of this method is that it can be applied across multiple joint angle curves and their derivates. Thus, they believed that it could be a valuable clinical tool that distinguished the gait of normal healthy children and children who were born prematurely.

Schwartz, et al. proposed Hip Flexor Index (HFI) which utilized PCA from five kinematic and kinetic variables [7]. These variables were collected from 23 normal and healthy individuals and six patients diagnosed with celebral palsy. These five variables are the maximum pelvic tilt, pelvic tilt range, maximum hip extension in stance phase, timing of crossover, and hip flexion power during late stance phase. HFI were proven to correspond well with the subjective clinical evaluation that was carried out by six clinicians. Thus, HFI can be a simple quantitative tool for clinicians to evaluate the patients' walking conditions.

Holzreiter and Kohle used Artificial Neural Networks (ANN) to classify normal gait and pathological gait [66]. Ground reaction force profiles of 94 healthy persons and 131 patients who had calcaneus fracture, artificial limbs and other diseases were measured and used as the main variables. Their experimental study achieved satisfactory results with

classification accuracy up to 95%. It demonstrated the capability of neural network to assist clinician's decision making.

Barton, et al. proposed Quantization Error (QE) derived from self-organizing neural networks to quantify the deviation of patients' abnormal walking gait from normal and healthy gait [64]. 3-D joint angles, moments and power of the lower limbs and the pelvis were used to train Kohonen ANN. 18 normal subjects and 79 patients with various gait problems due to cerebral palsy, head injury, spina bifida, neuropathy, amputees, ankle injury, autism, Parkinson's disease, and dystonia involved in their experimental study. This study validated the application of QE in clinical application to be a measure of gait quality that was normally inaccessible by quantitative gait analysis.

Xu, et al. combined neural network capabilities and fuzzy logic qualitative approaches to classify gait of normal and healthy persons and gait of patients with pes cavus and pes planus [67]. In their study, plantar pressure distributions of the feet were the main kinetic parameters. With this approach, they were able to achieve high classification accuracy of 96.15%, 92.5%, 93.33% for normal persons, and for patients who suffered from pes cavus and pes planus respectively. These accuracies were relatively higher than other neural network approaches.

In their recent publications, Schwartz and Rozumalski proposed a biometric method that was commonly used for human face identification, 'Eigenface' method [68]. In this method, a set of kinematic plots and joint angles were digitized and converted to vectors. This vector was then subjected to PCA. Subsequently, a distance metric was defined to measure the similarity of one gait feature to another gait feature. For validation, GDI was applied to the gait of patients with celebral palsy. From their experimental results, it could be observed that GDI successfully distinguished the affected and contralateral side for the hemiplegia while confirming that the contralateral side did not exhibit a normal gait pattern. Hence, they concluded that GDI could be a practical tool to measure the overall gait pathology of a patient.

Despite of their implementations in several clinical applications, waveform classifiers have a high computational requirement. Hence, they consume significant time to generate the results and can only be implemented offline. Moreover, most of the classifiers still use conventional motion capture systems i.e. optical motion capture systems and force platforms. Lastly, waveform classifiers require a large set of normative data that have to be

collected from normal and healthy individuals. Prior knowledge on the pathological gait patterns is also one of the important elements to distinguish patient's gait from healthy individual's gait.

To address these limitations, this research proposes the use of Coefficient of Determination (*CoD*) to provide quantitative gait index. It serves as a discrete measure that represents all data points in every gait cycle. Since it does not require extensive computation, *CoD* can be implemented as one of the online processes. Thus, quantitative gait assessment can be performed while a person is walking on a treadmill or on the ground. In addition, various temporal gait parameters such as duration of stride (T_{stride}), stance phase (T_{stance}), and swing phase (T_{swing}) can also be calculated to compliment the online gait assessment and to provide comprehensive information on a person's walking condition.

2.4 Gait Asymmetry

Gait asymmetry is one of the most important gait characteristics. Gait symmetry is defined as a perfect agreement between the actions of the lower limbs and/or when no statistical differences are noted on parameters measured bilaterally. Gait of a healthy individual is fairly symmetrical with acceptable deviations. Symmetrical gait offers both stable and adaptive walking patterns, minimizes energy expenditures and minimizes the risk of fall. On the contrary, asymmetrical gait is commonly found in patients who suffer from celebral palsy [4],[69], hemiplegic [8],[9],[10], amputation [12],[13],[70], limb length discrepancy [71] and Parkinson disease [16]. Significant bilateral differences can be found in both kinematic and kinetic parameters such as the duration of stride, stance phase, and swing phase [72]-[73], ground reaction force profile [73]-[75] and range of motion of the lower limbs [76]. Fundamental approaches used to define gait asymmetry are the Symmetry Index (SI), the Symmetry Ratio index (SR) and the statistical approach [77].

2.4.1 Symmetry Index (SI)

Symmetry index or SI was initially proposed by Robinson, et al. [78]. It evaluates the degree of symmetric behavior using the calculated differences between the left and right limbs for a given parameter divided by their bilateral average. Zero SI indicates that the gait is perfectly symmetrical. Becker, et al. demonstrated the usefulness of SI in the rehabilitation of young adults who underwent surgical treatment of ankle fracture [79]. Using SI, they found that significant load asymmetries particularly in the lateral

forefoot of the injured leg. Asymmetrical loading suggested that patients used compensation mechanisms to regain gait symmetry after ankle alteration.

Kim and Eng used SI to identify gait asymmetry in individuals with chronic stroke [73]. Using patients' ground reaction force profiles to derive SI, they found that stroke patients' gait speed was correlated with the symmetry of temporal measures and ground reaction force. In addition, they also described that symmetry in patients' ground reaction force was correlated with symmetry in temporal parameters with $p < 0.05$.

Perttunen et al. applied SI to study the gait asymmetry in patients with leg length discrepancy [71]. Plantar pressures distribution, ground reaction force profile and muscle activities of 25 patients were measured and recorded to compare the bilateral difference between the left and right limbs. They found that vertical ground reaction force of the longer limb was greater than the shorter limb. Similar observation was also apparent in the maximum isometric torque. Their experimental results implied that foot loading pattern shifted more to the forefoot of the longer limb to compensate walking disturbances.

Despite the wide implementation of SI in various clinical applications, SI suffers from several drawbacks. One of the drawbacks is that SI requires a reference value which is typically different from case to case [75]. Besides that, SI is prone to artificial inflation as highlighted in [78],[80]. It was reported that maximum SI value of 13,000% could occur when the difference between sides was divided by a much smaller value [75].

2.4.2 Symmetry Ratio (SR)

Symmetry Ratio or SR is calculated based on the ratio of a gait parameter between the left and right limbs. The gait is symmetrical if and only if SR is close to one. Balasubramanian, et al. utilized SR to observe the step length and walking performance of individuals with chronic hemiparesis [8]. Patients' walking speed, step length, and the duration of swing phase and pre-swing were collected using an instrumented mat and force plates to determine gait asymmetry. Their study suggested that patients generated least paretic propulsion when walking with relatively longer paretic steps.

On a different application, Andres and Stimmel applied SR to assess the lower limb prosthetic alignment [12]. Stride length, step length, the duration of stride, stance phase,

swing phase and double support, walking velocity, joint angles and vertical displacement of the centre of gravity were used as the main parameters. Their research revealed that patients performed several compensatory mechanisms to reduce gait asymmetry. Hip angle asymmetries were found to compensate for knee angle asymmetries and swing phase lasted longer while the double support time decreased on the prosthetic side.

Similar to SI, SR may suffer from the artificial inflation as well. This effect may happen if both gait parameters are close to zero. Moreover, SR also requires a reference value, which may be different from one application to another. In spite of providing good indication of gait asymmetry, SI and SR only take into account single variable or limited set of points from left and right limbs. They do not analyze the motion in one complete gait cycle [76],[81].

2.4.3 Statistical Approaches

The statistical approaches are also used to identify gait asymmetry between the lower limbs in walking. Sadeghi applied PCA as a curve structure detection method to determine gait asymmetry [82]. They used the muscle moment of the lower limbs as the main variable. As the research outcome, they concluded that the gait of able-bodied subjects appeared to be symmetrical. This behavior was identified as a result of local asymmetry which indicated different levels of within and between muscle activities developed at each joint in one gait cycle.

Shorter, et al. proposed Regions of Deviation (RoD) analysis to quantify gait asymmetry between bilateral joint pairs and its behavior relative to the normative data [76]. RoD used kinematic parameters collected from an optical motion capture system. This analysis effectively identified the timing and magnitude of deviations throughout the gait cycle. It also provided information about the impact of a joint-mobility perturbation on neighboring joints. Thus, this analysis appeared to be useful for clinicians in detecting gait impairments and monitoring the changes in gait as a function of recovery process.

Allard et al. applied paired t-test ($\alpha < 0.05$) to determine the presence of gait asymmetry [83]. Kinematic and kinetic parameters collected from the force plates and optical motion capture system were used to identify the bilateral difference between the left and right limbs. From the experimental results, they found that right limb developed

a significantly greater total negative work than left limb. On the contrary, both limbs generated similar total positive work while maintaining the walking speed.

Regardless of their capabilities, statistical approaches require additional subjects and experiments to define gait asymmetry. In addition, they also need normative data from able-bodied subject as a reference.

To address limitations of these three different approaches i.e. SI, SR and statistical methods, this thesis introduces Normalized Cross-correlations (Cc_{norm}) to generate a discrete indicator that signifies the bilateral differences between the left and right limbs and to estimate the time shift (Ts) between them. This thesis also introduces Normalized Symmetry Index (SI_{norm}) to determine the gait asymmetry over one complete gait cycle. Unlike conventional SI, SI_{norm} is capable of identifying the timing and magnitude of gait asymmetry. It is also not prone to artificial inflation. Lastly, this thesis explores the viability of these methods in identifying gait asymmetry in both normal and abnormal walking patterns. Details of these approaches are discussed in Chapter 5.7, Chapter 5.8, and Chapter 5.9.

2.5 Gait Dynamic Stability

Gait dynamic stability is defined as the ability to maintain functional locomotion despite the presence of small kinematic disturbances or control errors [85]. Deterioration of gait stability is a sign of many pathologic conditions which commonly found in the elderly [92], patients with Down syndrome [93], patients with diabetic neuropathic [94] and patients with ACL deficient knee [97]. For this reason, stability is one of important factors in gait analysis.

In recent years, many researchers have attempted to investigate and to quantify human stability during walking [86]-[90]. In some of the studies, magnitude of kinematic variability was often referred as an estimate of stability. However, there were little evidences that support this assumption [91]-[92]. Gait variability generally quantifies only the average differences between strides and it is independent of the temporal order in which the strides occur. It also does not contain information on how the locomotor control system responds to perturbations either within or across strides [91]-[94]. Moreover, it is limited by its ability to quantify and to provide a discrete measure that represents all data points [92].

Due to these reasons, tools from nonlinear dynamical system theory were proposed to assess the point-to-point fluctuations in movement trajectories throughout the gait cycle [85],[91]-[92],[94]. Although the fluctuations in measurement data are often described as error or noise of a system, dynamical system theory provides a different explanation. It proposes that these fluctuations might be a consequence of the dynamic self-organization of a complex system. The most popular tool derived from this theory is the estimation of the maximum Lyapunov exponent (λ^*). While true Lyapunov exponents cannot be calculated from discrete time-series of biological system behavior (i.e. human walking), Rosenstein et al. [95]and Kantz and Schreiber [96] developed methods that can estimate λ^*, which dominates the entire system stability.

Dingwell and Kang examined the dynamic stability of older adults using λ^* [92]. They used trunk kinematics to estimate the dynamic stability of upper body during walking. Trunk kinematic was captured using optical motion capture system with six markers placed on the left and right acromias, C7 and T10 spinal processes and spines of each scapulae. Their experimental results indicated that older adults exhibited higher λ^* than younger adults. Higher λ^* implied that older adults had increased dynamic instability during walking compared to the younger ones. However, when they walked slower, they decreased their dynamic instability in spite of increased variability. Their findings suggested that older adults walked slower to increase their overall gait stability.

Buzzi and Ulrich examined dynamic gait stability of preadolescent children with and without Down syndrome [93]. They captured thigh, shank and foot movement using optical motion capture system. The kinematic variable i.e. angular displacement on the sagittal plane was used as the main variable to examine gait dynamic stability of these children. Their experimental study suggested that children with Down syndrome had increased dynamic instability during walking compared to healthy children.

Dingwell et al. used λ^* to examine dynamic stability of patients with diabetic neuropathic [94]. Single tri-axial accelerometer and three electrogoniometers were placed on the upper body, hip, knee and ankle to measure the kinematic variables of these segments during walking. Their experimental results indicated that patients with diabetic neuropathic adopted more stable gait patterns by slowing their self-selected walking speed even though they exhibited greater kinematic variability than healthy subjects. Additionally,

they also found that walking on a treadmill was slightly more stable than walking on the ground.

Stergiou et al. assessed functional dynamic knee stability of patients with Anterior Cruciate Ligament (ACL) deficient knee using λ* [97]. They used optical motion capture system to measure the sagittal knee angular displacement when the subjects walked on a motorized treadmill. They found that λ* of ACL deficient knee was higher than the contralateral knee. This finding implied that the deficient knee was more unstable than the contralateral knee. Thus, deficient knee was less adaptable to ever-changing environment.

Despite its wide clinical applications, the kinematic variables used to estimate λ* are generally derived from optical motion capture system [92]-[94],[97]-[102]. Although it is considered as gold standard in capturing human motion, the optical motion capture system is expensive, bulky and difficult to operate [23],[25]. Therefore, this research explores the advantages offered by the miniature sensor, particularly gyroscope, to estimate the gait dynamic stability. In this thesis, the estimation of λ* is implemented as one of the system offline processes. Offline process implies that λ* can only be estimated after the experiment is completed or when the experimental data is uploaded to the system. This is solely due to large amount of data, and substantial calculation and computational time involved in the estimation process. In this thesis, there are two different measures that are considered in estimating gait dynamic stability: short-term maximum Lyapunov exponent (λ_S^*) and long-term maximum Lyapunov exponent (λ_L^*). λ_S^* reflects the ability of human neuromuscular locomotor system in maintaining short-term stability whereas λ_L^* reflects the ability of human neuromuscular locomotor system in maintaining long-term stability.

Chapter 3

AMBULATORY GAIT MONITORING SYSTEM

The wireless ambulatory gait monitoring system is a system that utilizes the state-of-art wireless inertial sensors to capture human gait. It comprises real-time hardware/software co-design system architecture that provides an integrated process to monitor and to evaluate human gait over long period of time in indoor and outdoor environments. The developed system was designed to provide sufficient information that assists clinicians, biomechanists, and researchers in interpreting the gait data, monitoring patient's rehabilitation progress, assessing functional performances of the lower limb upon medical treatment or surgery, and devising appropriate treatments for the patients.

Figure 3.1 illustrates a general overview of the wireless ambulatory gait monitoring system. This system consists of several main components i.e. wireless Inertia-Link sensors, wireless transceivers, workstation and system software developed using LabVIEW 8.5. To monitor and to examine human gait, wireless sensors are attached to the abdomen, right thigh, right shank, left thigh and left shank. Each sensor measures and records 3-D acceleration and 3-D angular rate of its respective body segment in real-time. This sensor then converts the measurement data into a series of data packets and transmits them to the workstation through its wireless transceiver. Subsequently, the system software converts the data back to the relevant kinematic parameters i.e. acceleration and angular rate and displays them on graphs.

In this thesis, LabVIEW 8.5 was selected as the main programming platform. One of the main reasons is that it can provide a reliable real-time wireless communication interface

between the wireless inertial sensors and the workstation. It also supports the simultaneous real-time data streaming from wireless inertial sensors. Lastly, it offers an interactive and user-friendly Graphical User Interface (GUI) so that a novice user can use the software without much difficulty. A detailed description of the software architecture is presented in Chapter 4.

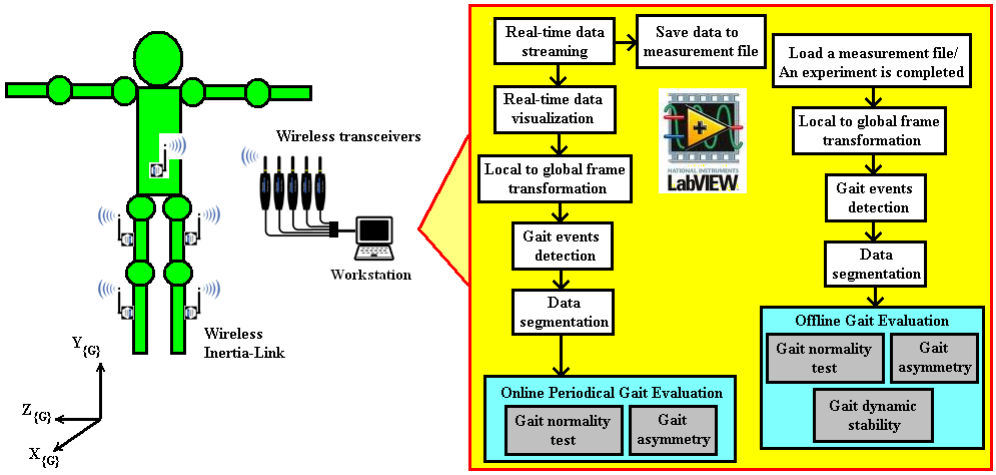

Figure 3.1 An overview of the ambulatory gait monitoring system.

It is important to note that this system consists of two operational modes: online periodical gait evaluation mode and offline gait evaluation mode (Figure 3.1). In this context, the word 'Online' refer to the real-time data streaming and data visualization. Therefore, online periodical gait evaluation mode implies that the gait evaluation occurs periodically during the real-time data streaming. On the contrary, offline gait evaluation mode refers to the system capability in performing similar gait evaluation after the experiment ends or when a measurement file is loaded into the software.

When online periodical gait evaluation mode is selected, measurement data collected during the experiment are evaluated periodically every five seconds. Prior to the evaluation process, the sensor coordinate frame is transformed to a global coordinate frame. Subsequently, Hybrid Multi-resolution Wavelet Decomposition (HMWD) method is applied to the shank angular rate to identify mid-swing (MS), heel-strike (HS) and toe-off (TO). The occurrences of these gait events can be then used to estimate T_{stride}, T_{stance}, and T_{swing}. They also allow the data to be segmented on stride-to-stride basis. A detailed description of HMWD is presented in Chapter 5.2.

The first operational mode has two different evaluation categories: gait normality test and gait asymmetry analysis. Gait normality test is an evaluation that compares the lower extremity

movements to the ideal movements of a healthy individual. This test provides the following information: The mean and standard deviation of T_{stride}, T_{stance}, T_{swing}, and CoD. T_{stride}, T_{stance}, and T_{swing} define the temporal gait parameters of a person. CoD provides single discrete measure that determines the normality of a person's gait. Detailed descriptions of T_{stride}, T_{stance}, T_{swing}, and CoD are discussed in Chapter 5.3 and Chapter 5.5.

Gait asymmetry analysis is an evaluation that examines the bilateral differences between the left and right limbs. This evaluation uses temporal SI i.e. SI_{stride}, SI_{swing} and SI_{stance}, Cc_{norm}, Ts and SI_{norm} as the main parameters. Temporal SI defines the differences in T_{stride}, T_{stance}, and T_{swing} between the left and right limbs. Cc_{norm} defines the similarity between left limb angular rate and right limb angular rate. Ts determines the time shift between them. SI_{norm} identifies the timing and magnitude of gait asymmetry throughout the gait cycle. Detail definitions of these parameters are described in Chapter 5.7, Chapter 5.8 and Chapter 5.9.

When offline gait evaluation mode is selected, gait data are processed after the experiment is completed or when a measurement file is uploaded to the system software. Unlike the previous operational mode, this mode provides three gait evaluation methods i.e. gait normality test, gait asymmetry analysis and estimation of gait dynamic stability. The first two evaluations use similar methods to those described earlier whereas the last evaluation examines human gait stability. Gait dynamic stability is assessed using λ*. λ* provide a discrete measure that reflects human neuromuscular ability responding to the kinematic perturbations (stride-to-stride variability) while maintaining body balance. This system provides two different measures of λ*: λ_S^* and λ_L^*. λ_S^* dictates the capability of human neuromuscular locomotor system in maintaining short-term stability. λ_L^* dictates the capability of human neuromuscular locomotor system in maintaining long-term walking stability Complete description of these parameters is provided in Chapter 5.10.

3.1 Wireless Inertial Sensor: Inertia-Link

Wireless Inertia-Link was selected as the main sensing device to measure and to record human lower extremity motion during walking. Inertia-Link is a small, light-weight and low power-consumption inertial sensor. It combines a tri-axial accelerometer, a tri-axial gyroscope and an onboard processor to measure the acceleration and angular rate of an object in a 3-D space. The sensing axes of wireless Inertia-Link are depicted in Figure 3.2. Inertia-Link is widely used in various application including [103]:

- Inertial aiding and location tracking i.e. INS (Inertial Navigational System) and GPS (Global Positioning System).
- Unmanned vehicles and robotics.
- Computer science and biomedical engineering.
- Platform stabilization.

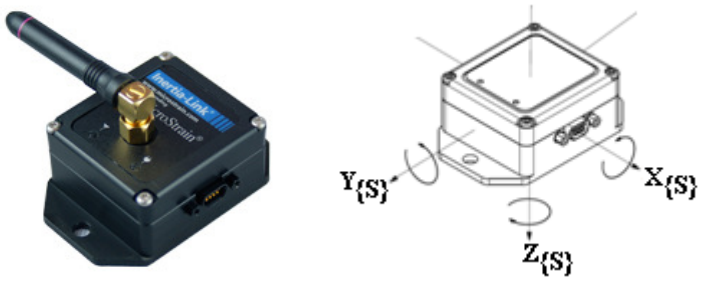

Figure 3.2 Wireless Inertia-Link with its sensing axes [103].

A complete set of wireless Inertia-Link consists of one wireless inertial sensor and one USB wireless transceiver. Since the developed system uses five inertial sensors, five wireless transceivers are utilized and connected to the workstation (Figure 3.3). The inertial sensor comes with a 9V Lithium battery pack which can last up to 4 hours. Based on specific preset configuration, Inertial-Link onboard processor can generate different type of output data i.e. acceleration, angular rate, Euler angles, orientation matrix, differences in angle and differences in angular rate. All these data are fully temperature compensated and corrected to minimize the measurement errors [84]. Since it is a commercially available high performance inertial sensor, no data disruption is expected when it is operating within the permissible transmission range (approximately 10 m). This sensor is also accompanied with a high sampling rate of up to 300 Hz. Its embedded accelerometer provides measuring range of ±9.81 m/s^2 with bias stability of ± 0.0981 m/s^2 and nonlinearity of 0.2 % whereas the gyroscope is capable of measuring range of ±5.235 rad/s with bias stability ±0.00349 rad/s and nonlinearity of 0.2%.

As illustrated in Figure 3.1, developed system places inertial sensors on a person's upper body (abdomen), right thigh, right shank, left thigh and left shank. Since each Inertia-Link has its own local sensing axes to measure 3-D acceleration and 3D angular rate (Figure 3.2), a local-to-global coordinate frame transformation is required to provide accurate measurement of the movement of each body segment. Detailed mathematical description of this transformation is presented in Chapter 5.1.

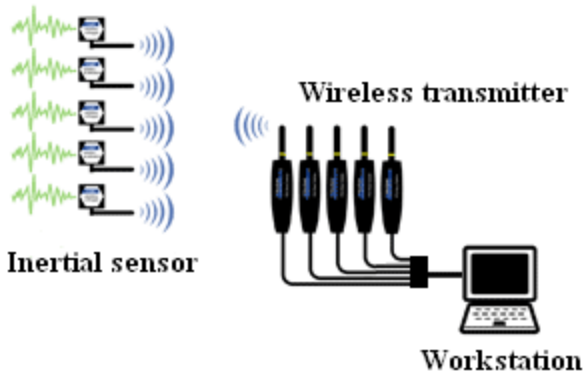

Figure 3.3 Wireless Inertia-Link system configuration.

Several configurations are set to enable simultaneous real-time data streaming from the sensors, to minimize data disruption and to prevent cross-talk between inertial sensors and transceivers. Firstly, each inertial sensor is assigned to a unique identification number ranging from 1 to 99 [106]. Secondly, it is allocated to a specific operating channel. Operating channels ranging from channel 1 to channel 26 are fixed by the manufacturer, thus further adjustment is not allowed. Thirdly, every wireless transceiver is assigned to an operating channel that is similar to one inertial sensor. This approach allows the wireless transceiver to be able to communicate with only one inertial sensor. The sensor identification numbers and their respective operating channel are presented in Table 3.1. In order to capture sufficient data samples during walking, the sampling frequency of this system is set to 200 Hz.

Table 3.1 Sensors ID and their operating channels

Sensor ID	Sensor placement	Operating channel
53	Abdomen	24
56	Right thigh	14
88	Left thigh	20
50	Right shank	22
54	Left shank	16

In spite of sensor capabilities in measuring acceleration and angular rate, only the angular rate of the lower extremity on sagittal plane were selected and considered in this thesis, therefore wireless Inertia-Link sensors were regarded as the wireless gyroscopes. The main reasons are:

- Unlike accelerometers, gyroscopes are not affected by gravity and/or any linear acceleration [21],[40],[51].
- The orientation of the lower extremity can be estimated by simple integration [21],[40],[51].
- Gyroscopes are able to produce similar measurement results regardless of the minor differences in the attachment sites on a human body [21],[40],[51].
- No calibration is required prior to the data acquisition process.
- Movements of the lower extremity on sagittal plane are commonly used in clinical settings and rehabilitations. Thus, they are better established than frontal plane and horizontal plane [2],[3], [21],[63],[68],[104]
- Highest data reliability was reported on the sagittal plane [105].

Even so, angular rate of the lower extremity on frontal plane and horizontal plane are still measured and recorded to provide a realistic and natural 3-D animation of human gait. Additionally, acceleration of the lower extremity on all three planes: sagittal plane, frontal plane and horizontal plane are also stored in real-time into single measurement file (*.csv).

3.2 The Inertia-Link Lower Extremity Suit

Optical motion capture system relies heavily on the skill of assessors in accurately placing reflective markers on human body. From their study, Mc Ginley et al. suggested that marker placements can contribute to the principal source of measurement error which leads to less accurate measurement [105]. To minimize this effect, a simple suit which is called 'The Inertia-Link Lower Extremity Suit' was designed and developed in this thesis. This suit is made of bulk straps, Velco^{TM} straps, bucklers, and buckler locks. This suit was designed such that

- The subject can wear this suit comfortably regardless of his/her anthropometry.
- The sensors can be firmly placed on the abdomen, right thigh, right shank, left thigh and left shank.
- It does not hinder the movements of the lower extremity during walking.
- It provides consistent sensors placements on the subject's lower extremity hence minimizing the measurement errors and offering reliable data across the subjects and/or experiments.
- It reduces the overall system setup time.

The lower extremity suit has several sets of bucklers and buckler locks, which are arranged horizontally and vertically. These sets of bucklers and buckler locks can be adjusted in a manner shown in Figure 3.4 according to the length and circumference of subject's lower limbs.

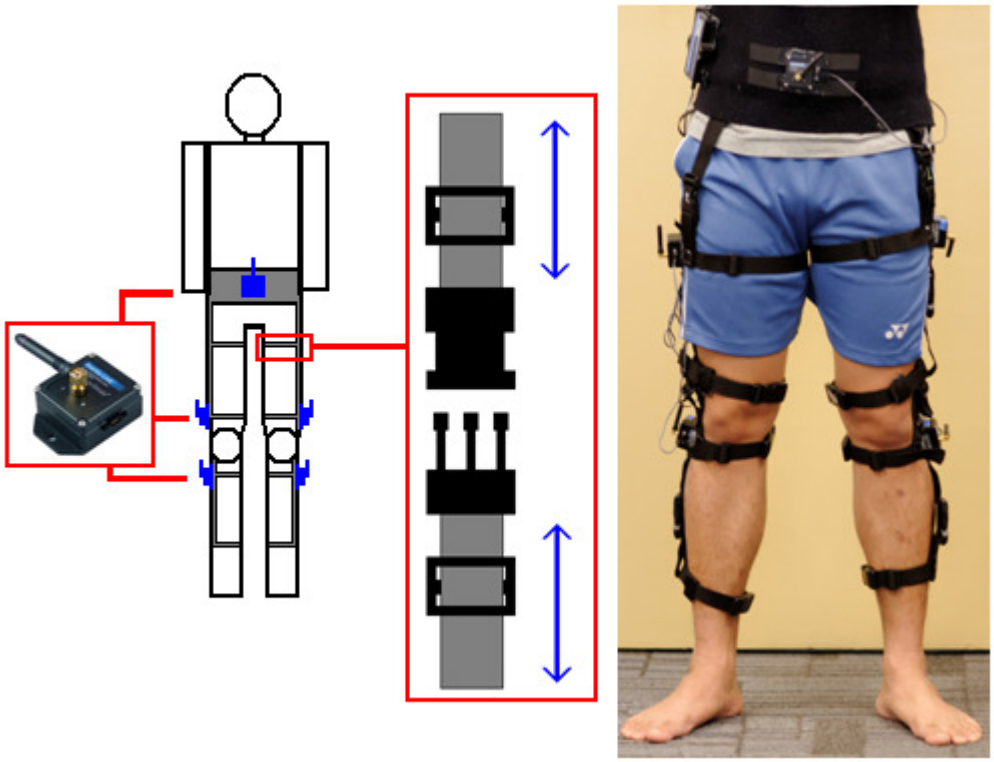

Figure 3.4 Inertia-Link Lower Extremity Suit.

3.3 Inertia-Link USB Transceivers

Five USB transceivers are utilized to transfer the measurement data from five wireless Inertia-Link sensors to the workstation. These transceivers are properly placed inside a carrier to reduce the system setup time. Indirectly, it also increases the mobility of the system because it can be easily stored and moved to another experiment site or to another workstation. The overall setup of the USB transceivers is presented in Figure 3.5.

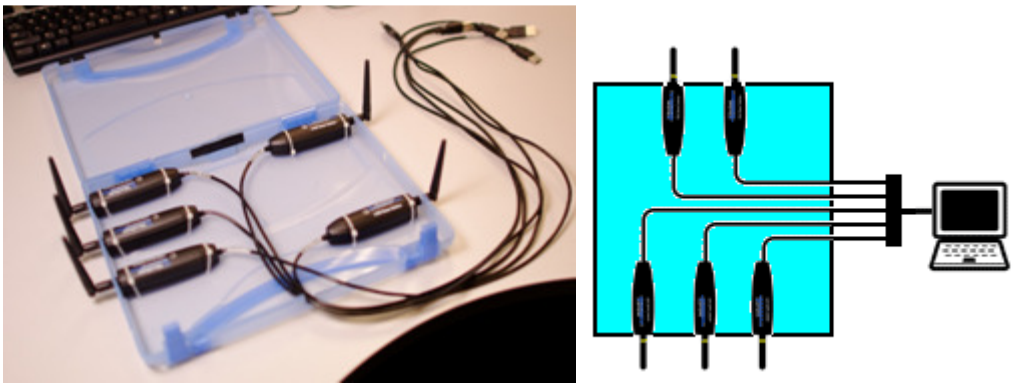

Figure 3.5 Arrangement of the USB wireless transceivers inside a carrier.

Chapter 4

SOFTWARE ARCHITECTURE

The gait monitoring system software was developed using LabVIEW 8.5 to enable bidirectional communication between the wireless inertial sensors and the workstation, to stream the measurement data in real-time, and to cater to different data processes including the local-to-global coordinate frame transformation, periodical gait evaluation, and basic 3-D animation. This software was developed incorporating an interactive and user-friendly GUI that allows novice users to conveniently acquire the measurement data and perform the necessary computations.

Based on its functionality, this software can be categorized into two different operational modes: Online periodical gait evaluation mode (Figure 4.1) and offline gait evaluation mode (Figure 4.2 and Figure 4.3). The first mode allows the user to collect real-time measurement data and to perform periodical gait evaluation while the subject is walking on a treadmill or on the ground. The software architecture of this process is depicted in Figure 4.4. Prior to each experiment, wireless communications between the workstation and wireless transceivers, and between the wireless transceivers and inertial sensors have to be initiated and verified. Once the communication links are established, inertial sensors start to measure human lower extremity motion and transmit the measurement data in form of wireless data packets to the workstation. The workstation then verifies the data packets and converts them into six different entities: X, Y and Z accelerations and X, Y and Z angular rates. These data are displayed on their respective graphs and are recorded into a measurement file (*.csv). Simultaneously, angular rates are collected for duration of five seconds and are stored in a temporary buffer. Gait evaluation is then conducted depending on the objectives of the experiments; either evaluation of subject's

gait relative to normal/healthy individual's gait (Refer to Chapter 4.5), or evaluation of subject's gait asymmetry (Refer to Chapter 4.6). In this thesis, the former evaluation is referred as the gait normality test whereas the latter assessment is referred as the gait asymmetry analysis. Regardless of the evaluation methods, the results are updated every five seconds and presented on relevant graphs so that clinicians and researchers can periodically examine subject's gait when he/she is walking on the treadmill or on the ground (Figure 4.1).

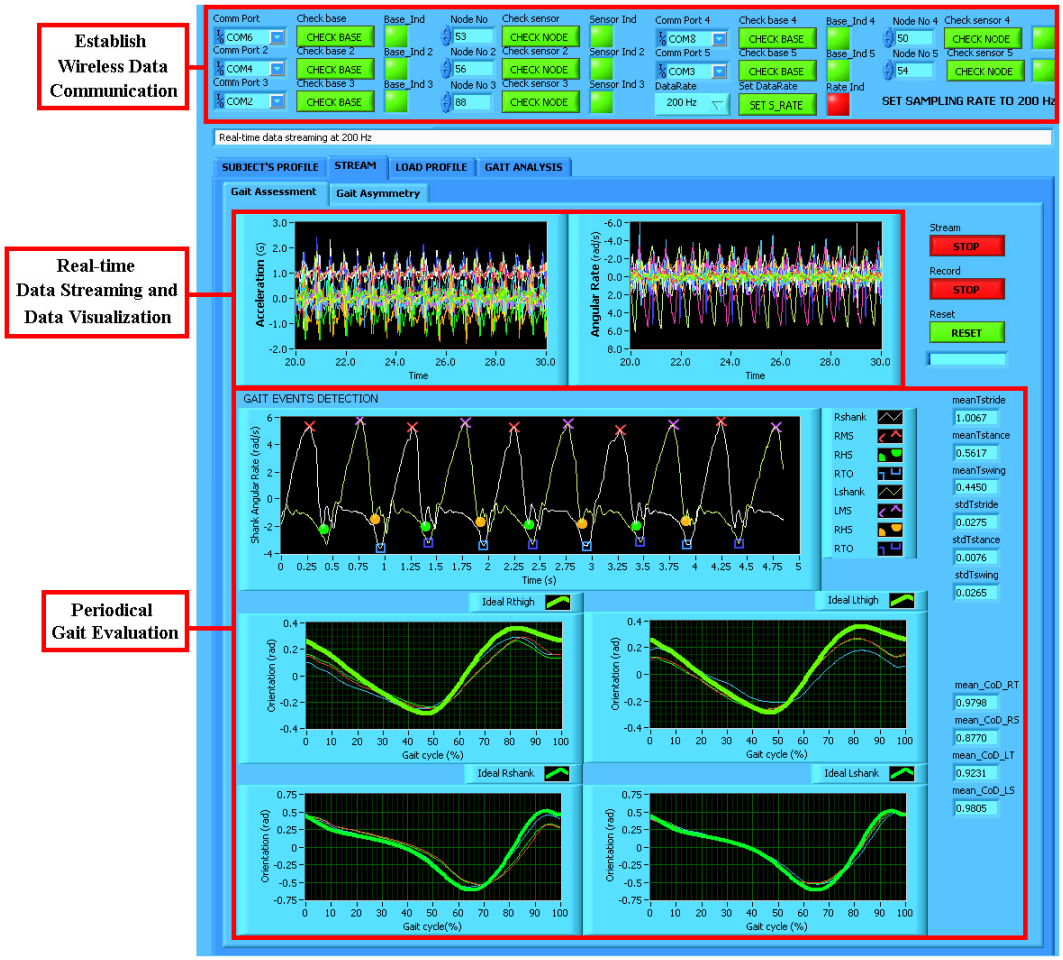

Figure 4.1 Periodical gait evaluation (Gait normality test) during real-time data streaming and data visualization.

When offline gait evaluation mode is selected, two options become available. In the first option, the user can examine subject's gait after the experiment has been conducted. In the second option, the user can upload a measurement file recorded from previous experiment to the software and perform the necessary analysis. When an experimental data are uploaded to the software, they are separated into two components and are displayed individually. First component displays subject's details and the experimental descriptions. Second component

displays 3-D acceleration and 3-D angular rate collected throughout the experiment. A Region of Interest (RoI) can then be selected. RoI is a subset of the complete experimental data which are selected for gait evaluation purposes. Similar to the online gait evaluation mode, gait normality test and gait asymmetry analysis are also available in this mode. Another gait evaluation method embedded into this mode is the estimation of gait dynamic stability. This method examines human gait stability using non-linear time series analysis (Refer to Chapter 4.7). Once the evaluation is completed, a Hyper Text Markup Language (HTML)-based report can be generated for documentation and reporting purposes (Refer to Chapter 4.11). Apart from three different gait evaluations, this mode also provides an additional feature that can animate a person's gait in a 3-D plot (Refer to Chapter 4.10). This feature is provided so that the user can view subject's walking pattern using this software instead of requesting him/her to walk in front of the user repetitively. A flowchart of the offline gait evaluation is presented in Figure 4.5.

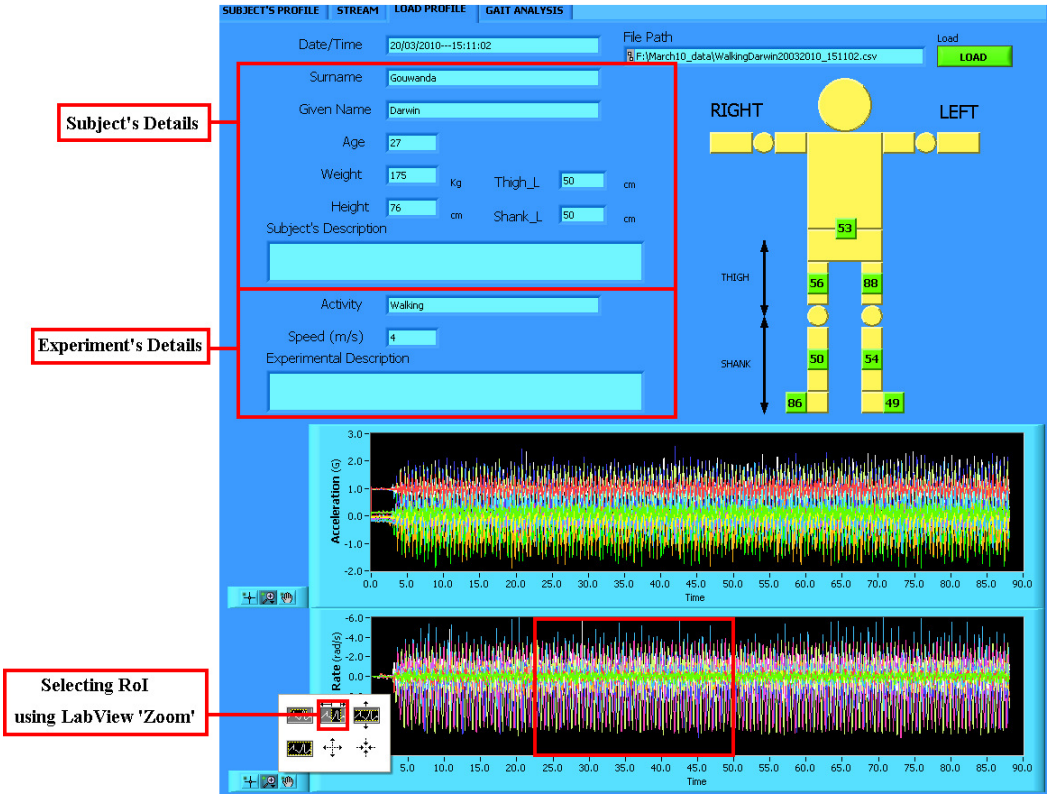

Figure 4.2 Loading a measurement file into the system software.

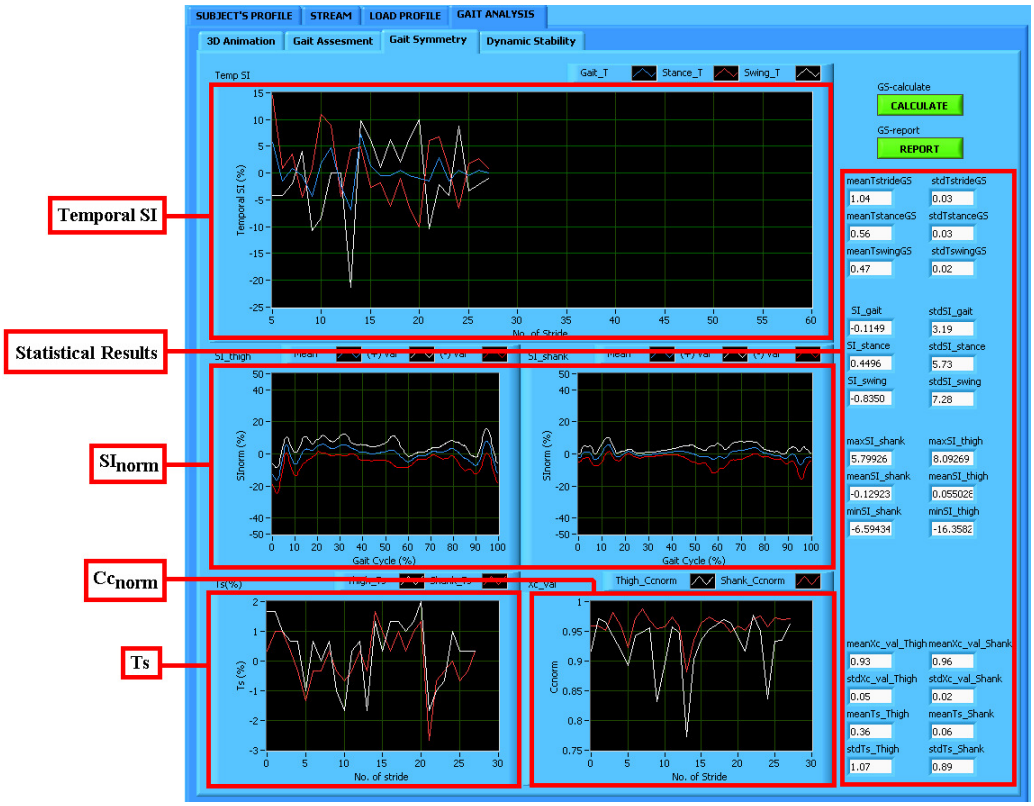

Figure 4.3 Offline gait evaluation (Gait asymmetry analysis).

In addition to the software functionalities, it is important to mention that the communication between the wireless inertial sensor and its transceiver is based on Inertia-Link data communication protocol developed by Microstrain, Inc. [106]. In this protocol, communication is established in form of data packets. Each data packet contains the start of packet, delivery flags, data type, sensor ID, command data, and checksum. Inertial-Link communication protocol will not be discussed in details because it is not the main concern of this thesis. However, other functionalities available for the user to perform real-time data streaming and periodical gait evaluations are discussed in the following sections.

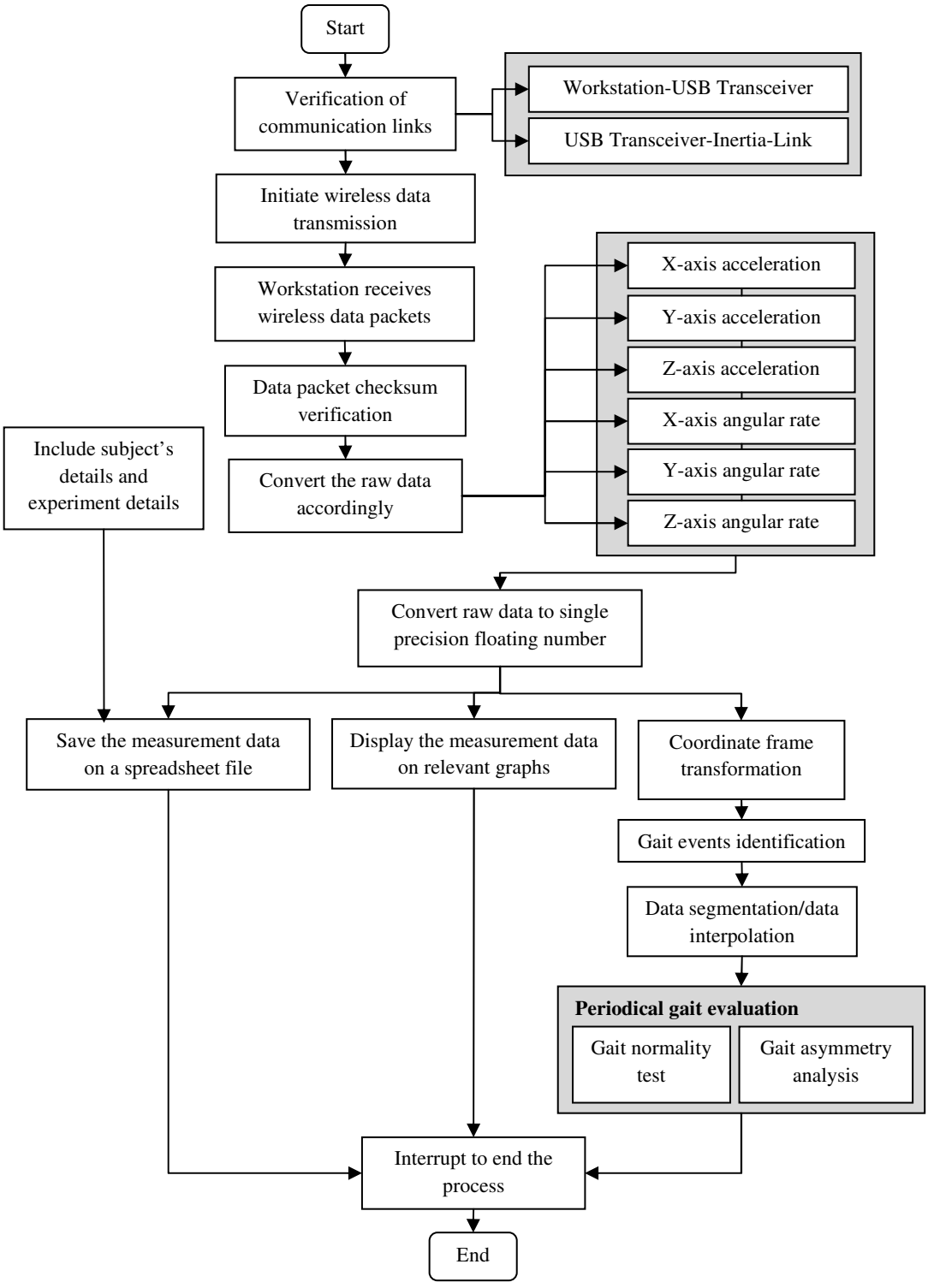

Figure 4.4 General flowchart of the real-time data streaming with periodical gait normality test and gait asymmetry analysis.

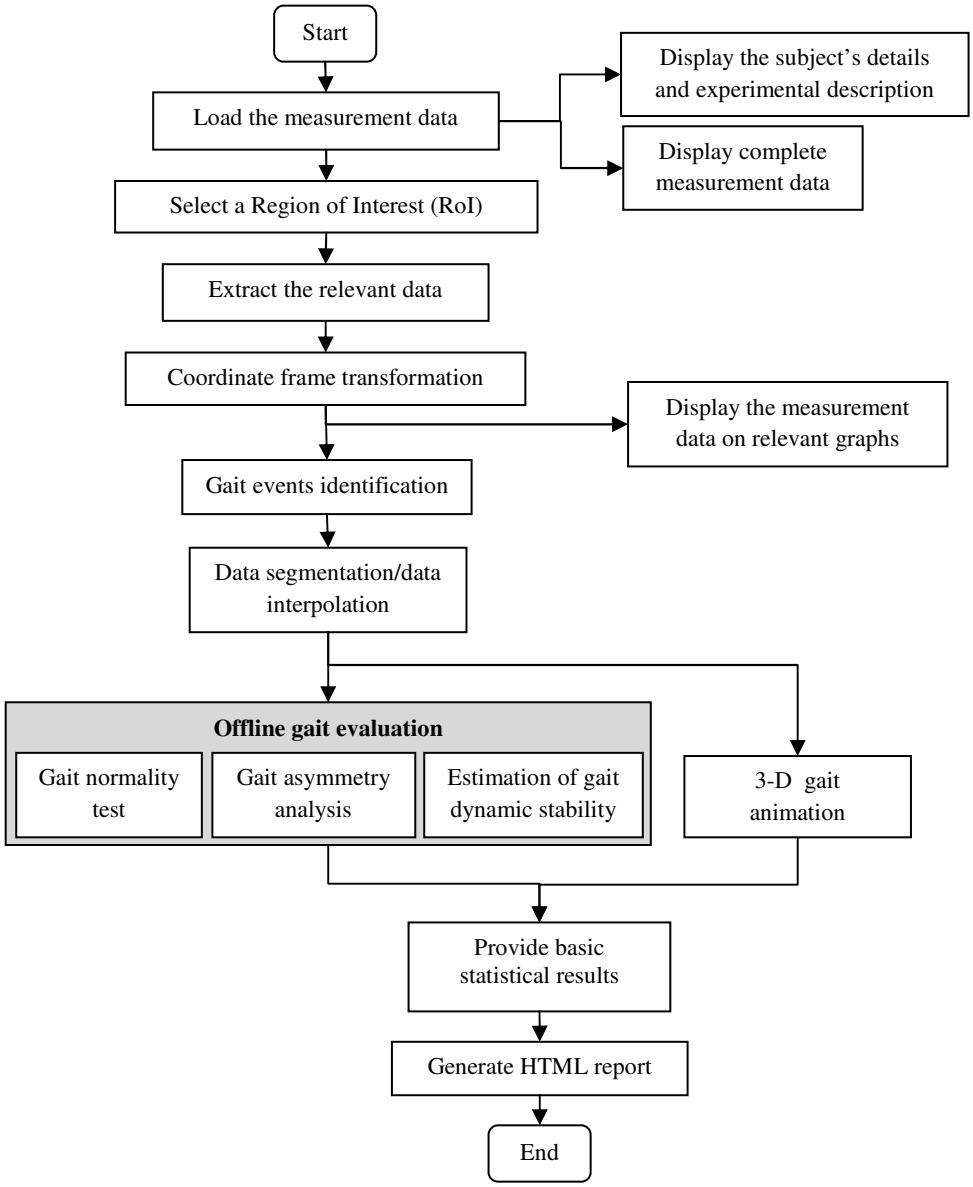

Figure 4.5 General flowchart of the offline gait evaluation.

4.1 Verification of the Communication Port

Ensuring each communication port i.e. status of the USB port for wireless data transmission, is the first step in real-time data streaming. For verification, the developed software initializes the communication port by sending a 'Ping' command, '0x01' to the wireless transceiver. As a response, wireless transceiver sends '0x01' to indicate its readiness for real-time wireless data transmission or '0x21' to indicate its difficulty in communicating with the workstation. A flow chart of this process is presented in Figure 4.6.

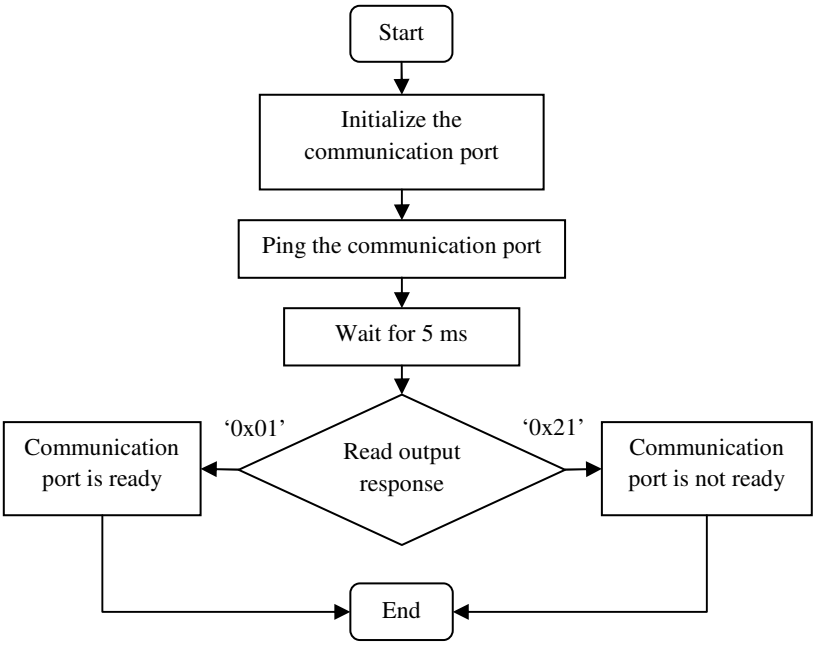

Figure 4.6 Flowchart of the communication port verification.

4.2 Verification of the Wireless Inertial-Link

This feature ensures each wireless inertial sensor communicating with its respective wireless transceiver. Similar to the previous feature, the software initializes the relevant communication ports, and sends a 'Ping' command ('0x02' and sensor unique ID) to the sensor. Wireless inertial sensor then responds to the command by sending '0x01' to indicate that the communication link between the sensor and the transceiver has been established. If the communication link is not established, the wireless transceiver generates an output response of '0x21'. A flowchart of this feature is illustrated in Figure 4.7.

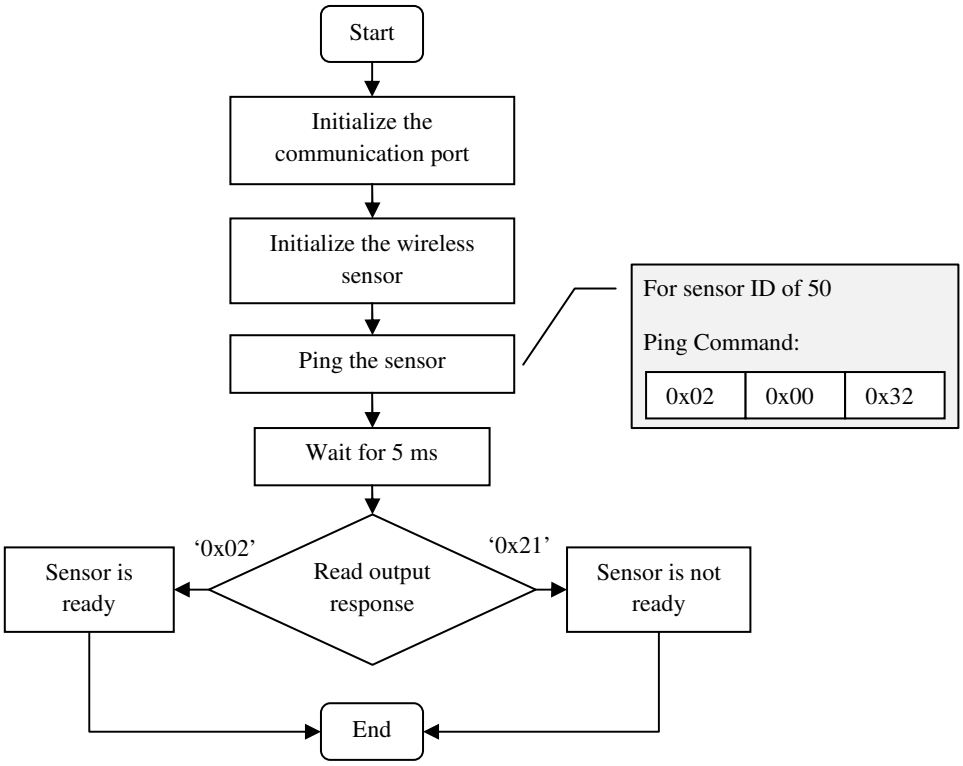

Figure 4.7 Flowchart of wireless sensor verification.

4.3 Real-time Data Streaming

The flowchart of the real-time data streaming is presented in Figure 4.8. As the first step, wireless sensors and wireless transceivers are configured to 'Continuous mode' [106]. This mode allows wireless sensors to measure acceleration and angular rate in a pre-determined sampling rate (200Hz) and continuously transmit them to the workstation. Next, the developed software signals the sensors to measure the lower extremity motions by sending a 'Stream' command. After five milliseconds, the sensors start to measure the motions and send the measurement data to the workstation in form of wireless data packets. The data packet checksum is then verified to ensure that the workstation receives the correct data packet. Data packet is discarded if the checksum is incorrect. Once the verification is completed, data packets are separated into six different components: XYZ axes accelerations and XYZ axes angular rates based on Inertia-Link data communications protocol [106]. These data packets are then converted to single precision floating number according to IEEE754 standards. Converted measurement data are displayed on relevant graphs and saved into a spreadsheet file (*.csv). Measurement data stored in a spreadsheet

file contains the format shown in Figure 4.9. These data are stored sequentially as presented in Table 4.1

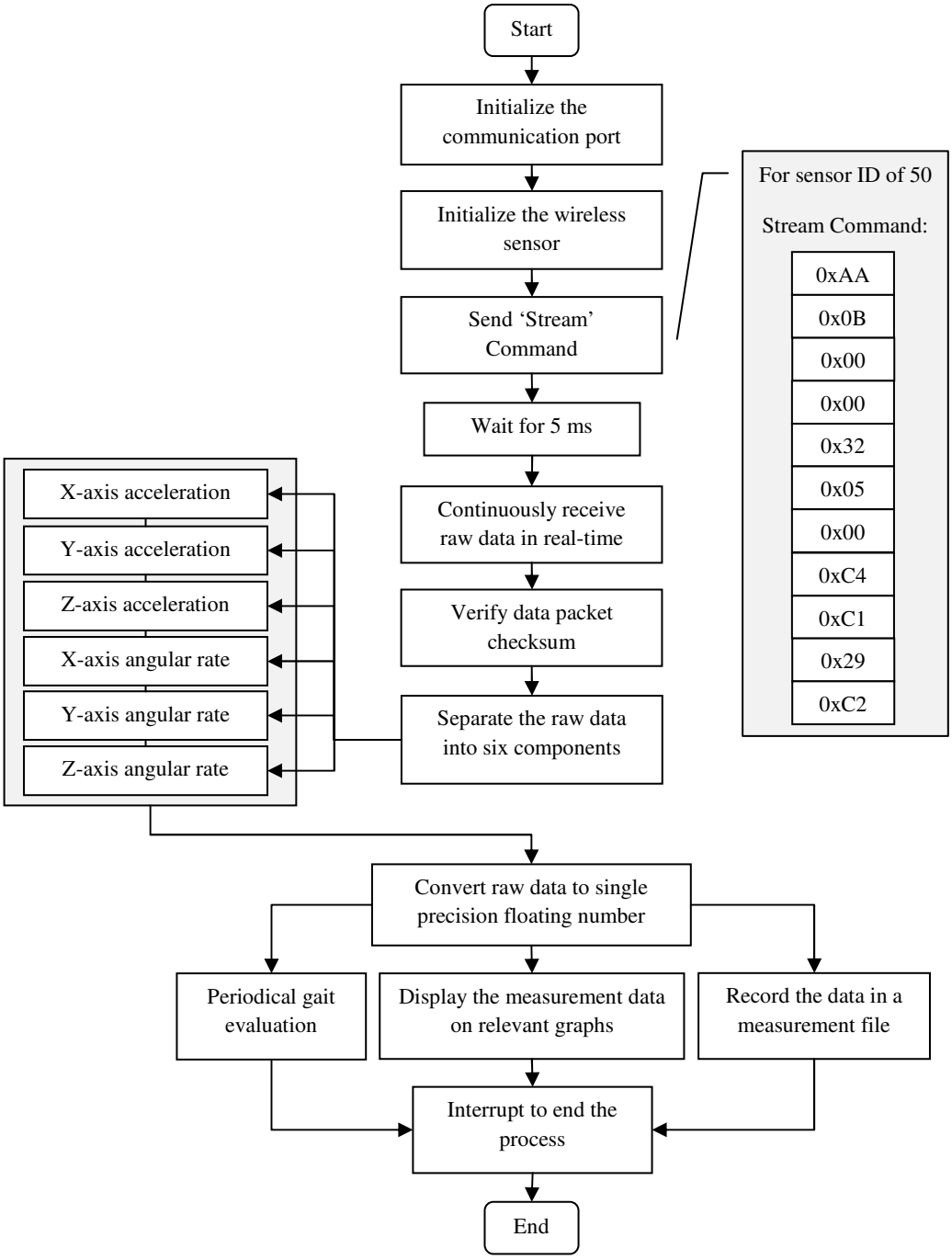

Figure 4.8 Real-time data streaming flowchart.

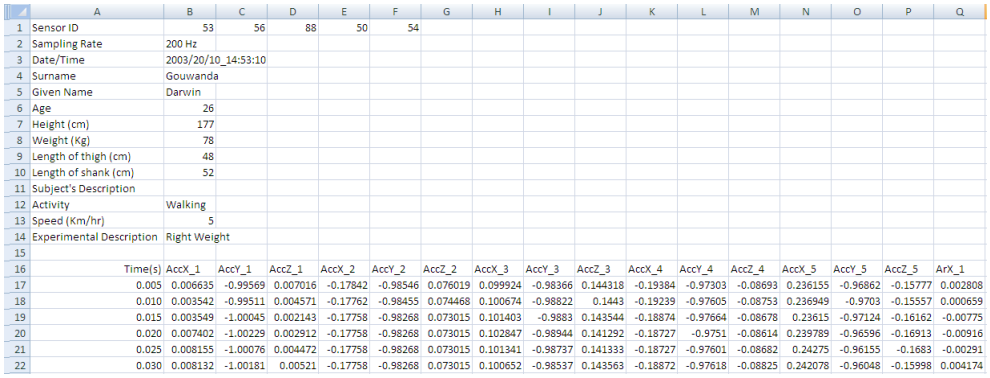

	A	B	C	D	E	F	G	H	I	J	K	L	M	N	O	P	Q
1	Sensor ID	53	56	88	50	54											
2	Sampling Rate	200 Hz															
3	Date/Time	2003/20/10_14:53:10															
4	Surname	Gouwanda															
5	Given Name	Darwin															
6	Age	26															
7	Height (cm)	177															
8	Weight (Kg)	78															
9	Length of thigh (cm)	48															
10	Length of shank (cm)	52															
11	Subject's Description																
12	Activity	Walking															
13	Speed (Km/hr)	5															
14	Experimental Description	Right Weight															
15																	
16	Time(s)	AccX_1	AccY_1	AccZ_1	AccX_2	AccY_2	AccZ_2	AccX_3	AccY_3	AccZ_3	AccX_4	AccY_4	AccZ_4	AccX_5	AccY_5	AccZ_5	ArX_1
17	0.005	0.006635	-0.99569	0.007016	-0.17842	-0.98546	0.076019	0.099924	-0.98366	0.144318	-0.19384	-0.97303	-0.08693	0.236155	-0.96862	-0.15777	0.002808
18	0.010	0.003542	-0.99511	0.004571	-0.17762	-0.98455	0.074468	0.100674	-0.98822	0.1443	-0.19239	-0.97605	-0.08753	0.236949	-0.9703	-0.15557	0.000659
19	0.015	0.003549	-1.00045	0.002143	-0.17758	-0.98268	0.073015	0.101403	-0.9883	0.143544	-0.18874	-0.97664	-0.08678	0.23615	-0.97124	-0.16162	-0.00775
20	0.020	0.007402	-1.00229	0.002912	-0.17758	-0.98268	0.073015	0.102847	-0.98944	0.141292	-0.18727	-0.9751	-0.08614	0.239789	-0.96596	-0.16913	-0.00916
21	0.025	0.008155	-1.00076	0.004472	-0.17758	-0.98268	0.073015	0.101341	-0.98737	0.141333	-0.18727	-0.97601	-0.08682	0.24275	-0.96155	-0.1683	-0.00291
22	0.030	0.008132	-1.00181	0.00521	-0.17758	-0.98268	0.073015	0.100652	-0.98537	0.143563	-0.18872	-0.97618	-0.08825	0.242078	-0.96048	-0.15998	0.004174

Figure 4.9 Measurement file format.

Table 4.1 Measurement data format in a measurement file

Body segment	**Data type**	**Column number**
	Sensor internal sampling clock	Column 1
	Acceleration	Column 2 – column 4
Abdomen	Angular rate	Column 17 – column 19
	Acceleration	Column 5 – column 7
Right thigh	Angular rate	Column 20 – column 22
	Acceleration	Column 8 – column 10
Left thigh	Angular rate	Column 23 – column 25
	Acceleration	Column 11 – column 13
Right shank	Angular rate	Column 26 – column 28
	Acceleration	Column 14 – column 16
Left shank	Angular rate	Column 29 – column 31

4.4 Gait Event Identification and Gait Data Segmentation

Gait event identification is one of the important elements in gait analysis. Gait events i.e. HS and TO are commonly used in clinical applications to examine patient's gait before/after medical treatment or surgery, to monitor rehabilitation progress of patients with pathologic gait and celebral palsy, and to aid the design and development of prosthetic limb and FES system [27],[52]-[54].

In this thesis, HMWD is implemented to identify HS, TO and MS in each gait cycle [107]. A detailed description of this method is discussed in Chapter 5.2. Determining the occurrences of these events allows estimation of T_{stride}, T_{stance}, and T_{swing}. The mathematical definitions of these parameters are described in Chapter 5.3. Identification of the gait events also allows the data to be segmented on stride-to-stride basis. Given that the segmented data have different data length depending on a person's walking speed and stride length, segmented data are linearly interpolated to 100% gait cycle. Detailed descriptions of data segmentation and data interpolation are presented in Chapter 5.4.

During online mode, this feature uses shank angular rate collected during the five seconds interval to identify the gait events. This feature is enabled automatically thus no user intervention is required. During offline mode, it uses shank angular rate lying within RoI to identify the gait events. A general overview of this feature is depicted in Figure 4.10.

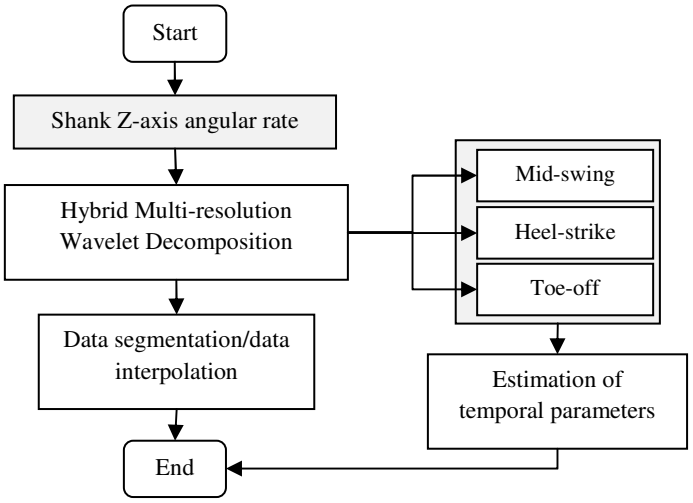

Figure 4.10 Gait event identification and data segmentation.

4.5 Gait Normality Test

Gait normality test provides qualitative and quantitative information of a person's gait. Qualitative information is represented through graphical comparisons between the orientation of a person's lower extremity and the ideal orientations established in [2]-[3], [104]. Minor and acceptable discrepancies are expected on a young and healthy individual with different anthropometric properties e.g. different height and different weight. An illustration of this comparison is shown in Figure 4.11. Green color thick line represents the

ideal orientation of human lower extremity. This line serves as the reference to visually compare the actual orientations of the lower extremity, which are represented as multicolor thinner lines (Each gait cycle is assigned to a unique color). This feature allows clinician or biomechanist to examine a person's walking condition and to determine his/her gait normality. On the other hand, quantitative information is presented as the computational results of *CoD* of each body segment, T_{stride}, T_{stance}, and T_{swing}. Definitions of these parameters are described in Chapter 5.5.

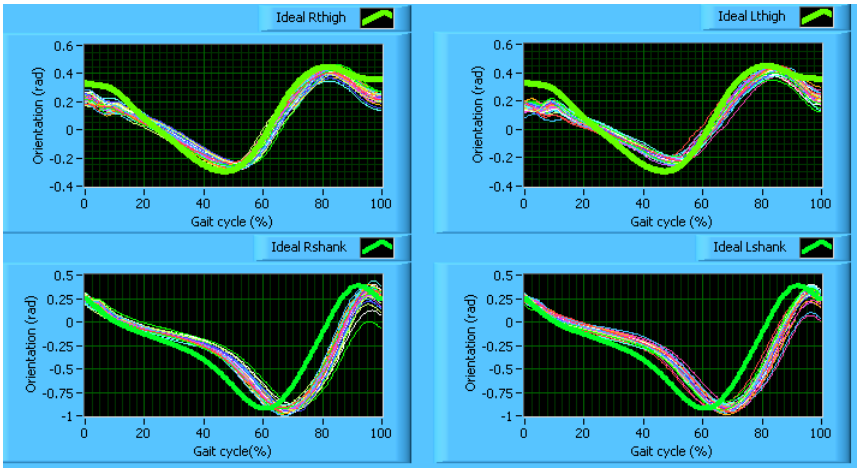

Figure 4.11 Comparison between ideal (thick green line) and actual (thin multicolor line) orientations of the lower extremity.

During the online mode, angular rates of thigh and shank are periodically stored in a temporary buffer. HMWD is then applied to shank angular rate to identify HS, TO and MS. Subsequently, temporal parameters are estimated and the angular rate of thigh and shank are segmented on stride-to-stride basis. Next, orientations of the lower extremity are estimated and compared with the ideal ones. Lastly, *CoD* is computed to quantify the similarity between them. The statistical results are presented to the user in form of the mean and standard deviation of *CoD*, T_{stride}, T_{stance}, and T_{swing}. It is important to note that this process has been optimized by minimizing the computations and processing time so that it will not affect the real-time data acquisition. A flowchart of this feature is depicted in Figure 4.12

During the offline mode, data can only be processed after the experiment has been completed or when a measurement file is uploaded to the software. The user can then use RoI to select the desired measurement data. Subsequently, the software performs similar tasks as describe earlier to provide qualitative and quantitative information of a person's gait. A flowchart of the offline gait normality test is presented in Figure 4.13.

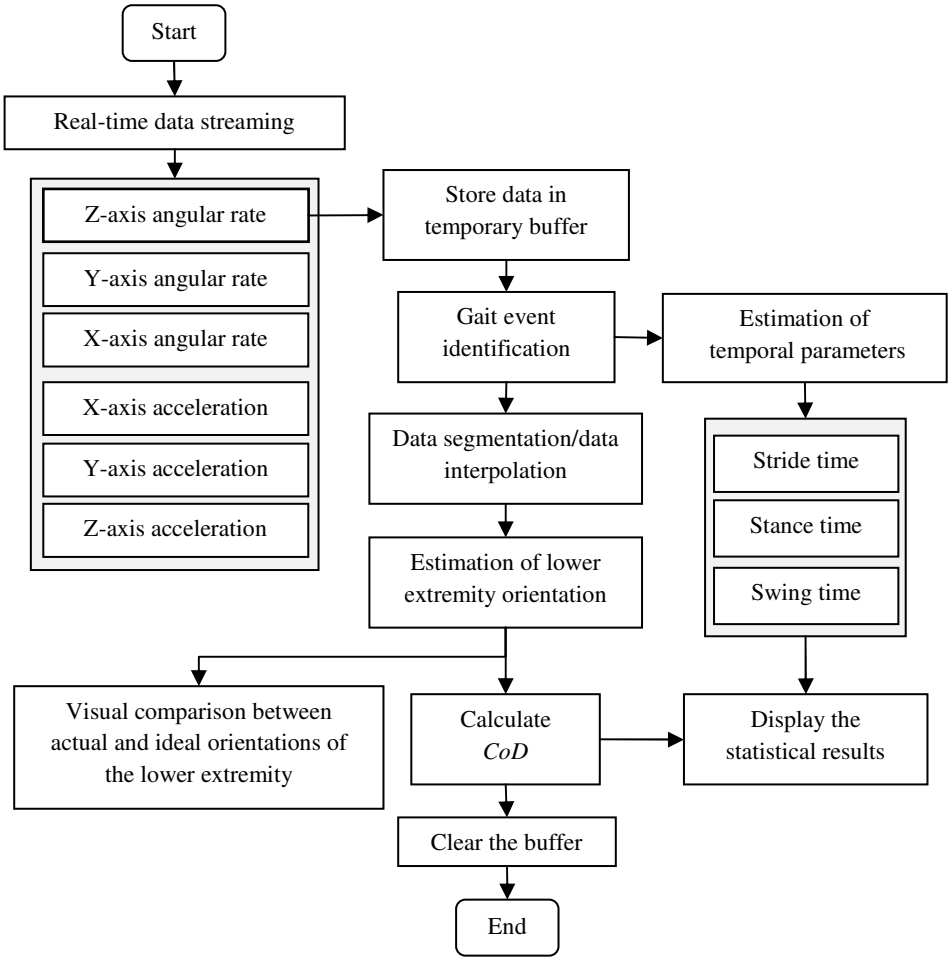

Figure 4.12 Online periodical gait normality test.

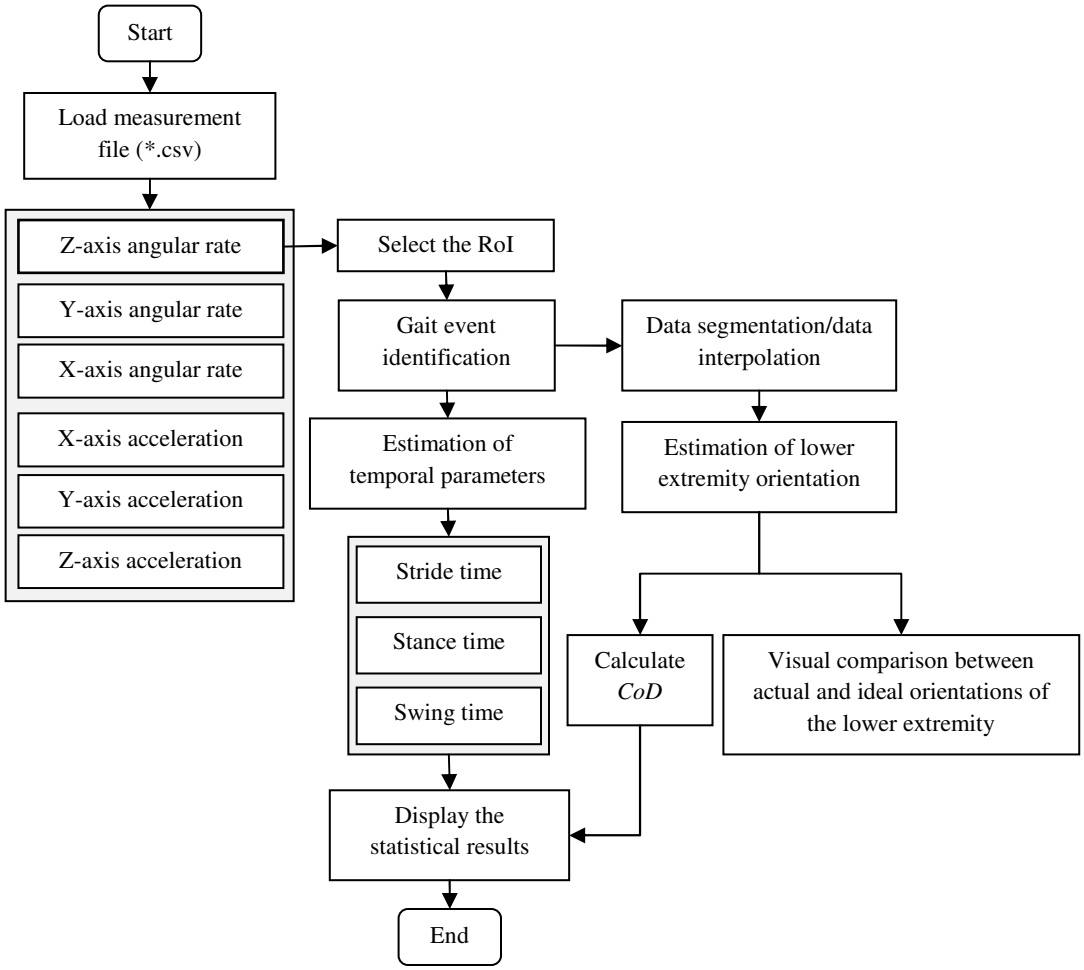

Figure 4.13 Offline gait normality test.

4.6 Gait Asymmetry Analysis

Asymmetrical gait is found in several pathological conditions [4],[8]-[9],[12]-[13] [70]-[76]. Hence, gait asymmetry is regarded as one of the important factors in examining a human walking condition and tracking a patient's rehabilitation progress. Therefore, gait asymmetry analysis is implemented as one of the prominent features of this software. The intention of this analysis is to determine the bilateral differences between the left and right lower extremity in both spatial and temporal parameters. In this thesis, Cc_{norm} is introduced a discrete measure that evaluates the signal patterns generated by left limb and right limb motions in each gait cycle. Cc_{norm} close to one implies that the gait is symmetrical. Detailed mathematical definition of Cc_{norm} is discussed in Chapter 5.7. Furthermore, SI_{norm} is also introduced to quantify the differences between left limb and right limb motions throughout the gait cycle. SI_{norm} is described in further details in Chapter 5.9. The bilateral differences between left and right limbs temporal gait parameters are computed using conventional *SI*. Detailed description of these parameters is presented in Chapter 5.8.

During online mode, shank ($\dot{\theta}_{shank}$) and thigh angular rates ($\dot{\theta}_{thigh}$) are stored in a temporary buffer. HMWD is then applied to identify HS and TO and to segment the angular rates on stride-to-stride basis. Segmented angular rates are then compared bilaterally to obtain Cc_{norm}, *Ts*, and SI_{norm} and display them on their respective graphs. The occurrences of heel-strike and toe-off are also used to determine the temporal differences between left limb and right limb, particularly the differences in duration of stride (SI_{stride}), stance phase (SI_{stance}) and swing phase (SI_{swing}). In order to ease data interpretations, mean and standard deviation of the SI_{stride}, SI_{stance}, and SI_{swing} and SI_{norm} are presented. A flow chart of the online gait asymmetry analysis is presented in Figure 4.14.

During the offline mode, measurement file must be preloaded into the software. A RoI can then be selected to exclude redundant data. Subsequently, the software identifies HS and segments the measurement data on stride-to-stride basis. Segmented angular rate of thigh and shank are then compared bilaterally to obtain the Cc_{norm}, *Ts* and SI_{norm} and display them on their respective graphs. At the same time, SI_{stride}, SI_{stance}, SI_{swing} are being calculated too. Similarly, statistical results such as mean and standard deviation of Cc_{norm}, and *Ts*, and mean and variation of SI_{norm} are presented to ease data interpretation. The flowchart of the offline gait asymmetry analysis is presented in Figure 4.15

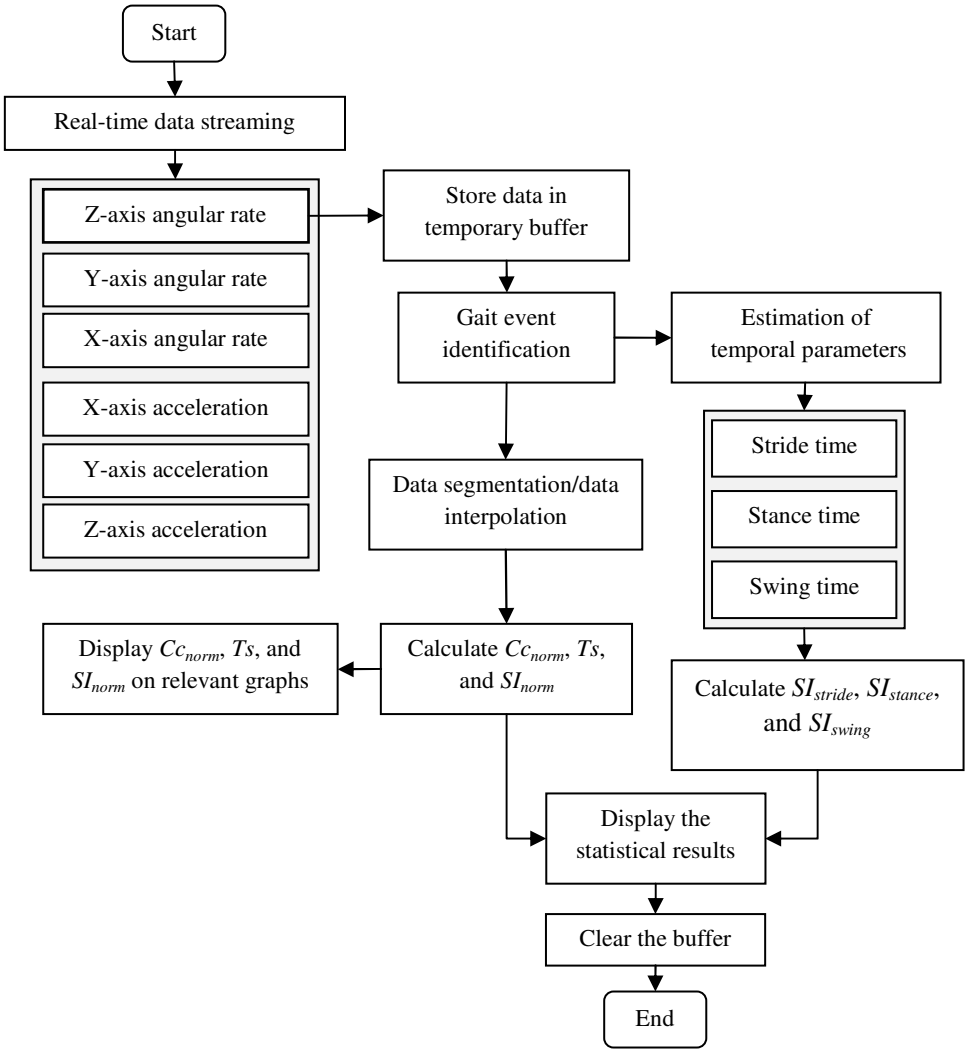

Figure 4.14 Online gait asymmetry analysis.

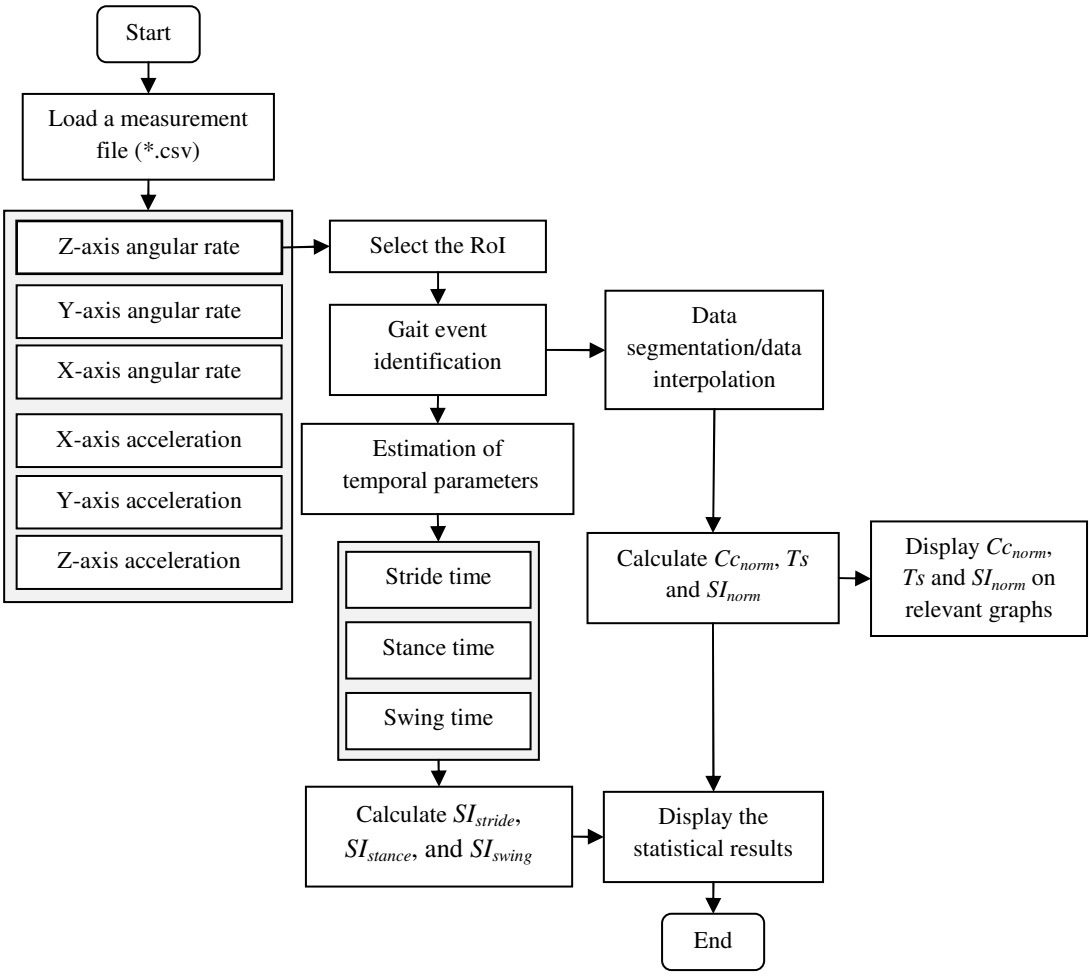

Figure 4.15 Offline gait asymmetry.

4.7 Estimation of Gait Dynamic Stability

Gait stability is also a key feature of gait analysis. Hence, an algorithm that quantifies human walking stability is implemented as one of the main components of this system. This system uses an algorithm developed by Rosenstein et al. [95] to estimate the λ* from discrete time-series measurement data. In gait analysis, λ* is a measurement that indicates how human body responds to kinematic perturbations (stride-to-stride variability) and maintains body balance during walking [85],[91]-[94],[97]-[102]. Instead of using kinematic parameters obtained from optical motion capture system, this system uses angular rates of the thigh and shank as the key parameters.

This system employs tools available in TISEAN (Time Series Analysis) package [96],[108] to perform various non-linear time series analysis i.e. Mutual Information (MI), False Nearest Neighbours (FNN) and estimation of λ*. It is important to highlight that MI and FNN are processes used to obtain the optimum time delay and embedding dimensions needed to reconstruct the state space representation of the kinematic variable and to estimate λ*. Preliminary study conducted in this thesis suggested that the time delay of 14 data points and embedding dimensions of 9 were the optimum parameters. These parameters are only valid for male subject with age: 25.3 ± 1.7 years old, height: 173.9 ± 4.8 cm and weight: 70.5 ± 9.3 kg.

There are two different measures that are used to represent a person's gait stability: λ_S^* and $\lambda_L^*.\lambda_S^*$ corresponds to the ability of human neuromuscular locomotor system in maintain short-term gait stability whereas λ_L^* corresponds to ability of human neuromuscular locomotor system in maintaining long-term stability. Detailed description of FNN, MI and the estimation of λ_S^* and λ_L^* are presented in Chapter 5.10. A flowchart of the estimation of λ* is depicted in Figure 4.16.

Due to large computational data and extensive computations involved in estimating λ*, this feature is only available in the offline mode. There are several data preprocesses are included in this feature. One of the processes is the data segmentation. HMWD is initially applied to the shank angular rate [107]. This method identifies the occurrences of HS and TO. Since the first 30 continuous strides are needed to estimate λ* [85], only the measurement data lying between 2nd HS and 32nd HS are considered (As a standard in gait analysis, first gait cycle is neglected).

Given that the time to complete one gait cycle varies according to the walking velocity while the sampling rate is fixed, segmented angular rate of thigh and shank may have different data length. Therefore, measurement data of the first 30 strides are linearly interpolated into 3000 data points. This approach preserves the stride-to-stride temporal variation, which is one of the important elements of Lyapunov stability analysis [85]. It also normalizes the measurement data such that the number of data points is similar for every experiment.

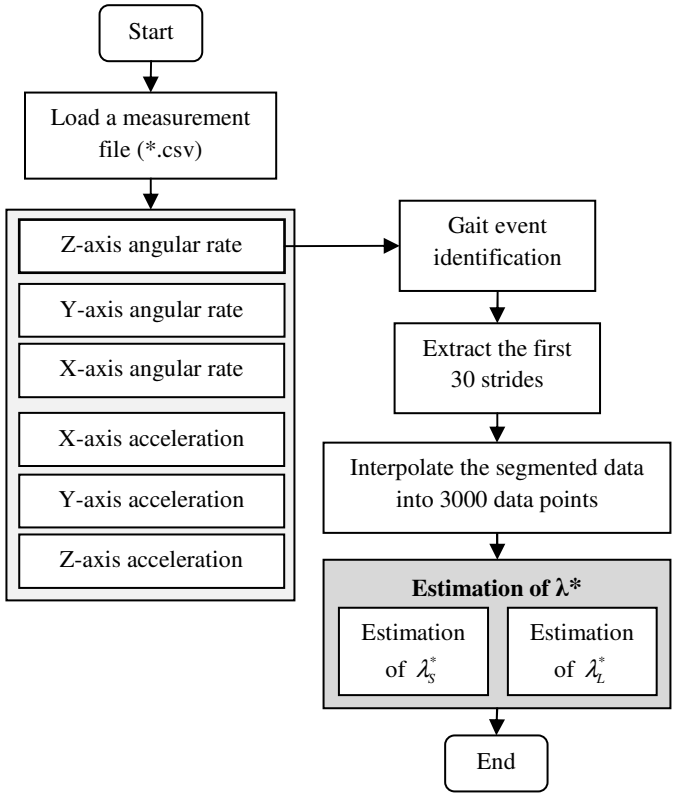

Figure 4.16 Offline estimation of the maximum Lyapunov exponent.

4.8 Sensor Reset

The main function of 'Sensor reset' is to disable real-time data streaming from the wireless inertial sensor to the workstation. As the first step, the communication port and wireless sensor are reinitialized and reconfigured. Afterward, a reset command is sent to all wireless sensors via its respective transceivers. A flowchart of this feature is presented in Figure 4.17.

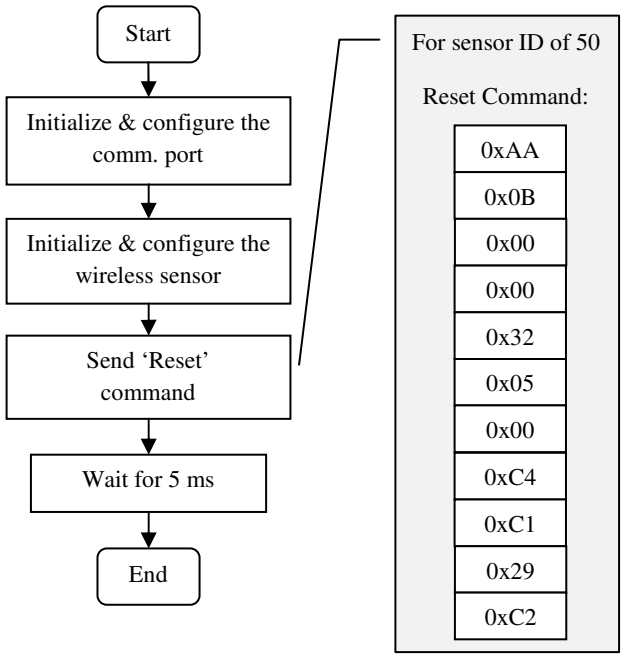

Figure 4.17 A flowchart of sensor reset function.

4.9 Uploading a Measurement File

Measurement files collected from the previous experiments can be uploaded to the software using this feature. It uploads the measurement data, subject's personal details i.e. name, height, weight and age, and the experimental descriptions. It then displays them on the software GUI (Figure 4.2). This feature comes with RoI, which allows the user to select the desired measurement data and to eliminate redundant data that should not be included in gait analysis. Using RoI, user can also exclude the first and last gait cycles as a standard procedure.

4.10 3-D Animation of the Human Lower Extremity

This tool provides a 3-D visualization of a person's walking pattern. Experienced users can use this feature to observe a person's gait and to determine his/her gait normality. In this thesis, a simple human stick figure is constructed in 3-D space to reduce unnecessary computations and to minimize processing time so that it can be used in a general purpose workstation. Computational details of this feature are presented in Chapter 5.6.

For better visualization, each body segment is assigned to different color. The upper body is black; the right thigh is red; right shank is blue; left thigh is green and left shank is yellow. An illustration of the 3-D animation of the lower extremity is shown in Figure 4.18. This feature is only available offline. The experimental data collected from the previous session has to be preloaded into the software to animate the 3-D walking motion.

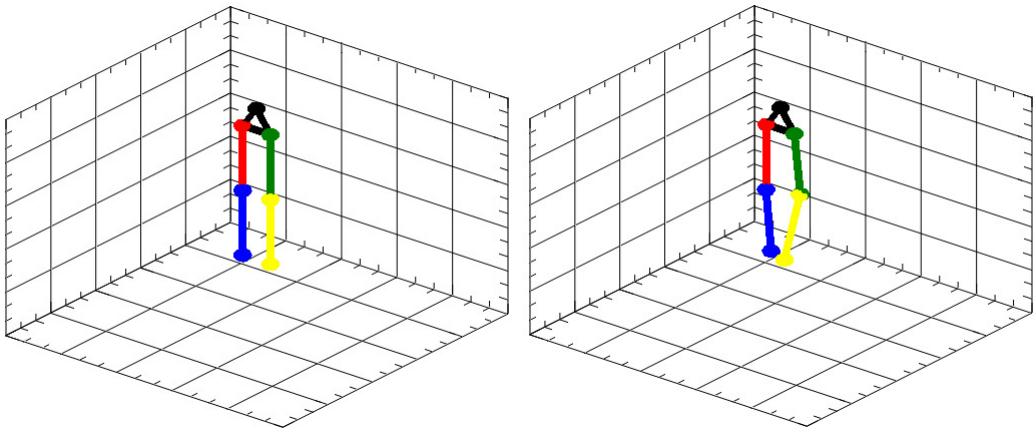

Figure 4.18 3-D animation of the lower extremity during walking.

4.11 Report Generation

Reporting a person's gait evaluation result is important in rehabilitations and clinical settings. It provides biomechanists, researchers and/or clinicians with a document to present their findings to their patients and for further analysis. This document is also widely stored as a part of patients' medical history. For this reason, this system implements a feature that can produce a HTML-based report. HTML report is selected because it can be viewed by any conventional web browser. More importantly, the file size is relatively small in spite of storing several images and tables. A sample of the experimental results presented in a HTML report is depicted in Figure 4.19.

************Report on GAIT NORMALITY TEST ************

==========

Subject's Personal Details :

Date/Time	20/03/2010---15:11:02
Surname	Gouwanda
Given Name	Darwin
Age	27
Weight	175
Height	76
Additional Description	
Activity	Walking
Walking Speed	4
Experimental Descripiton	

Right Shank Angular Rate Graph

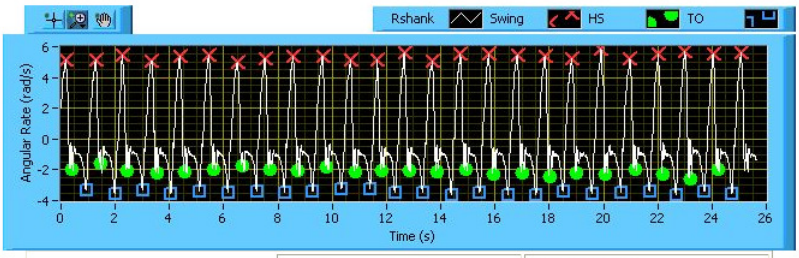

	Mean	Standard dev
Stride time	1.036304	0.030008
Stance time	0.564130	0.025165
Swing time	0.472174	0.024018

Figure 4.19 A sample of HTML report on gait normality test results.

Report generated by this feature is different depending on the gait evaluation method selected by the user. However, subject's details and the experimental descriptions are retained in the report. Detailed experimental results available in this report are presented in Table 4.2.

Table 4.2 HTML-based report content

Gait normality test	Gait asymmetry analysis	Gait dynamic stability
❖ Mean and standard deviation of T_{stride}, T_{stance} and T_{swing} ❖ Estimated orientation of thigh (θ_{thigh}) in each gait cycle ❖ Estimated orientation of shank (θ_{shank}) in each gait cycle ❖ Mean and standard deviation of *CoD*	❖ Mean and standard deviation of T_{stride}, T_{stance} and T_{swing} ❖ Mean and standard deviation of SI_{stride}, SI_{stance} and SI_{swing} ❖ Mean and variation of SI_{norm} ❖ Mean and standard deviation of Cc_{norm} and *Ts*	❖ Mean and standard deviation of λ_S^* of thigh and shank ❖ Mean and standard deviation of λ_L^* of thigh and shank

Chapter 5

COMPUTATIONAL METHODS

Computational methods were implemented into the wireless gait monitoring system to obtain the relevant parameters that represent a person's walking condition and to ease the data interpretation. Among them are the computations of *CoD,* Cc_{norm}, SI_{norm}, SI_{stride}, SI_{stance}, and SI_{swing}. The computational methods embedded into this system are discussed in the following sections.

5.1 Coordinate Frame Transformation

International Society of Biomechanics (ISB) proposed a general reporting standard for joint kinematics in [109]-[110]. This standard makes the application and interpretation of biomechanical findings easier and more welcoming to various research groups, biomechanists, physicians, physical therapists, and other related interest groups. It also allows direct comparisons among the literatures that had been published so far.

In this thesis, ISB coordinate system is regarded as the global coordinate system {G} while sensor coordinate system is regarded as the local coordinate system {S}. A graphical representation of {G} and {S} are illustrated in Figure 5.1. In order to define the sensor local coordinate frame {S} relative to the global coordinate frame {G}, ${}^{G}P_{Sorg}$, a rotation matrix, ${}^{G}_{S}R$ has to be defined as follows in (1).

$$\{S\} = \{ {}^{G}_{S}R, {}^{G}P_{Sorg} \} \tag{1}$$

Since each inertial sensor has its measuring axes pointing to different directions, a rotation matrix has to be identified. Details of these rotation matrices are described in following sub-sections.

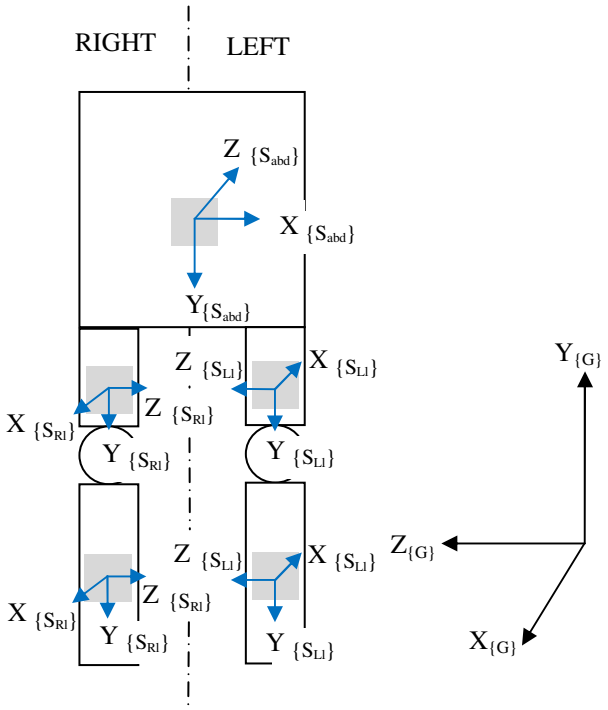

Figure 5.1 An illustration of the sensor local coordinate frame {S} and global coordinate frame {G}.

5.1.1 Upper Body

To map the sensor coordinate frame which is placed on the abdomen $\{S_{abd}\}$ to global coordinate frame {G}, $\{S_{abd}\}$ is rotated twice. The first rotation is performed along the X-axis with a magnitude of π. The second rotation is performed along the Y-axis with a magnitude of π/2. The rotation matrix, ${}^{G}_{Abd}R$ with respect to the {G} can be defined as (2) and (3):

$$ {}^{G}_{Abd}R = R_{Y(\pi/2)} R_{X(\pi)} \tag{2} $$

$$ {}^{G}_{Abd}R = \begin{bmatrix} \cos(\pi/2) & 0 & \sin(\pi/2) \\ 0 & 1 & 0 \\ -\sin(\pi/2) & 0 & \cos(\pi/2) \end{bmatrix} \begin{bmatrix} 1 & 0 & 0 \\ 0 & \cos(\pi) & -\sin(\pi) \\ 0 & \sin(\pi) & \cos(\pi) \end{bmatrix} = \begin{bmatrix} 0 & 0 & -1 \\ 0 & -1 & 0 \\ -1 & 0 & 0 \end{bmatrix} \tag{3} $$

5.1.2 Right Limb

Since sensors placed on right thigh and right shank have measuring axes not aligned to {G}, a rotation matrix, ${}^{G}_{Rl}R$ is required to align $\{S_{Rl}\}$ to {G}. As illustrated in Figure 5.1, $\{S_{Rl}\}$ has to be rotated along X-axis with a magnitude of π, thus ${}^{G}_{Rl}R$ can be defined as (4) and (5)

$$ {}^{G}_{Rl}R = R_{X(\pi)} \tag{4} $$

$$ {}^{G}_{Rl}R = \begin{bmatrix} 1 & 0 & 0 \\ 0 & \cos(\pi) & -\sin(\pi) \\ 0 & \sin(\pi) & \cos(\pi) \end{bmatrix} = \begin{bmatrix} 1 & 0 & 0 \\ 0 & -1 & 0 \\ 0 & 0 & -1 \end{bmatrix} \tag{5} $$

5.1.3 Left Limb

Similar to the right limb, sensors placed on the left limb do not have measuring axes aligned to {G}, thus a rotation matrix, ${}^{G}_{Ll}R$ is required to rotate the $\{S_{Ll}\}$ along the Y-axis with a magnitude of π. ${}^{G}_{Ll}R$ is expressed in (6) and (7)

$$ {}^{G}_{Ll}R = R_{Y(\pi)} \tag{6} $$

$$ {}^{G}_{Ll}R = \begin{bmatrix} \cos(\pi) & 0 & \sin(\pi) \\ 0 & 1 & 0 \\ -\sin(\pi) & 0 & \cos(\pi) \end{bmatrix} = \begin{bmatrix} 0 & 0 & 1 \\ 0 & 1 & 0 \\ -1 & 0 & 0 \end{bmatrix} \tag{7} $$

5.2 Hybrid Multi-resolution Wavelet Decomposition Method (HMWD)

The application of wavelet transform in science and engineering began in the early 1990s with rapid growth in the number of researchers turning their attention to wavelet transform analysis. Since then, wavelet transforms are widely used in various fields, ranging from engineering, medicine, finance, geophysics to astronomy [111]. In this thesis, wavelet transform is coupled with peak-valley detection algorithm to identify HS and TO from $\dot{\theta}_{shank}$ .This method is called Hybrid Multi-resolution Wavelet Decomposition method (HMWD).

HMWD is one of the significant outcomes of this thesis. It is a combination of the Multi-resolution Wavelet Decomposition method (MWD) proposed by [112] and the peak-valley detection algorithm (PD+VD). Alternatively, HMWD can be expressed as follows in (8).

$$HMWD = \{MWD, PD+VD\} \tag{8}$$

MWD is a method that uses wavelet transform to split the original signal (S_o) to two different components: the low frequency component called approximation signal (A_1) and high frequency component called detail signal (D_1). This method can be repeated n times with each successive approximation signal being decomposed to produce the next approximation signal (A_n) and detail signal (D_n), as described in Figure 5.2. Mathematically, decomposition of S_o is expressed as follows in (9).

$$S_o = A_n + D_n + D_{n-1} + \ldots + D_1 \tag{9}$$

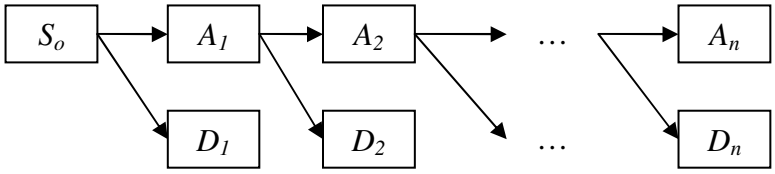

Figure 5.2 Multi-resolution wavelet decomposition method.

PD+VD differentiates the MWD output signal twice to produce a signal that has sharp spikes. In subsequent step, PD+VD places positive spikes and negative spikes into two separate arrays. It then performs local search to identify peaks and valleys that corresponds to HS, TO and MS

In this thesis, HMWD is applied to the right ($\dot{\theta}_{Rshank}$) and left shank angular rate ($\dot{\theta}_{Lshank}$). The main reason is that $\dot{\theta}_{shank}$ contains the three significant attributes corresponding to HS, TO and MS [21],[40],[51]. These attributes are depicted in Figure 5.3. For clarity, only $\dot{\theta}_{Rshank}$ is discussed in this section and it is regarded as $\dot{\theta}_{shank}$. Since human gait is a periodical movement, this pattern occurs repetitively. When a portion of $\dot{\theta}_{shank}$ is extracted, two valleys and two peaks can be found. The peaks correspond to MS whereas the valleys correspond to HS and TO respectively.

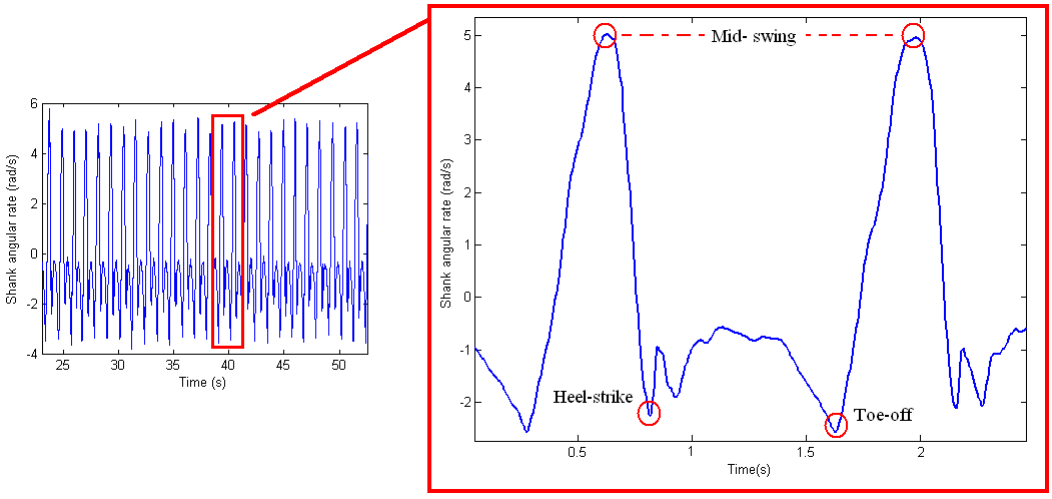

Figure 5.3 Shank angular rate with heel-strike, toe-off and mid-swing events.

Several assumptions are made to identify HS, TO and MS. These assumptions are:

- HS and TO occur between two successive MS.
- $\dot{\theta}_{shank}$ during HS and TO are less than 0 rad/s.
- $\dot{\theta}_{shank}$ during MS is greater than 0 rad/s.

To extract its significant attributes, $\dot{\theta}_{shank}$ is decomposed twice using symmlet2 wavelet transform. As a result, this process produces three main components: 2nd level approximation signal ($A_{\dot{\theta}2}$), 2nd level detail signal ($D_{\dot{\theta}2}$) and 1st level detail signal ($D_{\dot{\theta}1}$). From these components, only $A_{\dot{\theta}2}$ is used to identify HS, TO and MS while the other components, $D_{\dot{\theta}2}$ and $D_{\dot{\theta}1}$ are discarded. In the subsequent step, second derivatives of $A_{\dot{\theta}2}$ are calculated using finite difference equations to produce a series of positive and negative spikes as shown in Figure 5.4 . $A_{\dot{\theta}2}$ first derivative, $A'_{\dot{\theta}2}$ and second derivative, $A''_{\dot{\theta}2}$ are defined as (10) and (11) respectively, where Δt is 0.005s for sampling rate of 200 Hz

$$A'_{\dot{\theta}2(t)} = \frac{A_{\dot{\theta}2(t)} - A_{\dot{\theta}2(t-1)}}{\Delta t} \qquad (10)$$

$$A''_{\dot{\theta}2(t)} = \frac{A'_{\dot{\theta}2(t)} - A'_{\dot{\theta}2(t-1)}}{\Delta t} \qquad (11)$$

A group of positive spikes and negative spikes that are close to each other are separated and stored in different arrays. Subsequently, PD is conducted as a form of local search in array containing negative spikes ($A''_{\dot{\theta}2} < 0$). This search identifies the occurrence of MS (T_{MS}) in each gait cycle *m*, assuming that $\dot{\theta}_{shank}$ during MS, $\dot{\theta}_{shank\_MS}$, is greater than 0 rad/s. PD as a function of $A''_{\dot{\theta}2}$ and $\dot{\theta}_{shank\_MS}$ can be expressed as (12)

$$T_{MS(j)} = PD(A''_{\dot{\theta}2}, \dot{\theta}_{shank\_MS}) \tag{12}$$

Afterward, two successive mid-swing events, $T_{MS(m)}$ and $T_{MS(m+1)}$ are set as the main reference to identify the occurrences of HS (T_{HS}) and TO (T_{TO}). VD is conducted as a form of local search in array containing positive spikes ($A''_{\dot{\theta}2} > 0$). This search produces a series of indicators which shows the potential T_{HS} and T_{TO} in $\dot{\theta}_{Shank}$. Assuming that $\dot{\theta}_{shank}$ during HS ($\dot{\theta}_{shank\_HS}$) and during TO ($\dot{\theta}_{shank\_TO}$) are less than 0 rad/s and they happen in between $T_{MS(m)}$ and $T_{MS(m+1)}$, T_{HS} and T_{TO} to be identified as the first and last indicators respectively (Figure 5.4). In general, *VD* can be expressed as a function of T_{MS}, $A''_{\dot{\theta}2}$, $\dot{\theta}_{shank\_HS}$ and $\dot{\theta}_{shank\_TO}$ as indicated in (13). A flowchart is presented in Figure 5.5 to further enhance the understanding of this method.

$$T_{HS(j),TO(j)} = VD(A''_{\dot{\theta}2}, T_{MS(j)}, T_{MS(j+1)}, \dot{\theta}_{shank\_HS}, \dot{\theta}_{shank\_TO}) \tag{13}$$

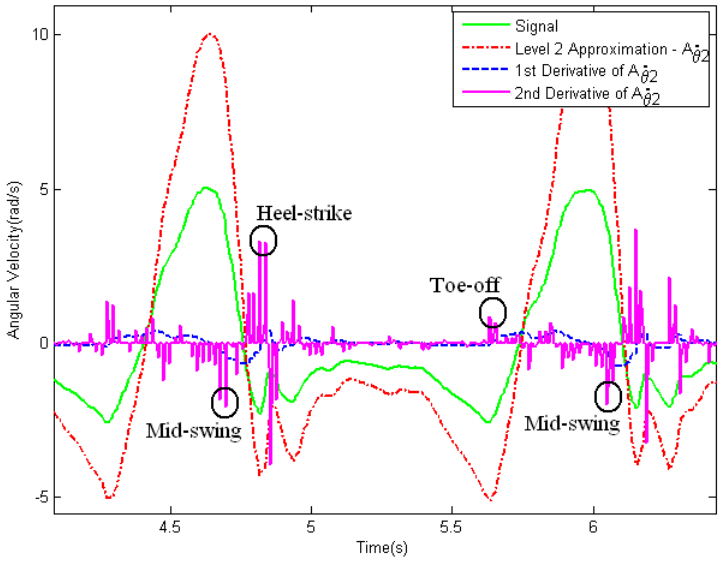

Figure 5.4 Identified mid-swing, heel-strike and toe-off in $A''_{\dot{\theta}2}$ ($A''_{\dot{\theta}2}$ is multiplied by 10 to improve its visibility).

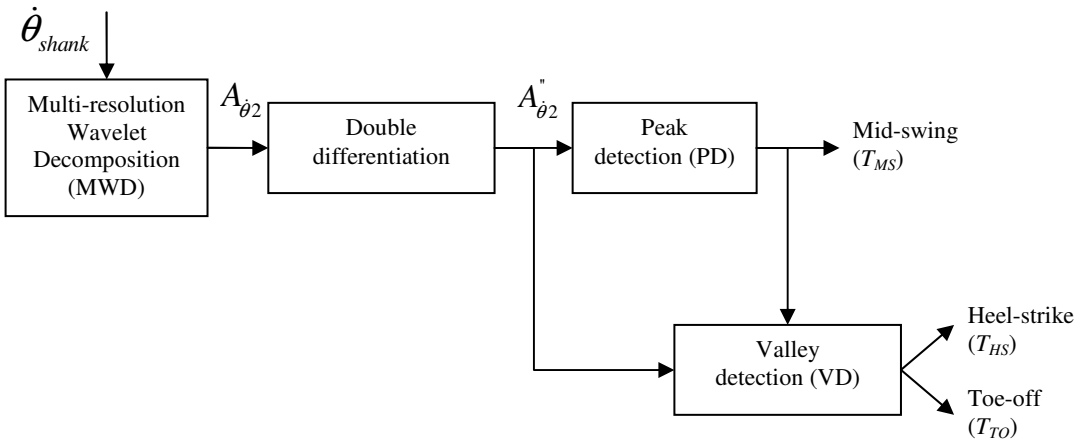

Figure 5.5 A flowchart of Hybrid Multi-resolution Wavelet Decomposition method (HMWD).

5.3 Estimation of Temporal Gait Parameters

Identifying T_{HS} and T_{TO} allows the estimation of temporal gait parameters i.e. T_{stride}, T_{stance}, and T_{swing}. These parameters can be calculated as follow in (14) – (16) for each gait cycle m.

$$T_{stride(m)} = T_{HS(m+1)} - T_{HS(m)} \tag{14}$$

$$T_{swing(m)} = T_{HS(m+1)} - T_{TO(m)} \tag{15}$$

$$T_{stance(m)} = T_{stride(m)} - T_{swing(m)} \tag{16}$$

In addition to these parameters, ratio of T_{stance} and T_{swing} over T_{stride} are also important because they provide direct comparison with previously published results. These ratios are calculated as follow in (17) and (18)

$$R_{stance(m)} = \frac{T_{stance(m)}}{T_{stride(m)}} \tag{17}$$

$$R_{swing(m)} = \frac{T_{swing(m)}}{T_{stride(m)}} \tag{18}$$

5.4 Gait Data Segmentation and Data Interpolation

Apart from temporal gait parameters, identification of T_{HS} in gait cycle allows the data to be segmented on stride-to-stride basis: $T_{HS(m)}$ to $T_{HS(m+1)}$. Data segmentation is important as it allows the spatial parameter i.e. the orientation of the lower extremity to be compared with previously published results in [2],[3] and [104]. Since each gait cycle possesses different time duration depending on the stride length and walking speed, segmented data may have different data length. Therefore, to ensure each of them has similar data length and to eliminate signal aliasing, angular rate of each body segment is linearly interpolated to N = 300 data points, which correspond to 100% gait cycle. Thus, angular rates measured from right thigh ($\dot{\theta}_{Rthigh}$), right shank ($\dot{\theta}_{Rshank}$), and left thigh ($\dot{\theta}_{Lthigh}$), and left shank ($\dot{\theta}_{Lshank}$) possess the following forms:

$$\dot{\theta}_{Rthigh} = \dot{\theta}_{Rthigh(1)}, \dot{\theta}_{Rthigh(2)}, \dot{\theta}_{Rthigh(3)}, ..., \dot{\theta}_{Rthigh(n)}, ..., \dot{\theta}_{Rthigh(300)} \quad (19)$$

$$\dot{\theta}_{Rshank} = \dot{\theta}_{Rshank(1)}, \dot{\theta}_{Rshank(2)}, \dot{\theta}_{Rshank(3)}, ..., \dot{\theta}_{Rshank(n)}, ..., \dot{\theta}_{Rshank(300)} \quad (20)$$

$$\dot{\theta}_{Lthigh} = \dot{\theta}_{Lthigh(1)}, \dot{\theta}_{Lthigh(2)}, \dot{\theta}_{Lthigh(3)}, ..., \dot{\theta}_{Lthigh(n)}, ..., \dot{\theta}_{Lthigh(300)} \quad (21)$$

$$\dot{\theta}_{Lshank} = \dot{\theta}_{Lshank(1)}, \dot{\theta}_{Lshank(2)}, \dot{\theta}_{Lshank(3)}, ..., \dot{\theta}_{Lshank(n)}, ..., \dot{\theta}_{Lshank(300)} \quad (22)$$

For the estimation of λ*, data segmentation and data interpolation are performed in a different way, as mentioned in Chapter 4.7. Measurement data from the first 30 gait cycles (excluding first gait cycle) are linearly interpolated to 3000 data points, as follow in (23) – (26). This method is intended to preserve stride-to-stride temporal variation which is important for Lyapunov stability analysis [85]. It also normalizes the measurement data so that the numbers of data points per stride are similar for every experiment.

$$\dot{\theta}_{Rthigh} = \dot{\theta}_{Rthigh(1)}, \dot{\theta}_{Rthigh(2)}, \dot{\theta}_{Rthigh(3)}, ..., \dot{\theta}_{Rthigh(n)}, ..., \dot{\theta}_{Rthigh(3000)} \quad (23)$$

$$\dot{\theta}_{Rshank} = \dot{\theta}_{Rshank(1)}, \dot{\theta}_{Rshank(2)}, \dot{\theta}_{Rshank(3)}, ..., \dot{\theta}_{Rshank(n)}, ..., \dot{\theta}_{Rshank(3000)} \quad (24)$$

$$\dot{\theta}_{Lthigh} = \dot{\theta}_{Lthigh(1)}, \dot{\theta}_{Lthigh(2)}, \dot{\theta}_{Lthigh(3)}, ..., \dot{\theta}_{Lthigh(n)}, ..., \dot{\theta}_{Lthigh(3000)} \quad (25)$$

$$\dot{\theta}_{Lshank} = \dot{\theta}_{Lshank(1)}, \dot{\theta}_{Lshank(2)}, \dot{\theta}_{Lshank(3)}, ..., \dot{\theta}_{Lshank(n)}, ..., \dot{\theta}_{Lshank(3000)} \quad (26)$$

5.5 Estimation and Evaluation of Human Lower Extremity

The orientations of the lower extremity i.e. right thigh (θ_{Rthigh}), right shank (θ_{Rshank}), left thigh (θ_{Lthigh}) and left shank (θ_{Lshank}) are the main kinematic parameters considered in both online and offline gait evaluations. To obtain these parameters, trapezoidal integration method is applied to the segmented angular rates described in (19) – (22). Trapezoidal integration method is selected because the input is discrete data with uniform spacing and the calculation is simpler than other methods.The estimated orientation is calculated as follows in (27), where $\theta_{(t)}$ is the estimated orientation at time t, $\dot{\theta}_{(t)}$ is the angular rate of either thigh or shank at time t and Δt is equal to 0.005s.

$$\theta_{(t)} = \Delta t \times \frac{\dot{\theta}_{(t)} + \dot{\theta}_{(t+1)}}{2} \quad (27)$$

For qualitative feedback, orientations of the lower extremity are arranged in array, as describe in (28) – (31), where m is the number of gait cycle, n is the number of data points, θ_{id_thigh} and θ_{id_shank} are the ideal orientation of thigh and shank reported in [2],[3],[104]. These arrays are then presented with the aid of graphical representations illustrated in Figure 4.11.

$$\theta_{Rthigh} = \begin{bmatrix} \theta_{id\_thigh(1)} & \theta_{id\_thigh(2)} & \theta_{id\_thigh(3)} & \cdots & \theta_{id\_thigh(n)} & \cdots & \theta_{id\_thigh(300)} \\ \theta_{Rthigh(1,1)} & \theta_{Rthigh(1,2)} & \theta_{Rthigh(1,3)} & \cdots & \theta_{Rthigh(1,n)} & \cdots & \theta_{Rthigh(1,300)} \\ \theta_{Rthigh(2,1)} & \theta_{Rthigh(2,2)} & \theta_{Rthigh(2,3)} & \cdots & \theta_{Rthigh(2,n)} & \cdots & \theta_{Rthigh(2,300)} \\ & & . & & & & \\ & & . & & & & \\ & & . & & & & \\ \theta_{Rthigh(m,1)} & \theta_{Rthigh(m,2)} & \theta_{Rthigh(m,3)} & \cdots & \theta_{Rthigh(m,n)} & \cdots & \theta_{Rthigh(m,300)} \end{bmatrix} \quad (28)$$

$$\theta_{Lthigh} = \begin{bmatrix} \theta_{id\_thigh(1)} & \theta_{id\_thigh(2)} & \theta_{id\_thigh(3)} & \cdots & \theta_{id\_thigh(n)} & \cdots & \theta_{id\_thigh(300)} \\ \theta_{Lthigh(1,1)} & \theta_{Lthigh(1,2)} & \theta_{Lthigh(1,3)} & \cdots & \theta_{Lthigh(1,n)} & \cdots & \theta_{Lthigh(1,300)} \\ \theta_{Lthigh(2,1)} & \theta_{Lthigh(2,2)} & \theta_{Lthigh(2,3)} & \cdots & \theta_{Lthigh(2,n)} & \cdots & \theta_{Lthigh(2,300)} \\ & & & . & & & \\ & & & . & & & \\ & & & . & & & \\ \theta_{Lthigh(m,1)} & \theta_{Lthigh(m,2)} & \theta_{Lthigh(m,3)} & \cdots & \theta_{Lthigh(m,n)} & \cdots & \theta_{Lthigh(m,300)} \end{bmatrix} \quad (29)$$

$$\theta_{Rshank} = \begin{bmatrix} \theta_{id\_shank(1)} & \theta_{id\_shank(1)} & \theta_{id\_shank(3)} & \cdots & \theta_{id\_shank(n)} & \cdots & \theta_{id\_shank(300)} \\ \theta_{Rshank(1,1)} & \theta_{Rshank(1,2)} & \theta_{Rshank(1,3)} & \cdots & \theta_{Rshank(1,n)} & \cdots & \theta_{Rshank(1,300)} \\ \theta_{Rshank(2,1)} & \theta_{Rshank(2,2)} & \theta_{Rshank(2,3)} & \cdots & \theta_{Rshank(2,n)} & \cdots & \theta_{Rshank(2,300)} \\ & & & . & & & \\ & & & . & & & \\ & & & . & & & \\ \theta_{Rshank(m,1)} & \theta_{Rshank(m,2)} & \theta_{Rshank(m,3)} & \cdots & \theta_{Rshank(m,n)} & \cdots & \theta_{Rshank(m,300)} \end{bmatrix} \quad (30)$$

$$\theta_{Rshank} = \begin{bmatrix} \theta_{id\_shank(1)} & \theta_{id\_shank(1)} & \theta_{id\_shank(3)} & \cdots & \theta_{id\_shank(n)} & \cdots & \theta_{id\_shank(300)} \\ \theta_{Rshank(1,1)} & \theta_{Rshank(1,2)} & \theta_{Rshank(1,3)} & \cdots & \theta_{Rshank(1,n)} & \cdots & \theta_{Rshank(1,300)} \\ \theta_{Rshank(2,1)} & \theta_{Rshank(2,2)} & \theta_{Rshank(2,3)} & \cdots & \theta_{Rshank(2,n)} & \cdots & \theta_{Rshank(2,300)} \\ & & & . & & & \\ & & & . & & & \\ & & & . & & & \\ \theta_{Rshank(m,1)} & \theta_{Rshank(m,2)} & \theta_{Rshank(m,3)} & \cdots & \theta_{Rshank(m,n)} & \cdots & \theta_{Rshank(m,300)} \end{bmatrix} \quad (31)$$

Quantitative feedbacks are provided in form of Coefficient of Determination (*CoD*) and statistical results of the temporal parameters. Mean stride time ($\overline{T}_{stride}$), mean stance time ($\overline{T}_{stance}$), mean swing time ($\overline{T}_{swing}$), and their standard deviations (σ_{stride}, σ_{stance}, and σ_{swing}) are calculated to indicate the timing performances of a person's gait. These statistical parameters are calculated as follow in (32) – (37) where *M* is the total number of gait cycle

$$\overline{T}_{stride} = \frac{1}{M}\sum_{m=1}^{M} T_{stride(m)} \quad (32)$$

$$\overline{T}_{stance} = \frac{1}{M}\sum_{m=1}^{M} T_{stance(m)} \quad (33)$$

$$\bar{T}_{swing} = \frac{1}{M}\sum_{m=1}^{M} T_{swing(m)} \tag{34}$$

$$\sigma_{stride} = \sqrt{\frac{1}{M}\sum_{m=1}^{M}(T_{stride(m)} - \bar{T}_{stride})^2} \tag{35}$$

$$\sigma_{stance} = \sqrt{\frac{1}{M}\sum_{m=1}^{M}(T_{stance(m)} - \bar{T}_{stance})^2} \tag{36}$$

$$\sigma_{swing} = \sqrt{\frac{1}{M}\sum_{m=1}^{M}(T_{swing(m)} - \bar{T}_{swing})^2} \tag{37}$$

Additionally, mean orientation $\bar{\theta}_{(n)}$ and standard deviation $\sigma_{\theta(n)}$ of the orientation of the lower extremity are calculated. These parameters are calculated in (38) – (39)

$$\bar{\theta}_{(n)} = \frac{1}{M}\sum_{M=1}^{M} \theta_{(m,n)} \tag{38}$$

$$\sigma_{\theta(n)} = \sqrt{\frac{1}{M}\sum_{m=1}^{m}(\theta_{(m,n)} - \bar{\theta}_{(n)})^2} \tag{39}$$

Coefficient of Determination (*CoD*) is a measure indicating how closely the ideal and actual orientations of the lower extremities are related. A value close to zero indicates that little relationship exists between the ideal and actual orientation and therefore gait abnormality shall be observed, whereas a value close to one indicates that strong relationship exists between the ideal and actual orientation and therefore healthy/normal gait shall be observed. *CoD* is calculated as shown in (40) where θ_{actual} is the actual orientation of the lower extremity, $\bar{\theta}_{actual}$ is the mean of the actual orientation of the lower extremity and θ_{ideal} is the ideal orientation of the lower extremity.

$$CoD = \frac{\sum(\theta_{actual} - \bar{\theta}_{actual})^2 - \sum(\theta_{ideal} - \bar{\theta}_{actual})^2}{\sum(\theta_{actual} - \bar{\theta}_{actual})^2} \tag{40}$$

5.6 3-D Animation of the Lower Extremity in Walking

3-D animation of a person's gait is simulated using a basic stick figure animation, as illustrated in Figure 5.6. This stick figure was designed in order to represent the human's lower extremity: upper body, right thigh, right shank, left thigh and left shank. Orientations of each body segment on sagittal plane, horizontal plane and frontal plane are taken into account to demonstrate the natural and realistic walking movements.

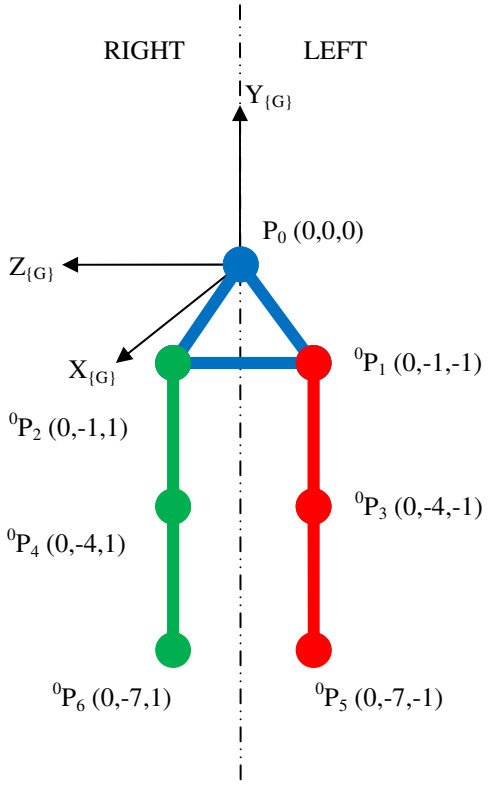

Figure 5.6 Initial positions of the 3-D lower extremity representation.

Considering that each body segment is able to rotate along three different axes: X-axis, Y-axis and Z-axis, a 4x4 transformation matrix is required to obtain the position of lower extremity over the time *t*. This matrix contains Z-Y-X euler angles rotational matrix and 3-D translational matrix, as expressed in (41), where c is cosine, s is sine, and α, β and γ are the rotations along Z-axis, Y-axis and X-axis respectively over time *t*. The unit for these rotations is in radian. *x0*, *y0* and *z0* is the origin of the rotation with respect to the origin of {G} (0,0,0).

$$T_{(t)} = \begin{bmatrix} \mathrm{c}\alpha\mathrm{c}\beta & \mathrm{c}\alpha\mathrm{s}\beta\mathrm{s}\gamma - \mathrm{s}\alpha\mathrm{c}\gamma & \mathrm{c}\alpha\mathrm{s}\beta\mathrm{c}\gamma + \mathrm{s}\alpha\mathrm{s}\gamma & x0 \\ \mathrm{s}\alpha\mathrm{c}\beta & \mathrm{s}\alpha\mathrm{s}\beta\mathrm{s}\gamma + \mathrm{c}\alpha\mathrm{c}\gamma & \mathrm{s}\alpha\mathrm{s}\beta\mathrm{c}\gamma - \mathrm{c}\alpha\mathrm{s}\gamma & y0 \\ -\mathrm{s}\beta & \mathrm{c}\beta\mathrm{s}\gamma & \mathrm{c}\beta\mathrm{c}\gamma & z0 \\ 0 & 0 & 0 & 1 \end{bmatrix} \quad (41)$$

For a 3-D animation of the stick figure, the coordinates of P_1 to P_6 defined by transformation matrix T has to be determined individually over time t. The mathematical definitions of these coordinates are presented in following sub-sections.

5.6.1 Upper Body

As illustrated in Figure 5.6, upper body of the stick figure is made of three coordinates in space: ${}^0P_1$, ${}^0P_2$ and P_0 as the origin of the rotation. To perform 3-D animation of the upper body, the position of ${}^0P_1$ and ${}^0P_2$ over time t are defined as (42) – (43)

$${}^0P_{1(t)} = T_{\alpha_{UB},\beta_{UB},\gamma_{UB}(t)} \times {}^0P_{1(0)} \quad (42)$$

$${}^0P_{2(t)} = T_{\alpha_{UB},\beta_{UB},\gamma_{UB}(t)} \times {}^0P_{2(0)} \quad (43)$$

Where

α_{UB} = estimated orientation of upper body along Z-axis;

β_{UB} = estimated orientation of upper body along Y-axis;

γ_{UB} = estimated orientation of upper body along X-axis;

$$T_{\alpha_{UB},\beta_{UB},\gamma_{UB}} = \begin{bmatrix} \mathrm{c}\alpha_{UB}\mathrm{c}\beta_{UB} & \mathrm{c}\alpha_{UB}\mathrm{s}\beta_{UB}\mathrm{s}\gamma_{UB} - \mathrm{s}\alpha_{UB}\mathrm{c}\gamma_{UB} & \mathrm{c}\alpha_{UB}\mathrm{s}\beta_{UB}\mathrm{c}\gamma_{UB} + \mathrm{s}\alpha_{UB}\mathrm{s}\gamma_{UB} & 0 \\ \mathrm{s}\alpha_{UB}\mathrm{c}\beta_{UB} & \mathrm{s}\alpha_{UB}\mathrm{s}\beta_{UB}\mathrm{s}\gamma_{UB} + \mathrm{c}\alpha_{UB}\mathrm{c}\gamma_{UB} & \mathrm{s}\alpha_{UB}\mathrm{s}\beta_{UB}\mathrm{c}\gamma_{UB} - \mathrm{c}\alpha_{UB}\mathrm{s}\gamma_{UB} & 0 \\ -\mathrm{s}\beta_{UB} & \mathrm{c}\beta_{UB}\mathrm{s}\gamma_{UB} & \mathrm{c}\beta_{UB}\mathrm{c}\gamma_{UB} & 0 \\ 0 & 0 & 0 & 1 \end{bmatrix}$$

5.6.2 Right Thigh

Right thigh is defined by two points in space: ${}^0P_1$ and ${}^0P_3$. ${}^0P_1$ is the origin of the 3-D transformation. Over time t, ${}^0P_{3(t)}$ is defined as (44)

$${}^0P_{3(t)} = T_{\alpha_{RT},\beta_{RT},\gamma_{RT}(t)} \times {}^1P_{3(0)} \quad (44)$$

Where

α_{RT} is the rotation of right thigh along Z-axis;

β_{RT} is the rotation of right thigh along Y-axis;

γ_{RT} is the rotation of right thigh along X-axis;

$$T_{\alpha_{RT},\beta_{RT},\gamma_{RT}} = \begin{bmatrix} \mathrm{c}\alpha_{RT}\,\mathrm{c}\beta_{RT} & \mathrm{c}\alpha_{RT}\,\mathrm{s}\beta_{RT}\,\mathrm{s}\gamma_{RT} - \mathrm{s}\alpha_{RT}\,\mathrm{c}\gamma_{RT} & \mathrm{c}\alpha_{RT}\,\mathrm{s}\beta_{RT}\,\mathrm{c}\gamma_{RT} + \mathrm{s}\alpha_{RT}\,\mathrm{s}\gamma_{RT} & {}^{0}P_{1(t)-X} \\ \mathrm{s}\alpha_{RT}\,\mathrm{c}\beta_{RT} & \mathrm{s}\alpha_{RT}\,\mathrm{s}\beta_{RT}\,\mathrm{s}\gamma_{RT} + \mathrm{c}\alpha_{RT}\,\mathrm{c}\gamma_{RT} & \mathrm{s}\alpha_{RT}\,\mathrm{s}\beta_{RT}\,\mathrm{c}\gamma_{RT} - \mathrm{c}\alpha_{RT}\,\mathrm{s}\gamma_{RT} & {}^{0}P_{1(t)-Y} \\ -\mathrm{s}\beta_{RT} & \mathrm{c}\beta_{RT}\,\mathrm{s}\gamma_{RT} & \mathrm{c}\beta_{RT}\,\mathrm{c}\gamma_{RT} & {}^{0}P_{1(t)-Z} \\ 0 & 0 & 0 & 1 \end{bmatrix}$$

$$^{1}P_{3(0)} = \begin{bmatrix} 0 \\ -3 \\ 0 \\ 1 \end{bmatrix}$$

5.6.3 Right Shank

Right shank is defined by two points in space: $^{0}P_{3}$ and $^{0}P_{5}$. $^{0}P_{3}$ is the origin of the transformation. The coordinate of $^{0}P_{5(t)}$ over time *t* is defined as (45)

$$^{0}P_{5(t)} = T_{\alpha_{RS},\beta_{RS},\gamma_{RS}(t)} \times {}^{3}P_{5(0)} \tag{45}$$

Where

α_{RS} is the rotation of right shank along Z-axis;

β_{RS} is the rotation of right shank along Y-axis;

γ_{RS} is the rotation of right shank along X-axis;

$$T_{\alpha_{RS},\beta_{RS},\gamma_{RS}} = \begin{bmatrix} \mathrm{c}\alpha_{RS}\,\mathrm{c}\beta_{RS} & \mathrm{c}\alpha_{RS}\,\mathrm{s}\beta_{RS}\,\mathrm{s}\gamma_{RS} - \mathrm{s}\alpha_{RS}\,\mathrm{c}\gamma_{RS} & \mathrm{c}\alpha_{RS}\,\mathrm{s}\beta_{RS}\,\mathrm{c}\gamma_{RS} + \mathrm{s}\alpha_{RS}\,\mathrm{s}\gamma_{RS} & {}^{0}P_{3(t)-X} \\ \mathrm{s}\alpha_{RS}\,\mathrm{c}\beta_{RS} & \mathrm{s}\alpha_{RS}\,\mathrm{s}\beta_{RS}\,\mathrm{s}\gamma_{RS} + \mathrm{c}\alpha_{RS}\,\mathrm{c}\gamma_{RS} & \mathrm{s}\alpha_{RS}\,\mathrm{s}\beta_{RS}\,\mathrm{c}\gamma_{RS} - \mathrm{c}\alpha_{RS}\,\mathrm{s}\gamma_{RS} & {}^{0}P_{3(t)-Y} \\ -\mathrm{s}\beta_{RS} & \mathrm{c}\beta_{RS}\,\mathrm{s}\gamma_{RS} & \mathrm{c}\beta_{RS}\,\mathrm{c}\gamma_{RS} & {}^{0}P_{3(t)-Z} \\ 0 & 0 & 0 & 1 \end{bmatrix}$$

$$^{3}P_{5(0)} = \begin{bmatrix} 0 \\ -3 \\ 0 \\ 1 \end{bmatrix}$$

5.6.4 Left Thigh

Left thigh is defined by two points in space: $^{0}P_{2}$ and $^{0}P_{4}$. $^{0}P_{2}$ is the origin of the 3-D transformation. $^{0}P_{4(t)}$ over time *t* is computed as follows in (46)

$$^{0}P_{4(t)} = T_{\alpha_{LT},\beta_{LT},\gamma_{LT}(t)} \times {}^{2}P_{4(0)} \tag{46}$$

Where

α_{LT} is the rotation of left thigh along Z-axis;

β_{LT} is the rotation of left thigh along Y-axis;

γ_{LT} is the rotation of left thigh along X-axis;

$$T_{\alpha_{LT},\beta_{LT},\gamma_{LT}} = \begin{bmatrix} \mathrm{c}\alpha_{LT}\,\mathrm{c}\beta_{LT} & \mathrm{c}\alpha_{LT}\,\mathrm{s}\beta_{LT}\,\mathrm{s}\gamma_{LT} - \mathrm{s}\alpha_{LT}\,\mathrm{c}\gamma_{LT} & \mathrm{c}\alpha_{LT}\,\mathrm{s}\beta_{LT}\,\mathrm{c}\gamma_{LT} + \mathrm{s}\alpha_{LT}\,\mathrm{s}\gamma_{LT} & {}^{0}P_{2(t)-X} \\ \mathrm{s}\alpha_{LT}\,\mathrm{c}\beta_{LT} & \mathrm{s}\alpha_{LT}\,\mathrm{s}\beta_{LT}\,\mathrm{s}\gamma_{LT} + \mathrm{c}\alpha_{LT}\,\mathrm{c}\gamma_{LT} & \mathrm{s}\alpha_{LT}\,\mathrm{s}\beta_{LT}\,\mathrm{c}\gamma_{LT} - \mathrm{c}\alpha_{LT}\,\mathrm{s}\gamma_{LT} & {}^{0}P_{2(t)-Y} \\ -\mathrm{s}\beta_{LT} & \mathrm{c}\beta_{LT}\,\mathrm{s}\gamma_{LT} & \mathrm{c}\beta_{LT}\,\mathrm{c}\gamma_{LT} & {}^{0}P_{2(t)-Z} \\ 0 & 0 & 0 & 1 \end{bmatrix}$$

$$^{2}P_{4(0)} = \begin{bmatrix} 0 \\ -3 \\ 0 \\ 1 \end{bmatrix}$$

5.6.5 Left Shank

Left shank is defined by $^{0}P_{4}$ and $^{0}P_{6}$. $^{0}P_{6}$ is the center of 3-D transformation. The coordinate of $^{0}P_{6(t)}$ over the time *t* is calculated as follows in (47)

$$^{0}P_{6(t)} = T_{\alpha_{LS},\beta_{LS},\gamma_{LS}(t)} \times {}^{4}P_{6(0)} \qquad (47)$$

Where

α_{LS} is the rotation of left shank along Z-axis;

β_{LS} is the rotation of left shank along Y-axis;

γ_{LS} is the rotation of left shank along X-axis;

$$T_{\alpha_{LS},\beta_{LS},\gamma_{LS}} = \begin{bmatrix} \mathrm{c}\alpha_{LS}\,\mathrm{c}\beta_{LS} & \mathrm{c}\alpha_{LS}\,\mathrm{s}\beta_{LS}\,\mathrm{s}\gamma_{LS} - \mathrm{s}\alpha_{LS}\,\mathrm{c}\gamma_{LS} & \mathrm{c}\alpha_{LS}\,\mathrm{s}\beta_{LS}\,\mathrm{c}\gamma_{LS} + \mathrm{s}\alpha_{LS}\,\mathrm{s}\gamma_{LS} & {}^{0}P_{1(t)-X} \\ \mathrm{s}\alpha_{LS}\,\mathrm{c}\beta_{LS} & \mathrm{s}\alpha_{LS}\,\mathrm{s}\beta_{LS}\,\mathrm{s}\gamma_{LS} + \mathrm{c}\alpha_{LS}\,\mathrm{c}\gamma_{LS} & \mathrm{s}\alpha_{LS}\,\mathrm{s}\beta_{LS}\,\mathrm{c}\gamma_{LS} - \mathrm{c}\alpha_{LS}\,\mathrm{s}\gamma_{LS} & {}^{0}P_{1(t)-Y} \\ -\mathrm{s}\beta_{LS} & \mathrm{c}\beta_{LS}\,\mathrm{s}\gamma_{LS} & \mathrm{c}\beta_{LS}\,\mathrm{c}\gamma_{LS} & {}^{0}P_{1(t)-Z} \\ 0 & 0 & 0 & 1 \end{bmatrix}$$

$$^{4}P_{6(0)} = \begin{bmatrix} 0 \\ -3 \\ 0 \\ 1 \end{bmatrix}$$

5.7 Normalized Cross-correlation (Cc_{norm})

Cross-correlation (Cc) is commonly used to determine the similarity of two signals and to determine the time delay between them. Cross-correlation of two signals is commonly used in radar, digital communications, geology, and other areas in engineering and science. In summary, cross-correlation performs the following operations: shifting one of the sequences, multiplication of the two sequences, and summing over all values of the product sequences [113].

In this thesis, Cc is computed to determine the bilateral differences between right limb and left limb motion in each gait cycle. The angular rate of the right limb ($\dot{\theta}_R$) is considered as the reference signal while the angular rate of the left limb ($\dot{\theta}_L$) is considered as the target signal. Hence, Cc can be computed as follows in (48).

$$Cc_{(k)} = \sum_{n=1}^{N} \dot{\theta}_{R(n)} \dot{\theta}_{L(n-k)} \qquad \begin{array}{c} k = 0, \pm 1, \pm 2, ..., \pm N - 1 \\ if\ \ n-k \le 0\ or\ n-k > N,\ then\ \ \dot{\theta}_{L(n-k)} = 0 \end{array} \tag{48}$$

Cc produces a distinctive peak, which is affected by the magnitude of $\dot{\theta}_R$ and $\dot{\theta}_L$. In order to address this limitation, auto-correlation of $\dot{\theta}_R$, AcR and $\dot{\theta}_L$, AcL are calculated using (49) – (51) to estimate Cc_{norm}. Cc_{norm} produces values ranging between zero and one where a value approaching one indicates a very strong correlation between $\dot{\theta}_R$ and $\dot{\theta}_L$.

$$AcR_{(k)} = \sum_{n=1}^{N} \dot{\theta}_{R(n)} \dot{\theta}_{R(n-k)} \qquad \begin{array}{c} k = 0, \pm 1, \pm 2, ..., \pm N - 1 \\ if\ \ n-k \le 0\ or\ n-k > N,\ then\ \ \dot{\theta}_{R(n-k)} = 0 \end{array} \tag{49}$$

$$AcL_{(k)} = \sum_{n=1}^{N} \dot{\theta}_{L(n)} \dot{\theta}_{L(n-k)} \qquad \begin{array}{c} k = 0, \pm 1, \pm 2, ..., \pm N - 1 \\ if\ \ n-k \le 0\ or\ n-k > N,\ then\ \ \dot{\theta}_{L(n-k)} = 0 \end{array} \tag{50}$$

$$Cc_{norm} = \frac{\max(Cc)}{\sqrt{AcR_{(0)} \times AcL_{(0)}}} \tag{51}$$

Cc also estimates the time delay between $\dot{\theta}_R$ and $\dot{\theta}_L$. Time delay between two signals (*Ts*) is defined as the time when the *Cc* reaches the maximum value. *Ts* is computed as indicated in (52). A positive *Ts* indicates that $\dot{\theta}_L$ is leading behind $\dot{\theta}_R$ whereas a negative *Ts* signifies that $\dot{\theta}_L$ is lagging behind $\dot{\theta}_R$. *Ts* is expressed as the percentage of gait cycle.

$$Ts = \frac{T_{max(Cc)}}{N} \times 100\% \tag{52}$$

5.8 Symmetry Index (SI) for the Temporal Gait Parameters

One of the popular methods to evaluate the gait asymmetry is the Symmetry Index (SI). SI is initially proposed by Robinson et al [78]. SI signifies the symmetrical behavior of human walking by calculating the difference between the left and right limbs of a given parameter and dividing the result by the bilateral average. Mathematically, SI is described as follows in (53).

$$SI = \frac{(X_R - X_L)}{0.5(X_R + X_L)} \times 100\% \tag{53}$$

Since the temporal parameters do not generate index values that are greater than 100%, conventional SI is used to determine the differences of T_{stride}, T_{stance} and T_{swing} between left limb and right limb. SI_{stride}, SI_{stance} and SI_{swing} are determined following (54) – (56). It is important to highlight that similar to all previous computations, right limb temporal parameters are used as the main reference.

$$SI_{stride} = \frac{(T_{Rstride} - T_{Lstride})}{0.5(T_{Rstride} + T_{Lstride})} \times 100\% \tag{54}$$

$$SI_{stance} = \frac{(T_{Rstance} - T_{Lstance})}{0.5(T_{Rstance} + T_{Lstance})} \times 100\% \tag{55}$$

$$SI_{swing} = \frac{(T_{Rswing} - T_{Lswing})}{0.5(T_{Rswing} + T_{Lswing})} \times 100\% \tag{56}$$

5.9 Normalized Gait Symmetry Index (SI_{norm})

SI suffers from one major drawback. It can generate index value up 13,000% when the difference between two sides was divided by a much smaller value [75]. It can occur when it is applied to spatial parameters i.e. ground reaction force profiles and the orientation of lower extremity. Therefore, SI_{norm} is proposed to overcome this limitation. SI_{norm} is also one of the significant outcomes of this research. The main parameters used to determine SI_{norm} are $\dot{\theta}_{Rthigh}$, $\dot{\theta}_{Rshank}$, $\dot{\theta}_{Lthigh}$, and $\dot{\theta}_{Lshank}$. Prior to the computation of the SI_{norm}, the angular rate of the lower extremity is normalized using min-max normalization approach. Min-max normalization is a transformation procedure that converts the data into a desired range, usually from zero to one. However, in this research, the angular rate is transformed to values greater than zero.

For consistency, angular rate of the right limb is regarded as the main reference. Normalized angular rate ($\dot{\theta}_{norm}$) can be computed as follows in (57), where $\dot{\theta}_{max}$ is the minimum angular rate of the right limb, $\dot{\theta}_{min}$ is the maximum angular rate of the right limb.

$$\dot{\theta}_{norm(n)} = \frac{(\dot{\theta}_{(n)} - \dot{\theta}_{min})}{\dot{\theta}_{max} - \dot{\theta}_{min}} + 1 \tag{57}$$

SI_{norm} is computed using (58), where $\dot{\theta}_{Rnorm}$ is the normalized angular rate of the right limb and $\dot{\theta}_{Lnorm}$ is the normalized angular rate of the left limb.

$$SI_{norm(n)} = \frac{\dot{\theta}_{Rnorm(n)} - \dot{\theta}_{Lnorm(n)}}{0.5(\dot{\theta}_{Rnorm(n)} + \dot{\theta}_{Lnorm(n)})} \times 100\% \tag{58}$$

5.10 Maximum Lyapunov Exponent (λ*)

A valid state space is a vector space that contains a sufficient number of independent coordinates to define the state of the system unequivocally at any point in time [91],[94]. This can be reconstructed from a single time series using the original data and its time-delayed copies as indicated in (59).

$$S(t) = [x(t), x(t+\tau), ..., x(t+(d_E - 1)\tau)] \tag{59}$$

Where *S(t)* represents the state vector, x(t) is the original one dimensional data, τ is the selected time delay and d_E is the embedding dimension.

It is essential to determine the appropriate time delay and embedding dimension in order to reconstruct appropriate representation of the dynamical system. In this thesis, τ was calculated from the first minimum of MI of the data. MI of the measurement data is calculated as follows in (60) [96],[114].

$$MI(\tau) = -\sum_{h=1}^{j}\sum_{k=1}^{j} P_{h,k}(\tau)\ln\frac{P_{h,k}(\tau)}{P_h P_k} \tag{60}$$

Where P_h and P_k denote the probabilities of a time series value x_i in the *h*th and *k*th bin respectively and P_{hk} is the joint probability that x_i is in bin *h* and $x_{i+\tau}$ is in bin *k*. Choosing an appropriate τ is important. If τ is too small, no additional information about the dynamics of a system will be contained in the state space. On the contrary, if τ is too large then information about the dynamics of the system will be lost and result in random information [97],[115]-[116]. Fraser et al. and Kennel et al. indicated that choosing the first minimum from MI provides appropriate τ with minimum redundancy [117]-[118]. Since MI is calculated using tools available in TISEAN package, several parameters have to be set. These parameters are presented in Table 5.1. It is important to highlight that only the measurement data of the first 30 strides are taken into account to estimate the λ*. These measurement data are linearly interpolated to 3000 data points, thus the number of data points used to determine MI is 3000 data points. From the preliminary research work, the first minimum was found to be ranging from 10 to 20 samples. For consistency, τ of 14 was selected and applied to all reconstructed state space.

Table 5.1 Parameters set to determine Mutual Information (MI)

Parameter	**Value**
Number of data points	3000
Number of bins	60
Maximal time delay	100

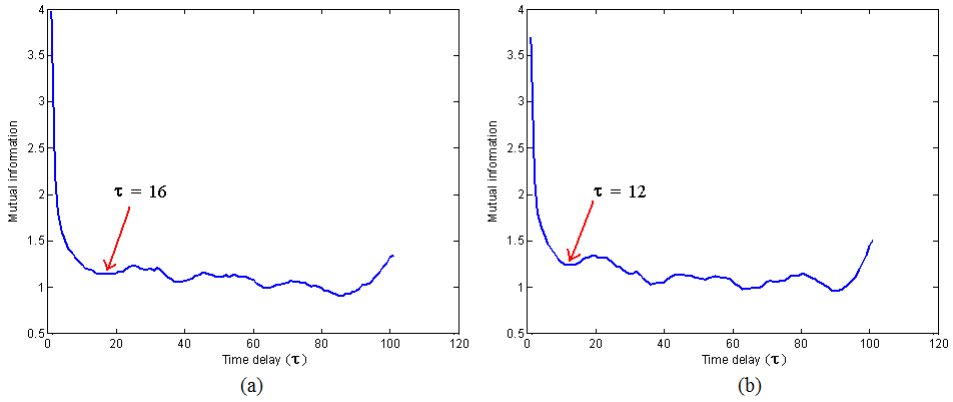

Figure 5.7 Determining the first minimum from MI (a) Thigh and (b) Shank of Participant A during walking at 3 km/h.

As mentioned earlier, d_E is one of the essential parameters required to reconstruct the state space. An inappropriate d_E may result in a projection of the dynamics of the system has orbital crossings in the state space due to false neighbors and not due to the actual dynamics of the system [114]-[115]. In this thesis, d_E was calculated from FNN analysis. FNN is known to be efficient in determining the minimal embedding dimension required to reveal the deterministic structure of the system in the reconstructed state space [114]-[116]. FNN compares the distances between neighboring trajectories in the reconstructed state space at successively higher dimensions. Given a point *p(i)* in the m-dimensional embedding space , *p(j)* is *p(i)* nearest neighbor if the normalized distance R_i is smaller than a given threshold R_t. *p(i)* is marked as having a false nearest neighbor if R_i is larger than R_t. R_i is computed using (61) [96],[114].

$$R_i = \frac{\left| x_{i+m\tau} - x_{j+m\tau} \right|}{\left\| p(i) - p(j) \right\|} \tag{61}$$

d_E is selected where the percentage of false neighbors approaches zero to provide a sufficient number of coordinates to define the system state at all points in time [118]. Similar to MI, several parameters need to be set to perform FNN analysis. These parameters are tabulated in Table 5.2. Most of these parameters are self-explanatory except the Theiler window. Since the data contains first 30 strides (excluding the first gait cycle), which are interpolated to 3000 data points, each stride has approximately 100 data points. Hence, Theiler window is set to 100 to eliminate dynamical correlations in the reconstructed state space [94],[119]. For consistency, d_E of 9 was selected and applied to the all reconstructed

state space because the percentages of false neighbor were less than one percent for both thigh and shank (Figure 5.8).

Table 5.2 Parameters used in False Nearest Neighbors analysis (FNN)

Parameter	**Value**
Number of data points	3000
Minimum embedding dimension	1
Maximum embedding dimension	10
Time delay	14
Theiler window	100

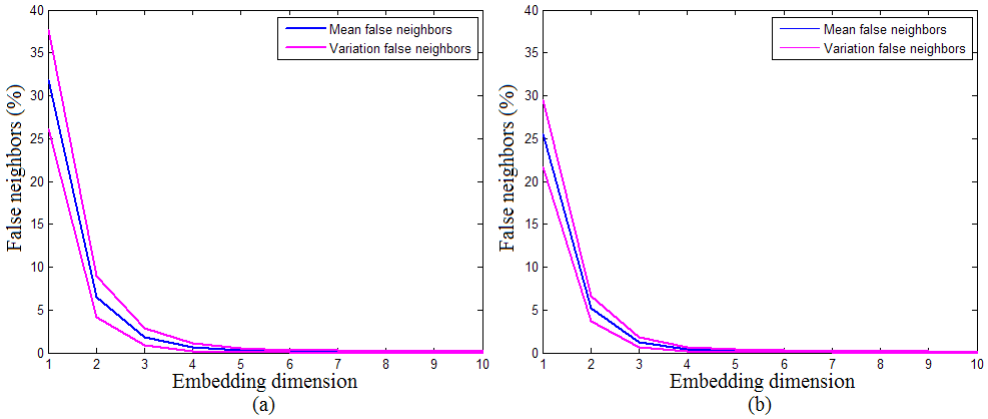

Figure 5.8 FNN analysis results of (a) Thigh and (b) Shank.

Lyapunov exponents quantify the average exponential rate of divergence of neighboring trajectories in the state space. They are a sensitivity measure of a system to infinitesimal perturbation [101]. For a complete description of the effects to such perturbation, the system needs to be described in all direction of the reconstructed state space thus yields to multiple Lyapunov exponents, which are called Lyapunov spectrum. However, in practice, analysis of the dynamic stability is restricted to the λ* because maximum Lyapunov exponent dominates the behavior of entire system. In gait analysis, the main significance of λ* is that it provides a direct indicator of human body dynamic stability [84],[95]-[96]. λ* is defined as follows in (62).

$$\ln d_j(i) \approx \ln C_j + \lambda^*(i\Delta t) \qquad (62)$$

Where Δt is the sampling time ($t = i\Delta t$), $d_j(i)$ is the Euclidean distance between the jth pair of nearest neighbors after ith discrete time steps and C_j is the initial separation between the jth pair of nearest neighbors. The jth pair of nearest neighbors at the ith discrete time step is obtained by pairing a data point of a reference trajectory after fixing the ith discrete time step and with another data point of the jth nearest neighbor trajectories in the whole range of data. Using the algorithm proposed by Rosenstein et al. [95], maximum Lyapunov exponent, λ* can be found by estimating the linear slopes of the curves generated by (63).

$$y(i) = \frac{1}{\Delta t}\left\langle \ln d_j(i) \right\rangle \tag{63}$$

Where $\langle . \rangle$ denotes the average over all values of j. Since each subject exhibited a different average stride time, the time axes of these curves are rescaled by multiplying the average stride frequency of each subject. A graphical illustration on how to estimate the maximum Lyapunov exponent is depicted in Figure 5.9.

In this thesis, $\left\langle \ln d_j(i) \right\rangle$ is computed using tool available in TISEAN package with parameters tabulated in Table 5.3. λ* are estimated over two different time scales [91]-[92],[98],[100]. Short-term λ* (λ_S^*) is calculated from the slope of a linear fit to the divergence curve between zero and one stride Figure 5.10. Long term λ* (λ_L^*) is calculated from the slopes between four and ten strides. This slope is estimated using linear least-squares regression method. The slope, m is calculated as follows:

$$m = \frac{n\sum_{i=1}^{n} x_i y_i - \sum_{i=1}^{n} x_i \sum_{i=1}^{n} y_i}{n\sum_{i=1}^{n} x_i^2 - (\sum_{i=1}^{n} x_i)^2}$$

Where i = {1,2,3, …, n};
n = number of data points;
x = data along the horizontal axis;
y = data along the vertical axis.

Periodic systems result in zero or negative λ*, whereas non periodic or random systems result in a positive λ*. Systems that are more dynamically stable exhibit lower λ* values whereas systems that are less dynamically stable exhibit higher λ* values.

Table 5.3 Parameters set to estimate y(i) using Rosenstein et al. method [95].

Parameter	Value
Number of data points	3000
Embedding dimension	9
Time delay	14
Theiler window	100
Number of iteration	1000

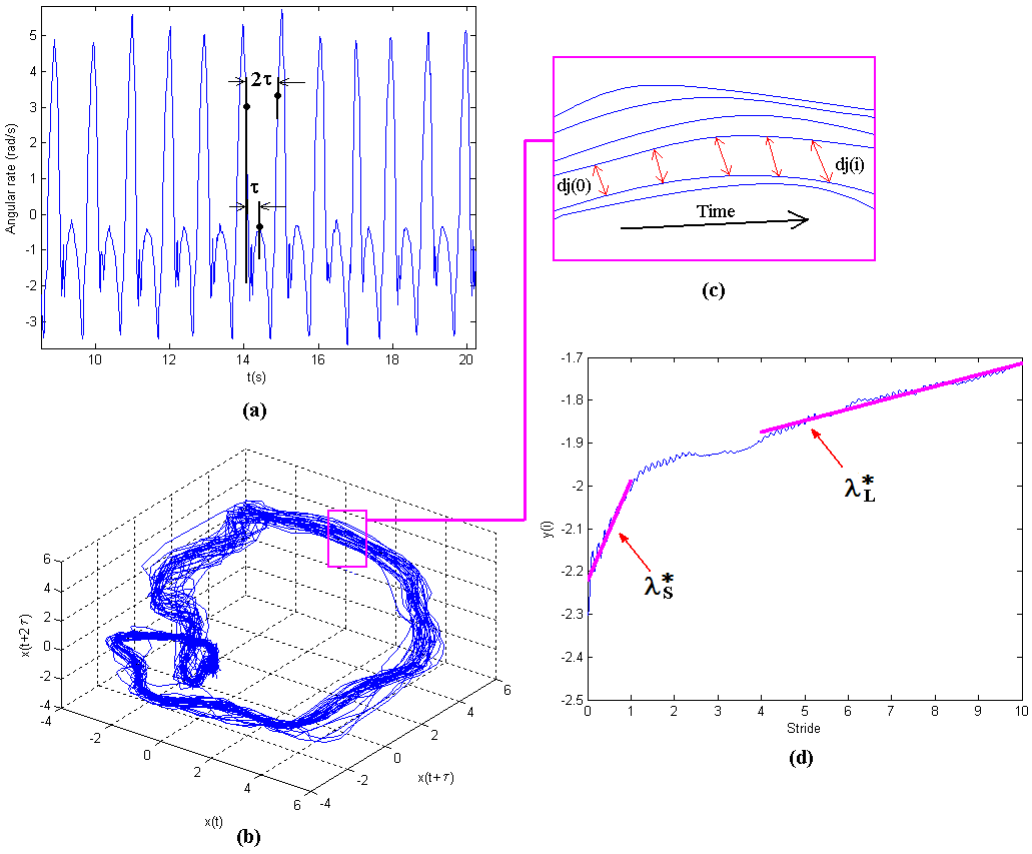

Figure 5.9 Schematic representation of local dynamic stability analysis. (a) original time series data i.e. shank angular rate (b) reconstructed state space with embedding dimension d_E of 3 and time delay τ of 10 (c) A closer view of a section of the reconstructed state space; for each data point, the nearest neighbor is calculated and divergence from this point was calculated as *dj(i).* (d) Average logarithmic rate of divergence, from λ_S^* and λ_L^* which are determined.

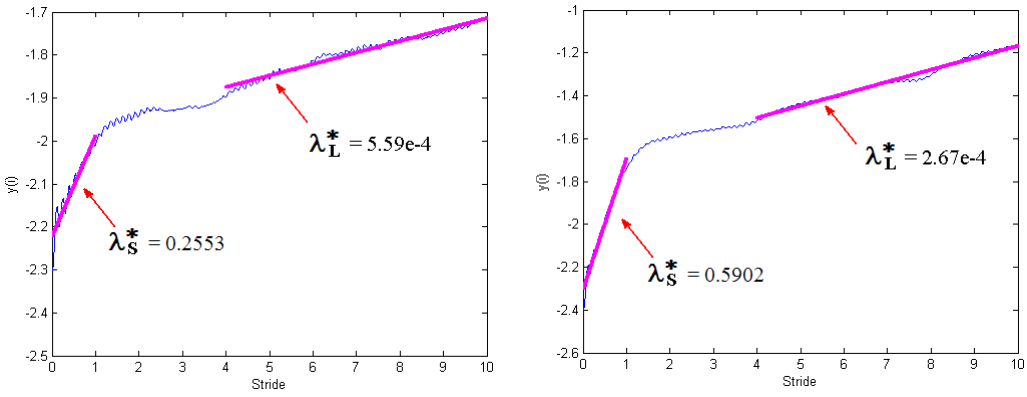

(a) (b)

Figure 5.10 Estimating λ* from (a) Thigh and (b) Shank of Participant A during walking at 3 km/h.

Chapter 6

EXPERIMENTAL SETUP

6.1 Participants

Eleven young and healthy male subjects with mean age 25.3 ± 1.7 years, mean height 173.9 ± 4.8 cm, and mean weight 70.5 ± 9.3 kg participated in this study. Participants were recruited from School of Engineering, Monash University Sunway campus. Participants with any known gait impairments were excluded from this study. Participants were briefed on the purpose of experiments and the experimental procedures before giving consent. In order to keep participants' anonymity, participants were labeled as Participant A to Participant K. This study was approved by Monash University Human Research Ethics Committee. Details of participant's age, weight and height are presented in Table 6.1.

Table 6.1 Participants' details

Participant	Age (years)	Weight (kg)	Height (m)
A	26	78	1.77
B	25	84	1.80
C	26	60	1.70
D	27	76	1.75
E	25	67	1.72
F	22	62	1.74
G	27	55	1.70
H	26	75	1.79
I	22	67	1.70
J	22	90	1.70
K	26	71	1.79

6.2 Experimental Procedures

Experiments were conducted to validate the performances of the system and to study the viability of the proposed methods. These experiments were mainly divided into two categories: treadmill walking and overground walking. Treadmill walking was an experiment where the participant walked on a treadmill for duration of one minute. On the other hand, overground walking was an experiment where the participant walked over a 10 m walkway.

To induce abnormal walking patterns, some of the experiments required the participants to load their lower shank and to wear a sandal on one side of the foot. Loading one of the limbs was intended to change the inertial properties of the loaded limb hence altering the spatio-temporal parameters of the loaded limb during walking [120]-[122]. This study selected 2.5 kg load to be placed on the left or right lower shank to induce abnormal gait (Figure 6.1). As reported in [120], 2.5 kg load shall alter both timing and magnitude of the lower limb kinematic parameters. Load less than 2.5 kg may not be sufficient to alter gait parameters. In contrast, load higher than 2.5 kg may cause stress at participants' joints. Other than loading one side of the limbs, abnormal gait was also simulated by walking with a custom-made sandal that has a thickness of 25 mm on one foot (Figure 6.2). This experiment was intended to simulate the gait of patients with leg length discrepancy [71],[123] Patients with gait disorder may exhibit one or more similar properties with gait simulated by placing a load on one side of the legs or by wearing a sandal on one foot. These properties may include R_{stance}, R_{swing}, and the timing and magnitude of θ_{thigh}, θ_{shank}, $\dot{\theta}_{thigh}$, and $\dot{\theta}_{shank}$.

There were total of nine experiments conducted on the treadmill. These experiments are:

- Normal walking at speed 3 km/hr (Norm3)
- Normal walking at speed 4 km/hr (Norm4)
- Normal walking at speed 5 km/hr (Norm5)
- Walking with load placed on the right limb at speed of 3 km/hr (Norm3Wr)
- Walking with load placed on the right limb at speed of 4 km/hr (Norm4Wr)
- Walking with load placed on the right limb at speed of 5 km/hr (Norm5Wr)
- Walking with load placed on the left limb at speed of 3 km/hr (Norm3Wl)
- Walking with load placed on the left limb at speed of 4 km/hr (Norm4Wl)
- Walking with load placed on the left limb at speed of 5 km/hr (Norm5Wl)

Figure 6.1 A 2.5 kg load is placed on one side of the limbs (right lower shank).

Figure 6.2 A custom-made sandal is worn on one side of the feet (right foot).

There were total of five experiments conducted on the ground. These experiments are:

- Normal walking at natural pace (Norm)
- Walking with load placed on the right limb (NormWr)
- Walking with load placed on the left limb (NormWl)
- Walking with sandal on the right foot (NormSr)
- Walking with sandal on the left foot (NormSl)

In each experiment, subjects were allowed to rest for a maximum time of two minutes before the subsequent experiment was conducted. It is important to note that walking experiments on a treadmill with sandal on one side of the feet were not conducted in this study due to safety concerns and risks that were associated with treadmill walking.

6.3 Statistical Analysis

Statistical analysis was conducted to examine whether there is any significant differences among the experiments conducted in this research. The alpha level/statistic significance was set at 0.01 for all statistical tests. One-way Analysis of Variance (ANOVA) was selected to examine the significance of *CoD*, Cc_{norm}, *Ts* and λ^* in different walking conditions and at different walking speeds. When the null hypothesis was rejected, Tukey-Kramer multiple comparison test was conducted in preference to paired t-test to identify the difference of a particular variable among the experiments. These tests were

conducted using Matlab Statistical Toolbox. Test results were compiled and discussed in Chapter 7.

As a standard procedure in gait analysis, measurement data collected during first stride and last stride were neglected. To examine the significant of *CoD,* Cc_{norm}, *Ts* and λ^*, first 30 strides of the measurement data collected from every treadmill experiment were used. When the participants walked over a 10 m walkway, inconsistent numbers of strides were found. Excluding first stride and last stride, the numbers of strides found to ranging between 6 to 8 strides. For consistency, only 6 strides were used in order to obtain correct statistical results.

Chapter 7

EXPERIMENTAL RESULTS

This chapter compiles and discusses the results of the experiments carried out to evaluate the overall system performances. It also presents the signal patterns generated by human lower extremity in different walking conditions. Additionally, it provides the statistical results on CoD, Cc_{norm}, Ts, λ_S^*, and λ_L^*. Lastly, it illustrates how the normal gait is different from artificially simulated abnormal gait in both spatial and temporal parameters.

7.1 Identification of Gait Events

As described in Chapter 5.2, $\dot{\theta}_{shank}$ produces a periodical signal that has several distinctive peaks and valleys. HMWD uses this property to identify MS, HS and TO. $\dot{\theta}_{shank}$ collected from different walking conditions are presented in Figure 7.1. It could be observed that despite having slightly different waveforms, HMWD was able to identify these gait events. Moreover, it identified those events correctly even though the timings and magnitudes of MS, HS and TO were different across the experiments. Lastly, the experimental results showed that HMWD did not disrupt real-time data streaming and no data loss was found when the system operated within the permissible transmission range. Experiments carried out in this thesis demonstrated the effectiveness of HMWD in periodically identifying gait events without disrupting the real-time data streaming.

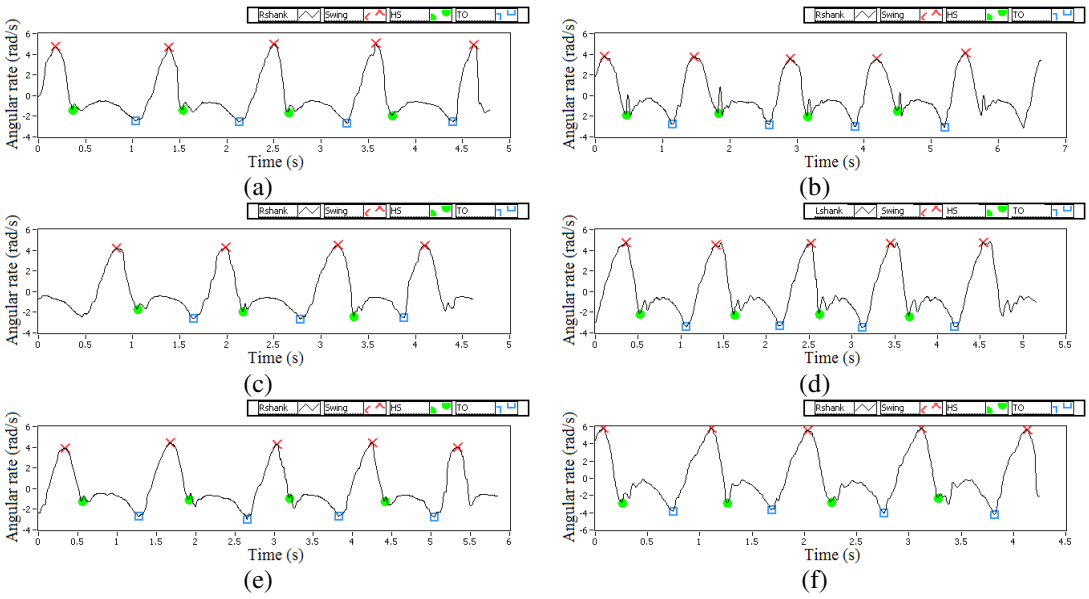

Figure 7.1 $\dot{\theta}_{shank}$ with MS (marked with 'x'), HS (marked with'.'), and TO (marked with '□') events during (a) Normal overground walking (b) Normal treadmill walking (c) Single limb-loaded overground walking (d) Single limb-loaded treadmill walking (e) Overground walking with sandal on one foot (f) Single limb-loaded treadmill walking.

7.2 Gait Normality Test Results

7.2.1 Qualitative Evaluation Results

Evaluating the normality of the participant's gait is one of the significant aspects of this thesis. Gait normality test examines participant's gait against the ideal gait of a normal and healthy individual published in [2],[3], and [104]. It also indicates how well the developed system discriminates normal and abnormal gait. As mentioned earlier, this test contains two main elements: qualitative and quantitative evaluations. Qualitative evaluation is achieved through a graphical comparison between the participant's gait and the ideal gait of a healthy individual, as illustrated Figure 7.2, Figure 7.3, Figure 7.4, and Figure 7.5. For clarity, only Participant A's right limb experimental results are presented and discussed in this thesis. Nevertheless, similar observations were found on the left limb.

As shown in Figure 7.2, Figure 7.3, Figure 7.4, and Figure 7.5, a thick green line is displayed on every graph. This thick line represents the ideal orientation of the lower extremity obtained from [2],[3], and [104]. This line is displayed along with the actual orientation of the participant's lower extremity i.e. multicolor thin lines. Presenting both

orientations within a same graph allow clinicians and biomechanists to distinguish normal and abnormal gait. They can also use qualitative evaluation results to assist them to devise an appropriate treatment that can improve patient's walking condition.

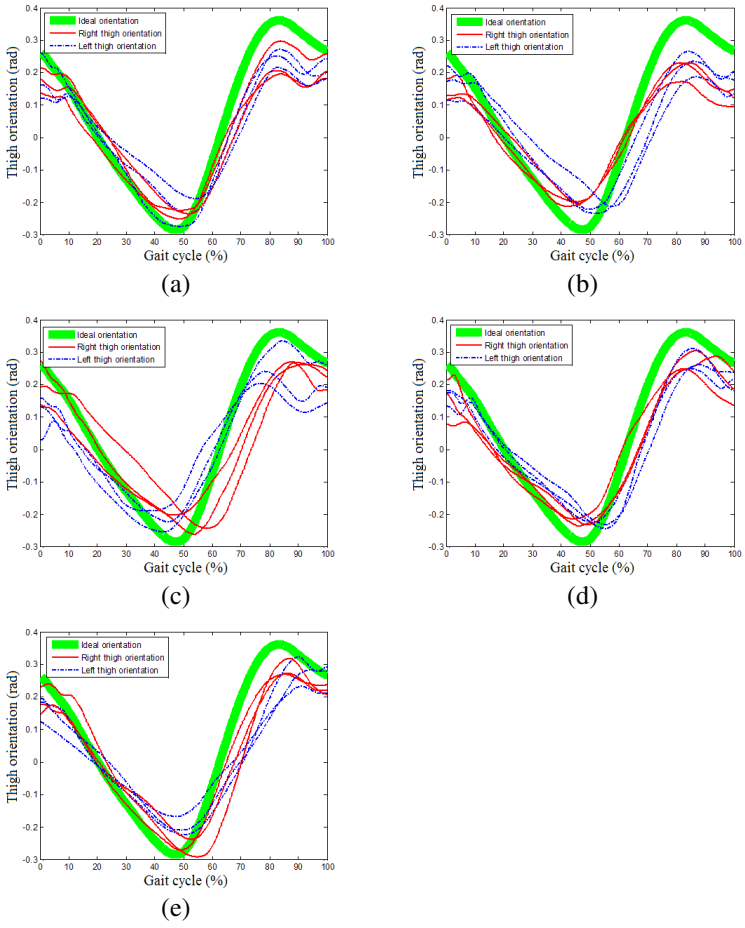

Figure 7.2 Participant A's θ_{thigh} during normal overground walking; θ_{thigh} during walking with a load placed on (b) right limb (c) left limb; θ_{thigh} during walking with sandal on (d) right foot (e) left foot (Thick green line represents θ_{id_thigh}; red thin line represents θ_{Rthigh}; and blue dash line represents θ_{Lthigh}).

Figure 7.2 and Figure 7.3 show θ_{Rthigh} and θ_{Rshank} during normal overground walking. When the participant walked on the ground with normal posture (Figure 7.2(a) and Figure 7.3(a)), θ_{Rthigh} and θ_{Rshank} were similar to θ_{id_thigh} and θ_{id_shank} with minor variations. The mean difference between participant's thigh orientations and the ideal one, $\Delta\overline{\theta}_{thigh}$ was approximately 0.037 rad. The mean difference between participant's shank orientation and the ideal one, $\Delta\overline{\theta}_{shank}$ was approximately 0.004 rad. When participant walked on the treadmill, $\Delta\overline{\theta}_{thigh}$ and $\Delta\overline{\theta}_{shank}$ were found to be approximately 0.038 rad

and 0.002 rad respectively (Figure 7.4(a) – Figure 7.4(c) and Figure 7.5(a) – Figure 7.5(c)). Comparing Figure 7.2(a) with Figure 7.4(a) – Figure 7.4(c) and Figure 7.3(a) with Figure 7.5(a) – Figure 7.5(c), it was apparent that variations of θ_{Rthigh} and θ_{Rshank} found during treadmill walking were less than the variations found during overground walking. These results were consistent with findings published in [91] that treadmill walking could reduce the gait variability.

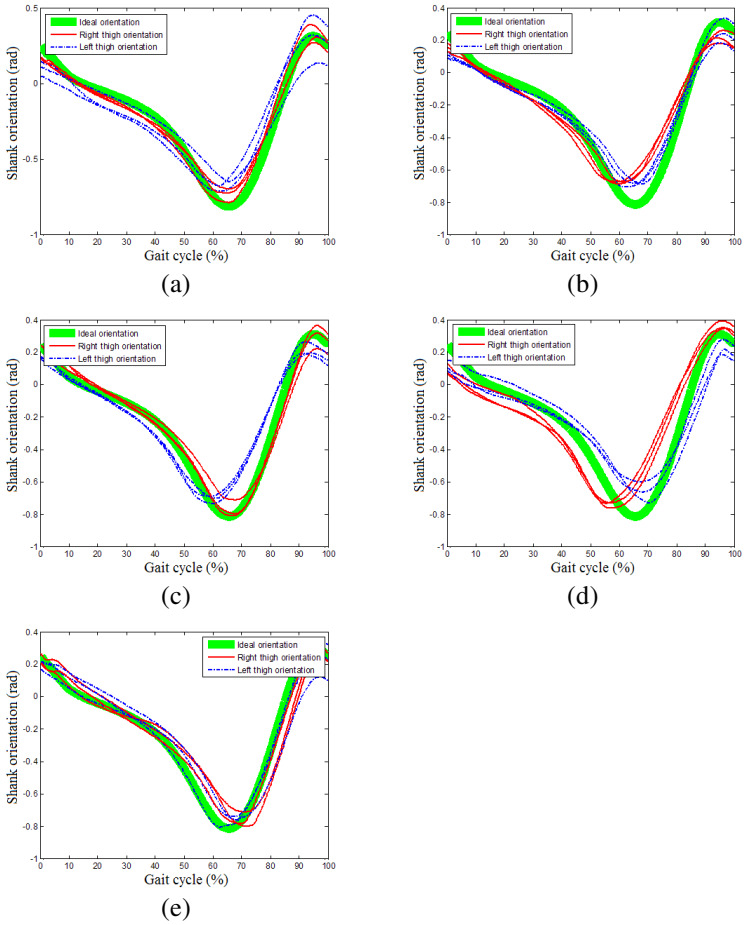

Figure 7.3 Participant A's θ_{shank} during normal overground walking; θ_{shank} during walking with a load placed on (b) right limb (c) left limb; θ_{shank} during walking with sandal on (d) right foot (e) left foot. (Thick green line represents θ_{id_shank}; red thin line represents θ_{Rshank}; and blue dash line represents θ_{Lshank}).

Other than normal gait, experimental results obtained from artificially simulated abnormal gait are also presented in Figure 7.2, Figure 7.3, Figure 7.4, and Figure 7.5. When the participant walked with a load placed on one side of the limbs, the loaded limb exhibited smaller thigh movement throughout the gait cycle (Figure 7.2(b) and Figure 7.4(d) – Figure 7.4(f)). $\Delta\overline{\theta}_{thigh}$ was found to be approximately 0.040 rad when

the participant walked on the ground and approximately 0.042 rad when participant walked on the treadmill. The largest differences ($\Delta\bar{\theta}_{thigh} \approx 0.13$ rad) occurred during the swing phase in overground and treadmill walking. This was expected as the load placed on the lower shank resisted the swinging motion of the thigh to move forward. On the other hand, non-loaded limb exhibited lower $\Delta\bar{\theta}_{thigh}$ of approximately 0.038 rad and 0.039 rad during overground and treadmill walking respectively (Figure 7.2(c) and Figure 7.4 (g) – Figure 7.4 (i)). Apart from the differences in its magnitude throughout the gait cycle, it was apparent that θ_{Rthigh} were slightly shifted to the left when the participant walked on the ground and on the treadmill. This time shift implied that the loaded limb exhibited shorter stance phase than the non-loaded limb. These findings agreed with the experimental results described later in Chapter 7.2.2. Similar observation was also found in θ_{Rshank}. Loaded shank exhibited smaller movement than non-loaded shank throughout the gait cycle. $\Delta\bar{\theta}_{shank}$ was approximately 0.005 rad and 0.003 rad when the participant walked on the ground and on a treadmill respectively (Figure 7.3(b) and Figure 7.5(d) – Figure 7.5(f)). On the other hand, the non-loaded shank exhibited smaller $\Delta\bar{\theta}_{shank}$ of approximately 0.004 rad and 0.002 rad during overground walking and treadmill walking respectively (Figure 7.3(c) and Figure 7.5(g) – Figure 7.5(i)).

In another experiment, when participant was requested to walk with a sandal on one foot, slight differences were found in θ_{Rthigh} and θ_{Rshank}. Affected limb (limb that wore a sandal on its foot) exhibited smaller thigh and shank motions throughout the gait cycle. $\Delta\bar{\theta}_{thigh}$ and $\Delta\bar{\theta}_{shank}$ were approximately 0.038 rad and 0.005 rad (Figure 7.2(d) and Figure 7.3(d)). Similar to the previous experiments, θ_{thigh} and θ_{shank} also exhibited significant time shift to the left. These occurrences indicated that the duration of stance phase was shorter than normal walking. On the contrary, non-affected limb exhibited θ_{Rthigh} and θ_{Rshank} that were similar to θ_{id_thigh} and θ_{id_shank}. $\Delta\bar{\theta}_{thigh}$ and $\Delta\bar{\theta}_{shank}$ were approximately 0.037 rad and 0.0047 rad (Figure 7.2(e) and Figure 7.3(e)). No time shift was found on θ_{thigh} and θ_{shank}.

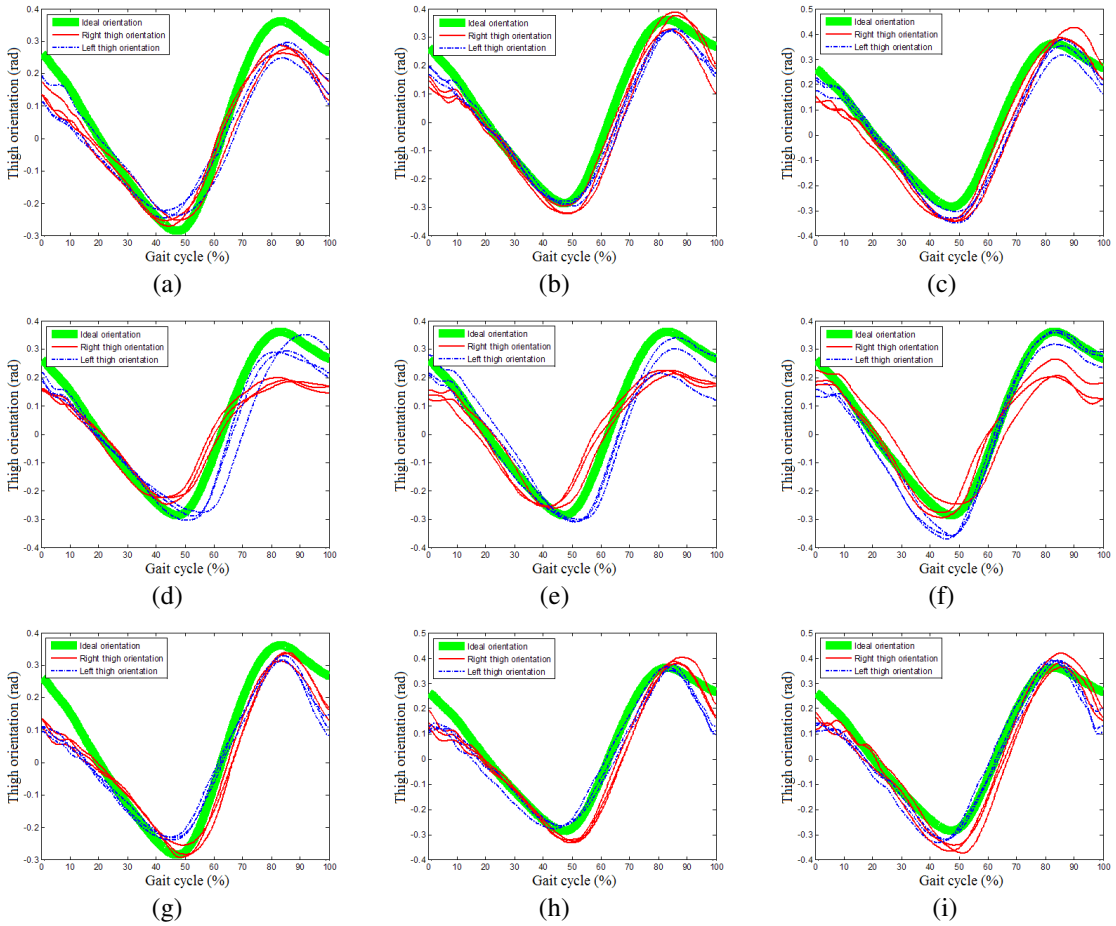

Figure 7.4 Participant A's θ_{thigh} during treadmill walking at (a) 3 km/h (b) 4 km/h (c) 5 km/h; θ_{thigh} during walking with a load on the right limb at (d) 3 km/h (e) 4 km/h (f) 5 km/h; θ_{thigh} during walking with a load on the left limb at (g) 3 km/h (h) 4 km/h (i) 5 km/h (Thick green line represents θ_{id_thigh}; red thin line represents θ_{Rthigh}; and blue dash line represents θ_{Lthigh}).

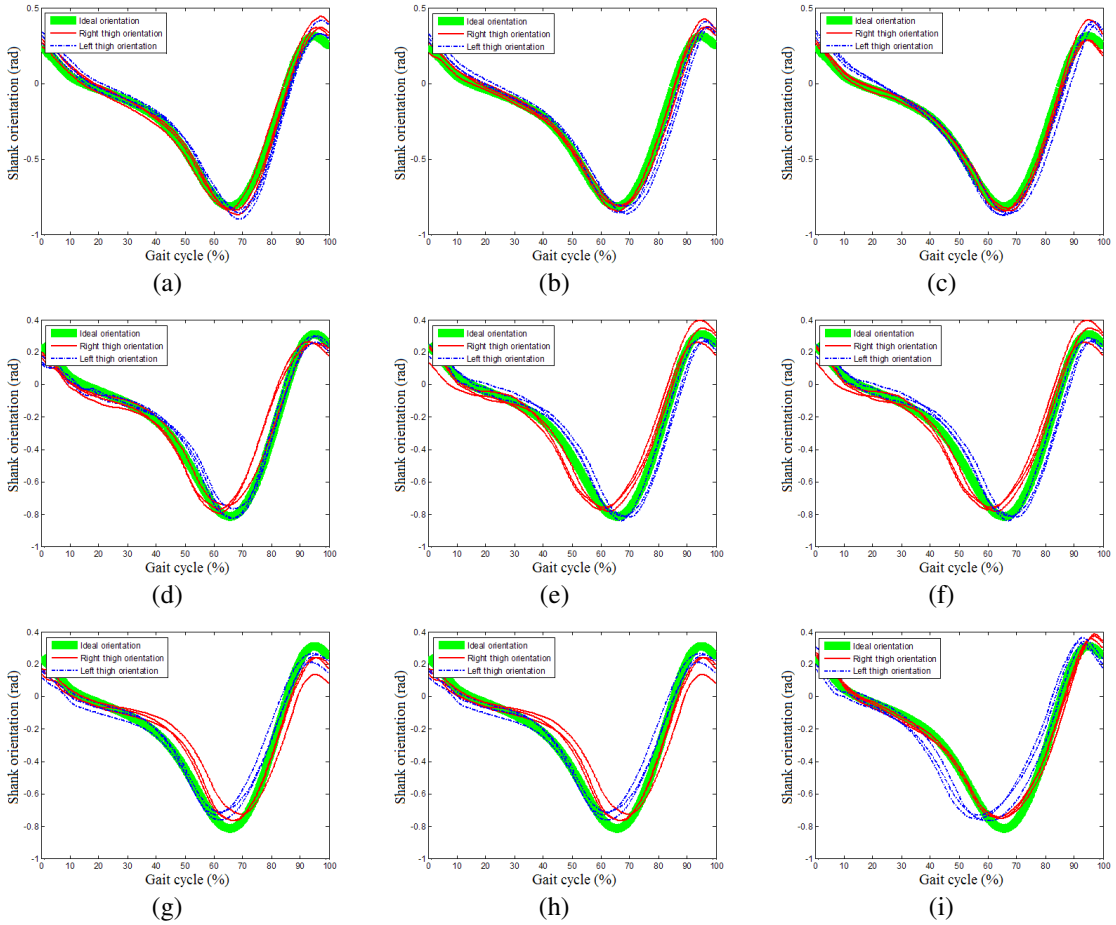

Figure 7.5 Participant A's θ_{shank} during treadmill walking at (a) 3 km/h (b) 4 km/h (c) 5 km/h; θ_{shank} during walking with a load on the right limb at (d) 3 km/h (e) 4 km/h (f) 5 km/h; θ_{shank} during walking with a load on the left limb at (g) 3 km/h (h) 4 km/h (i) 5 km/h. (Thick green line represents θ_{id_shank}; red thin line represents θ_{Rshank}; and blue dash line represents θ_{Lshank}).

7.2.2 Quantitative Evaluation Results

Quantitative evaluation, which is considered as a part of the gait normality test, is required to assist the data interpretation and to provide numerical representations of a person's gait. Quantitative evaluation provides two different parameters: temporal gait parameters and *CoD*. Temporal parameters are estimated based on the identification of HS and TO. These parameters include T_{stride}, T_{stance}, and T_{swing}. Mean of these parameters: $\overline{T}_{stride}$, $\overline{T}_{stance}$, and $\overline{T}_{swing}$ are presented in Table 7.1 and Table 7.2. Table 7.1 presents the temporal gait parameters from the overground walking experiments. Table 7.2 presents the temporal gait parameters compiled from the treadmill walking experiments.

Table 7.1 Mean temporal gait parameters during overground walking

			Norm	**NormWr**	**NormWl**	**NormSr**	**NormSl**
$\overline{T}_{stride}$ (s)	Right		1.0749	1.2099	1.1758	1.2491	1.2487
	Left		1.0840	1.1650	1.2073	1.2816	1.2219
Stance	Right	$\overline{T}_{stance}$ (s)	0.6441	0.7081	0.7191	0.7203	0.7546
		$\overline{R}_{stance}$ (%)	***59.92***	***58.53***	***61.16***	***57.67***	***60.43***
	Left	$\overline{T}_{stance}$ (s)	0.6527	0.7146	0.7109	0.7706	0.7209
		$\overline{R}_{stance}$ (%)	***60.21***	***61.34***	***58.88***	***60.13***	***59.00***
Swing	Right	$\overline{T}_{swing}$ (s)	0.4416	0.5018	0.4567	0.5288	0.4941
		$\overline{R}_{swing}$ (%)	***40.08***	***41.47***	***38.84***	***42.33***	***39.57***
	Left	$\overline{T}_{swing}$ (s)	0.4313	0.4504	0.4964	0.511	0.5010
		$\overline{R}_{swing}$ (%)	***39.79***	***38.66***	***41.12***	***39.87***	***41.00***

In normal overground walking, participants took less time to complete one gait cycle compared to other walking conditions. All participants took an average of 1.0749s and 1.0840s for the right limb and left limb respectively to complete one gait cycle. In other walking conditions, which were intended to simulate abnormal gait, all participants took longer time to complete one gait cycle. $\overline{T}_{stride}$ increased to maximum value of 1.2487s and 1.2816s for right limb and left limb respectively. This was expected as there was a resistance hindering the lower extremity motions in every gait cycle. More importantly, significant differences in $\overline{T}_{stride}$ can be observed between left limb and right limb. Placing a load on one side of the limbs caused the loaded limb to exhibit greater $\overline{T}_{stride}$ than the non-loaded limb. The discrepancy of $\overline{T}_{stride}$ between the

loaded limb and non-loaded limb was approximately 0.04s. Similar observations were found when participants walked with a sandal on one side of the feet. The affected limb exhibited greater $\overline{T}_{stride}$ than the non-affected limb with difference of approximately 0.03s. ANOVA results of T_{stride}, R_{stance} and R_{swing} are presented in Figure 7.6, Figure 7.7, and Figure 7.8.

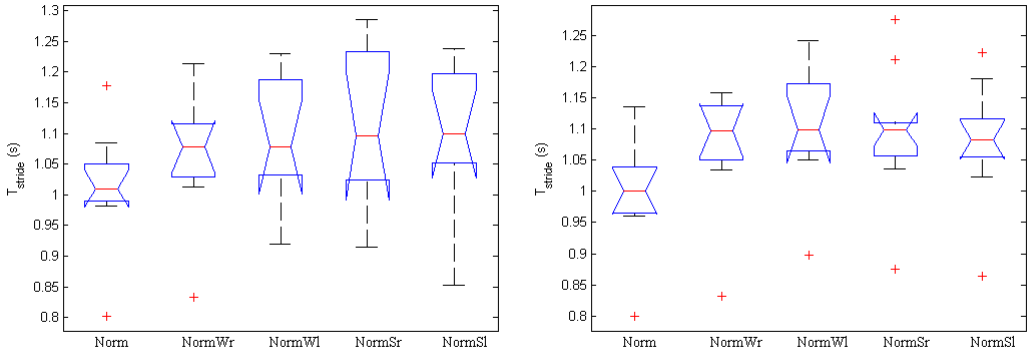

(a) (b)

Figure 7.6 Overground walking T_{stride} (a) right limb; (b) left limb during different walking conditions with $p < 0.01$.

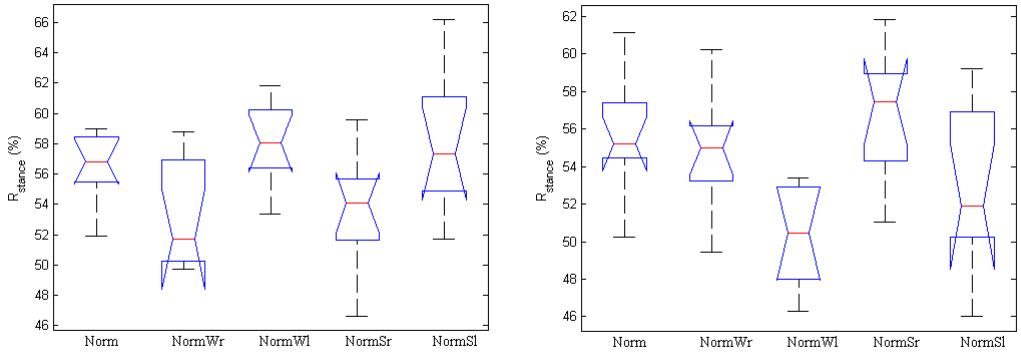

(a) (b)

Figure 7.7 Overground walking R_{stance} (a) right limb; (b) left limb during different walking conditions with $p < 0.01$.

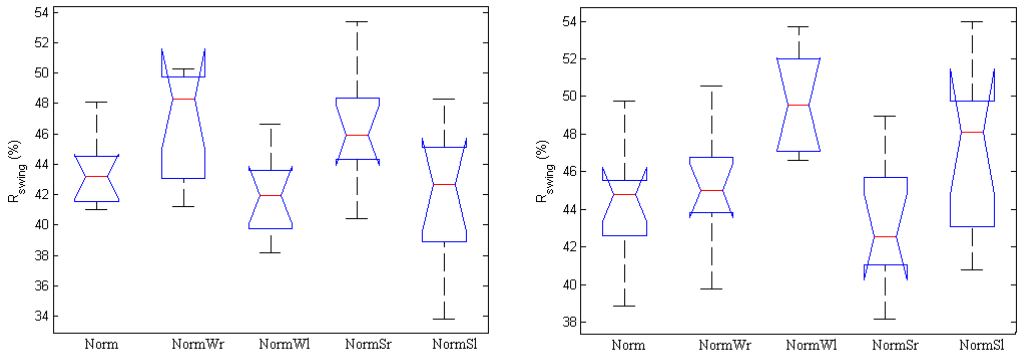

(a) (b)

Figure 7.8 Overground walking R_{swing} (a) right limb; (b) left limb during different walking conditions with $p < 0.01$.

Having determined $\overline{T}_{stride}$, $\overline{T}_{stance}$, and $\overline{T}_{swing}$, mean of R_{stance} ($\overline{R}_{stance}$) and mean of R_{swing} ($\overline{R}_{swing}$) were calculated so that temporal gait parameters obtained from the experimental study can be directly compared with other literatures. When the participants walked over the 10 m walkway with normal posture, $\overline{R}_{stance}$ lasted approximately 60 % whereas $\overline{R}_{swing}$ lasted approximately 40%. These results agreed with findings published in [2]-[3], and [137]-[139]. When the participants walked on the ground with a load placed on one side of the limbs, the loaded limb exhibited smaller $\overline{R}_{stance}$ than the non-loaded limb with difference of approximately 2.5%. It also exhibited greater $\overline{R}_{swing}$ than the non-loaded limb. Similar observations were found when the participants walked on the ground wearing sandal on one side of the foot. The affected limb or limb that wore a sandal on its foot exhibited smaller $\overline{R}_{stance}$ and greater $\overline{R}_{swing}$ than the non-affected limb with difference of approximately 2%.

Table 7.2 Mean temporal gait parameters during treadmill walking

			Norm3	Norm4	Norm5	Norm 3Wr	Norm 4Wr	Norm 5Wr	Norm 3Wl	Norm 4Wl	Norm 5Wl
$\overline{T}_{stride}$ (s)	Right		1.2830	1.1207	1.0189	1.2189	1.1149	1.0332	1.2259	1.1239	1.0349
	Left		1.2066	1.1828	1.0212	1.2197	1.1156	1.033	1.2257	1.1232	1.0344
Stance	Right	$\overline{T}_{stance}$ (s)	0.7513	0.6473	0.5805	0.6333	0.5963	0.5546	0.6952	0.6298	0.5883
		$\overline{R}_{stance}$ (%)	***58.56***	***57.76***	***56.97***	***51.92***	***53.45***	***53.69***	***56.72***	***55.98***	***56.87***
	Left	$\overline{T}_{stance}$ (s)	0.6987	0.6851	0.5839	0.6954	0.6347	0.5768	0.6342	0.5891	0.5673
		$\overline{R}_{stance}$ (%)	***57.91***	***57.92***	***57.18***	***57.05***	***56.93***	***55.83***	***51.73***	***52.42***	***54.82***
Swing	Right	$\overline{T}_{swing}$ (s)	0.5758	0.4734	0.4384	0.5864	0.5193	0.4784	0.5305	0.5423	0.4461
		$\overline{R}_{swing}$ (%)	***41.44***	***42.24***	***43.03***	***48.08***	***46.55***	***46.31***	***43.28***	***44.02***	***43.13***
	Left	$\overline{T}_{swing}$ (s)	0.5079	0.4977	0.4373	0.5235	0.4802	0.4919	0.5917	0.5687	0.4676
		$\overline{R}_{swing}$ (%)	***42.09***	***42.08***	***42.82***	***42.95***	***43.07***	***44.17***	***48.27***	***47.58***	***45.18***

Walking on a treadmill and on the ground are different [91],[137]-[139]. When a person walks on a treadmill, his/her temporal gait parameter, particularly T_{stride} greatly depends on the treadmill speed. Slow walking generally takes longer time to complete one gait cycle. In contrast, fast walking takes shorter time to complete one gait cycle. Similar conditions can be found in Table 7.2. When participants walked on the treadmill at speed of 3 km/h with normal posture, they took an average of 1.2830s and 1.2066s for right limb and left limb to complete one gait cycle. While they walked on a similar treadmill with speed of 5 km/h, $\overline{T}_{stride}$ decreases to 1.0189s and 1.0212s for right limb and left limb respectively. Similar observations were found when the participants walked abnormally with a load placed on one side of the limbs. The slower they walked, the longer they took to complete one gait cycle.

Observing the changes of $\overline{R}_{stance}$ in Table 7.2, it was apparent that the left limb and right limb exhibited similar $\overline{R}_{stance}$ and $\overline{R}_{swing}$ during normal treadmill walking regardless of the walking speeds. However, during other walking conditions, particularly when the participants walked with a load placed on one side of the limbs, the loaded limb exhibited smaller $\overline{R}_{stance}$ than the non-loaded limb. While participants were walking on a treadmill with speed of 3 km/h, $\overline{R}_{stance}$ were found to be 58.56% and 57.91% for right limb and left limb respectively. During similar walking speed, placing a load on left limb caused left limb to experience smaller $\overline{R}_{stance}$ ($\overline{R}_{stance}$ = 51.73%) than right limb ($\overline{R}_{stance}$ = 56.72%). When a load was placed on the right limb, left limb exhibited greater

$\overline{R}_{stance}$ ($\overline{R}_{stance}$ = 57.05%) than the right limb ($\overline{R}_{stance}$ = 51.92%). The opposite effect was found in $\overline{R}_{swing}$ when participants walked with a load placed on one side of the limbs. The loaded limb exhibited greater $\overline{R}_{swing}$ while the non-loaded limb exhibited smaller $\overline{R}_{swing}$. ANOVA results of T_{stride}, R_{stance} and R_{swing} are presented in

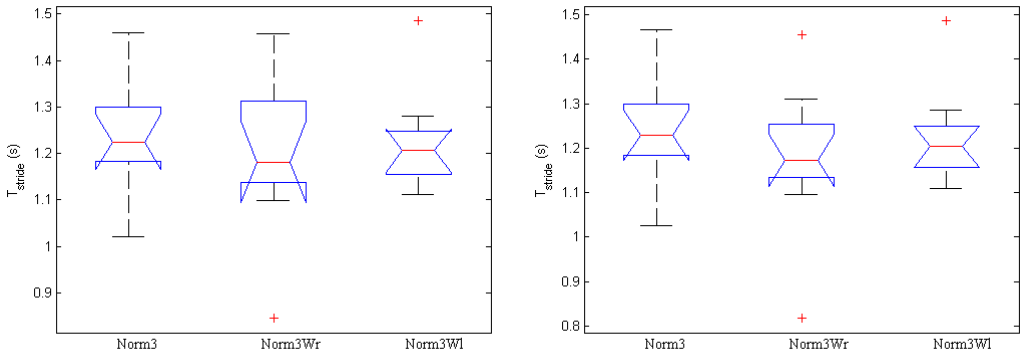

(a) (b)

Figure 7.9 T_{stride} (a) right limb; (b) left limb during treadmill walking at speed of 3 km/h with $p < 0.01$.

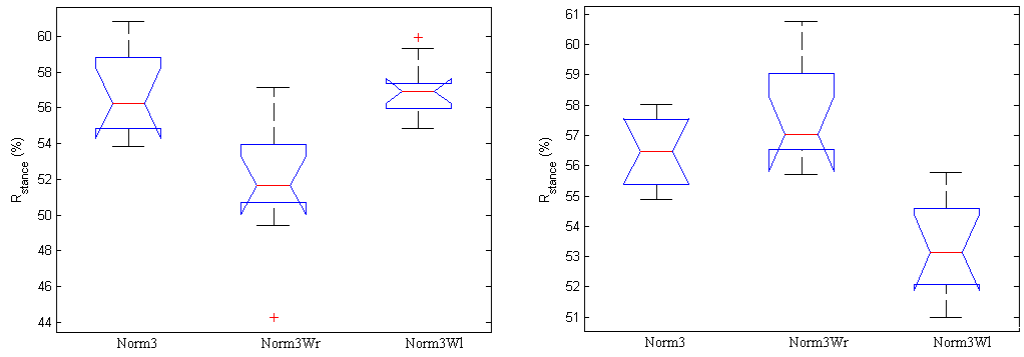

(a) (b)

Figure 7.10 R_{stance} (a) right limb; (b) left limb during treadmill walking at speed of 3 km/h with $p < 0.01$.

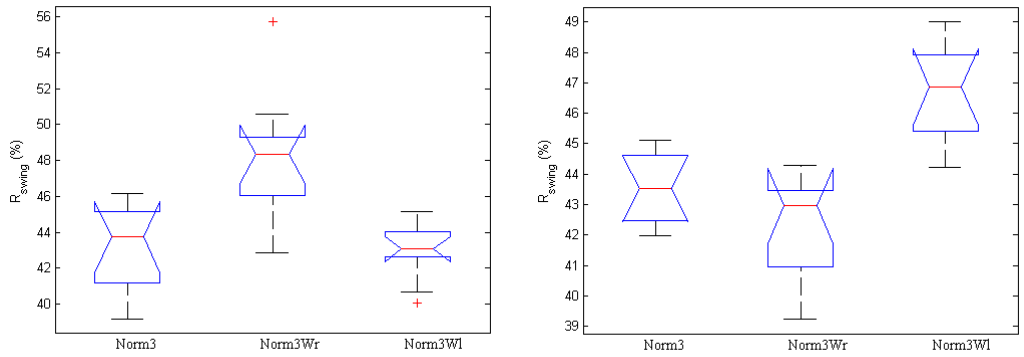

(a) (b)

Figure 7.11 R_{swing} (a) right limb; (b) left limb during treadmill walking at speed of 3 km/h with $p < 0.01$.

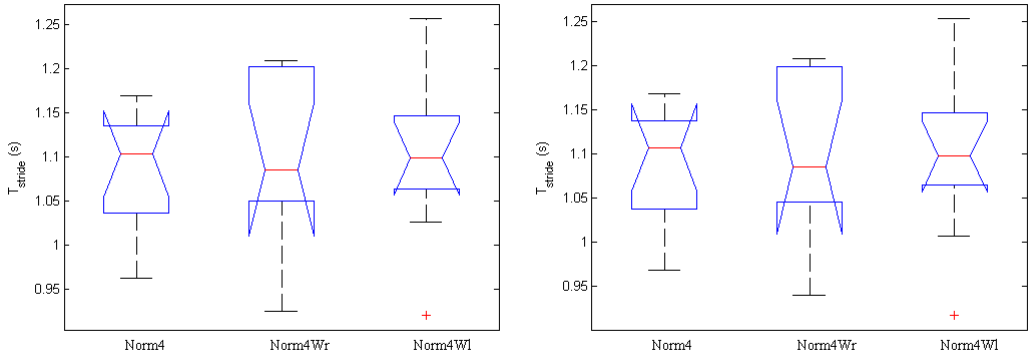

(a) (b)

Figure 7.12 T_{stride} (a) right limb; (b) left limb during treadmill walking at speed of 4 km/h with $p < 0.01$.

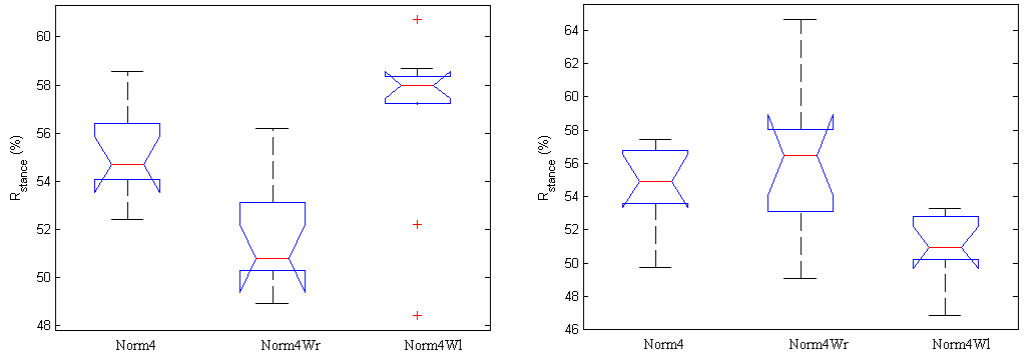

(a) (b)

Figure 7.13 R_{stance} (a) right limb; (b) left limb during treadmill walking at speed of 4 km/h with $p < 0.01$.

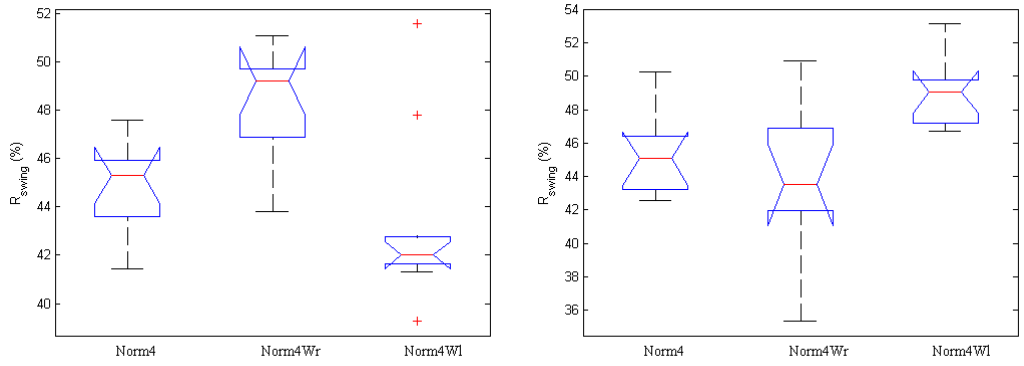

(a) (b)

Figure 7.14 R_{swing} (a) right limb; (b) left limb during treadmill walking at speed of 4 km/h with $p < 0.01$.

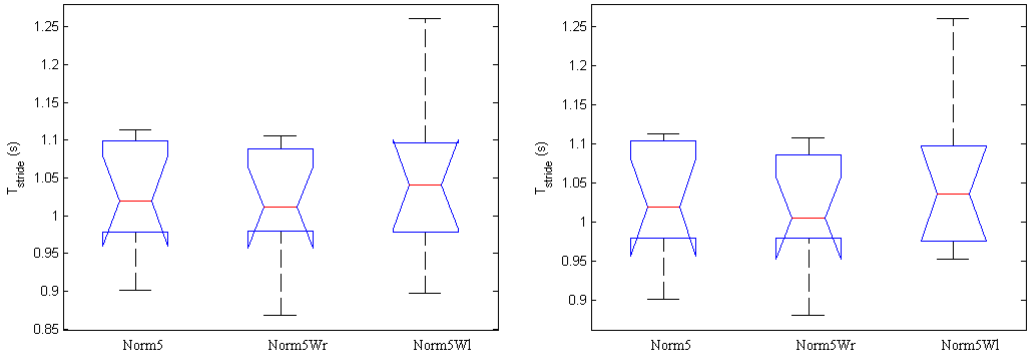

(a) (b)

Figure 7.15 T_{stride} (a) right limb; (b) left limb during treadmill walking at speed of 5 km/h with $p < 0.01$.

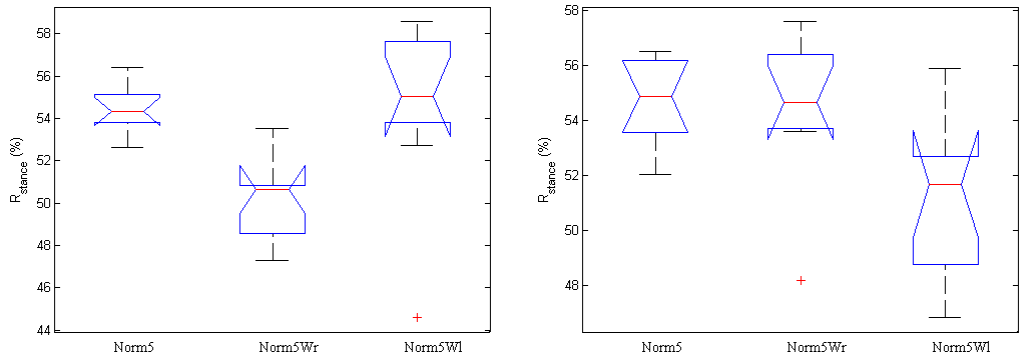

(a) (b)

Figure 7.16 R_{stance} (a) right limb; (b) left limb during treadmill walking at speed of 5 km/h with $p < 0.01$.

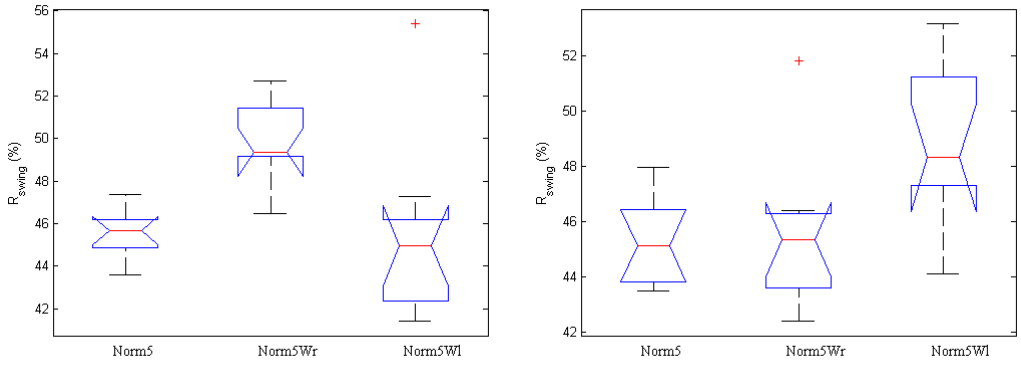

(a) (b)

Figure 7.17 R_{swing} (a) right limb; (b) left limb during treadmill walking at speed of 5 km/h with $p < 0.01$.

As mentioned in previous chapters, *CoD* determines the normality of a person's gait by comparing θ_{thigh} and θ_{shank} against θ_{id_thigh} and θ_{id_shank}. The overall *CoD* experimental results of each body segment i.e. right thigh, right shank, left thigh and left shank are depicted in Figure 7.18 and Figure 7.19. It could be clearly observed that in normal overground and treadmill walking, *CoD* values were close to one ($0.94 < CoD < 1.0$). In contrast, in artificially simulated abnormal gait, *CoD* was less than 0.94. It was also apparent that when participants walked with load placed on one side of the limbs or when they walked with a sandal on one side of the feet, the affected limb i.e. thigh and shank exhibited lower *CoD*. Lower *CoD* signified that the movement patterns of the participants' thigh and shank were different from movement patterns of thigh and shank of a healthy individual. These differences are illustrated in Figure 7.2, Figure 7.3, Figure 7.4, and Figure 7.5.

On the other hand, non-affected limb exhibited *CoD* that were close to one. Although only minor differences between the participants' lower extremity motion and the ideal lower extremity motions were found on this limb, these results were expected because the inertial property of the non-affected limb was not altered significantly and there was no abnormality encumbering its motion during walking. Statistical test results revealed that significant difference between the affected limb and non-affected limb was less than 0.01. Based on Tukey-kramer test results, when the participants walked on the ground and/or on the treadmill, the affected limb exhibited *CoD* value that was approximately 0.90 whereas the non-affected limb exhibited greater *CoD* ($CoD \approx 0.95$).

These experimental results demonstrated the capability of *CoD* in distinguishing normal and abnormal gait. They also established normative *CoD* data for normal overground and treadmill walking. Lastly, these results also indicated that this system was able to determine *CoD* periodically without disrupting real-time data streaming.

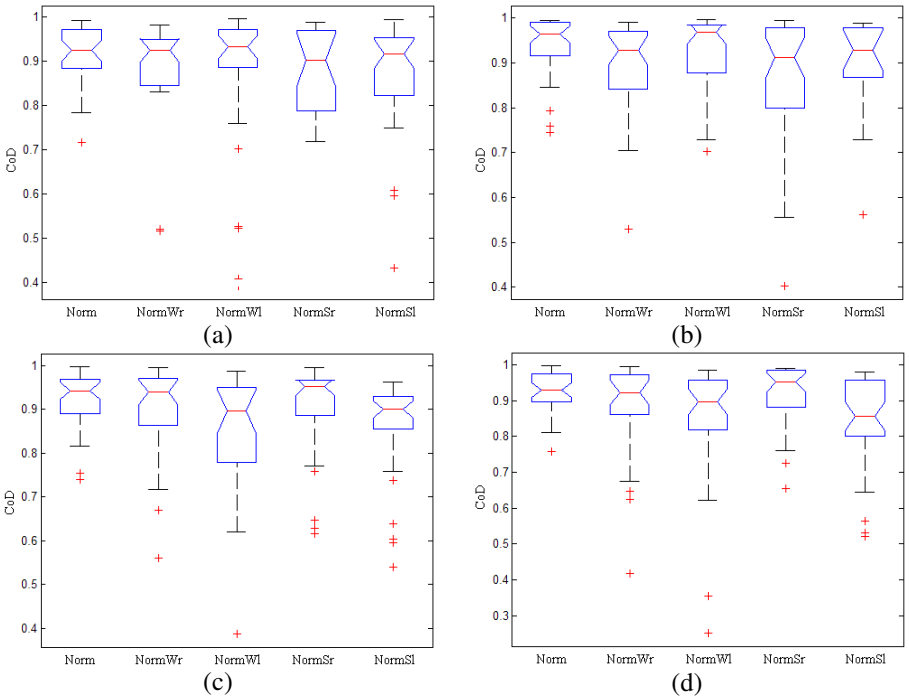

Figure 7.18 *CoD* of (a) Right thigh (b) Right shank (c) Left thigh (d) Left shank during different overground walking conditions.

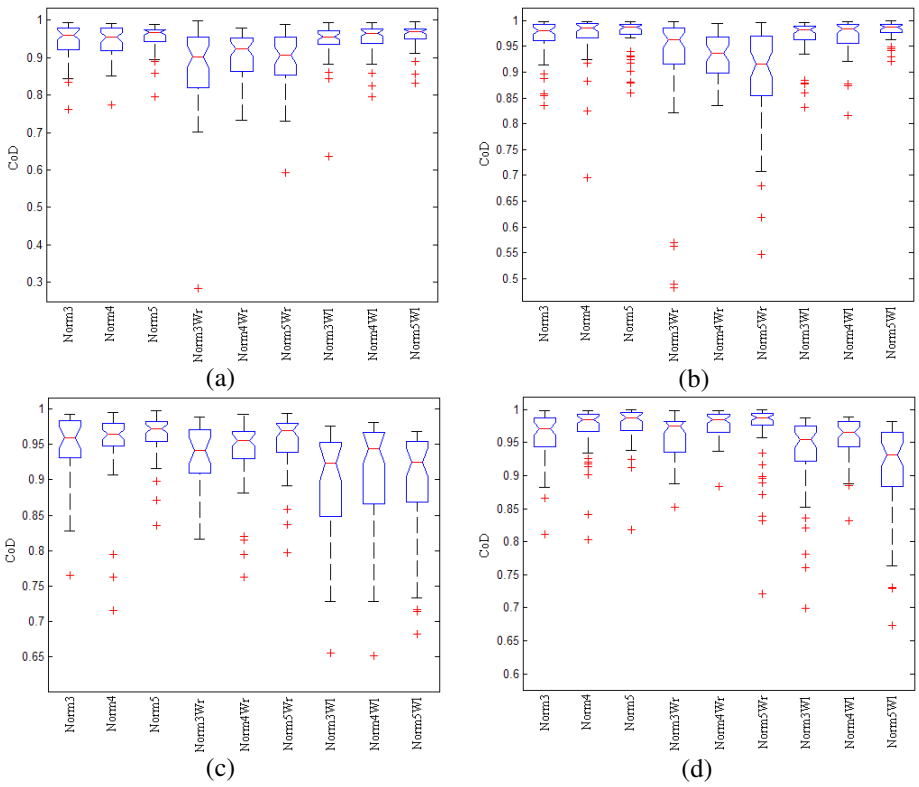

Figure 7.19 *CoD* of (a) Right thigh (b) Right shank (c) Left thigh (d) Left shank during different treadmill walking conditions.

7.3 3-D walking Animation

Simulating a 3-D walking animation allows clinicians and researchers to visually examine a person's gait. For experienced personnel in biomechanics and gait analysis, this feature helps them to determine whether the subject has normal and healthy gait. It also allows them to examine whether patient rehabilitation program has progressed well. In this thesis, 3-D animation of the lower extremity was successfully replicated using basic stick figure and the estimated orientations of the lower extremity. Screenshots of the 3-D animation of Participant A's walking movements are shown in Figure 7.20.

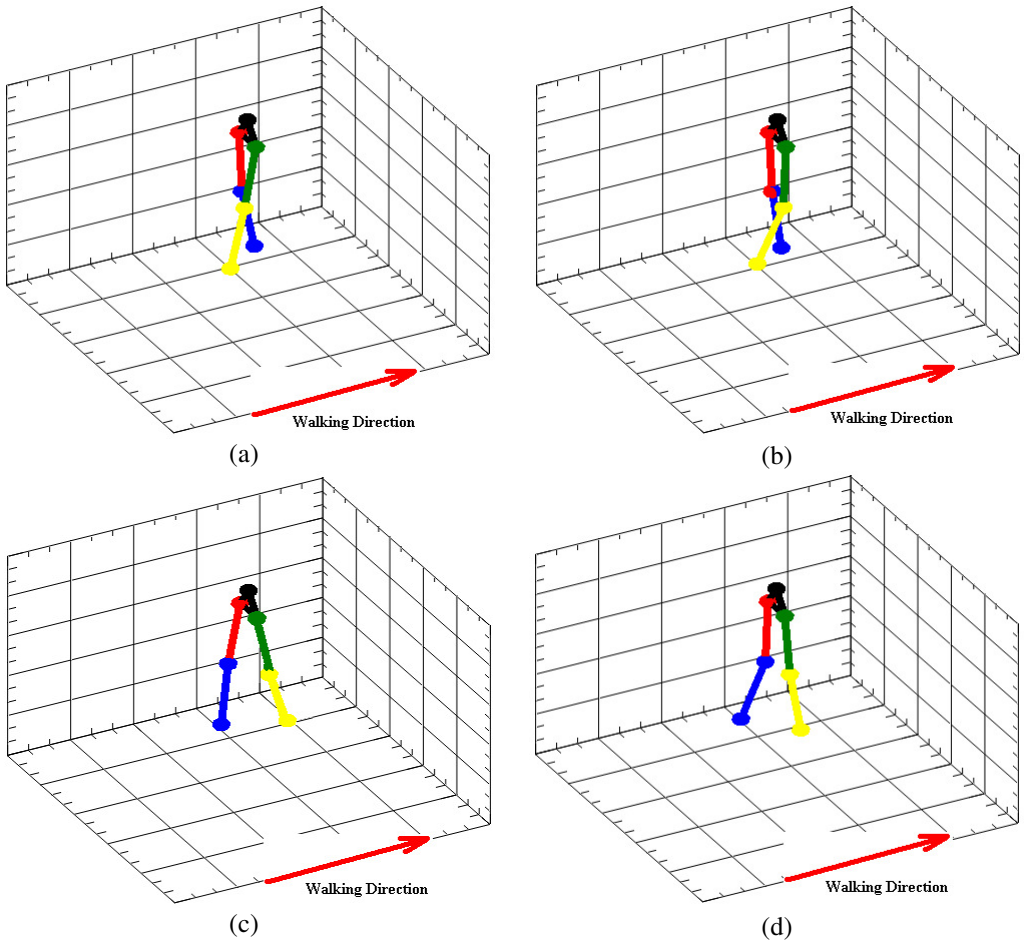

Figure 7.20 3-D animation of Participant A's walking movements during: (a) Mid-stance (b) Toe-off (c) Heel-strike (d) Mid-swing.

7.4 Gait Asymmetry Experimental Results

7.4.1 Normalized Cross-correlation (Cc_{norm}) Experimental Results

Cc_{norm} provides a discrete measure that signifies the similarity of angular rate waveforms generated by the left and right limbs in walking. Cc_{norm} results collected from the overground walking experiments are compiled and presented in Figure 7.21 and Figure 7.22. Experimental results from the treadmill walking are depicted in Figure 7.23 and Figure 7.24.

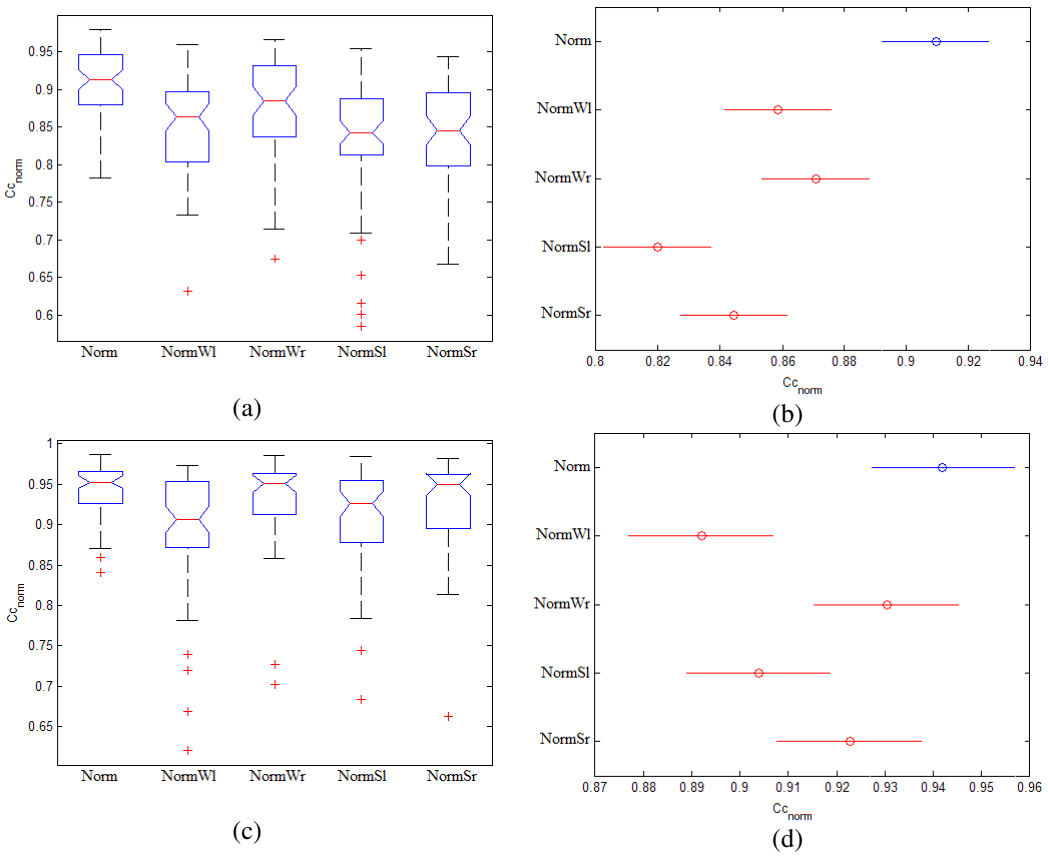

Figure 7.21 (a) $Cc_{norm\text{-}thigh}$ during overground walking conditions with (b) Tukey-Kramer comparison test result; (c) $Cc_{norm\text{-}shank}$ during different overground walking conditions with (d) Tukey-Kramer comparison test result.

When the participants walked on the ground, Cc_{norm} were close to one. However, when the participants walked with a load placed on one side of the limbs or with a sandal on one foot, asymmetrical gait was simulated. Experimental results indicated that asymmetrical gait had $Cc_{norm\text{-}thigh}$ of less than 0.9 and $Cc_{norm\text{-}shank}$ of less than 0.95. This was anticipated as significant bilateral differences existed in the lower extremity motion. These findings agreed with results depicted in Figure 7.2, Figure 7.3, Figure

7.4, and Figure 7.5. The larger the bilateral difference, the lower the Cc_{norm} value was. ANOVA test result indicated significant difference (p <0.01) in Cc_{norm} under different walking conditions. Tukey-Kramer comparison test revealed that $Cc_{norm\text{-}thigh}$ was able to clearly distinguish the differences between symmetrical and asymmetrical gait, except when asymmetrical gait was induced by placing a load on the left limb. This incident might happen because participants' neuromuscular system performed better in minimizing gait asymmetry when a load was placed on the left limb.

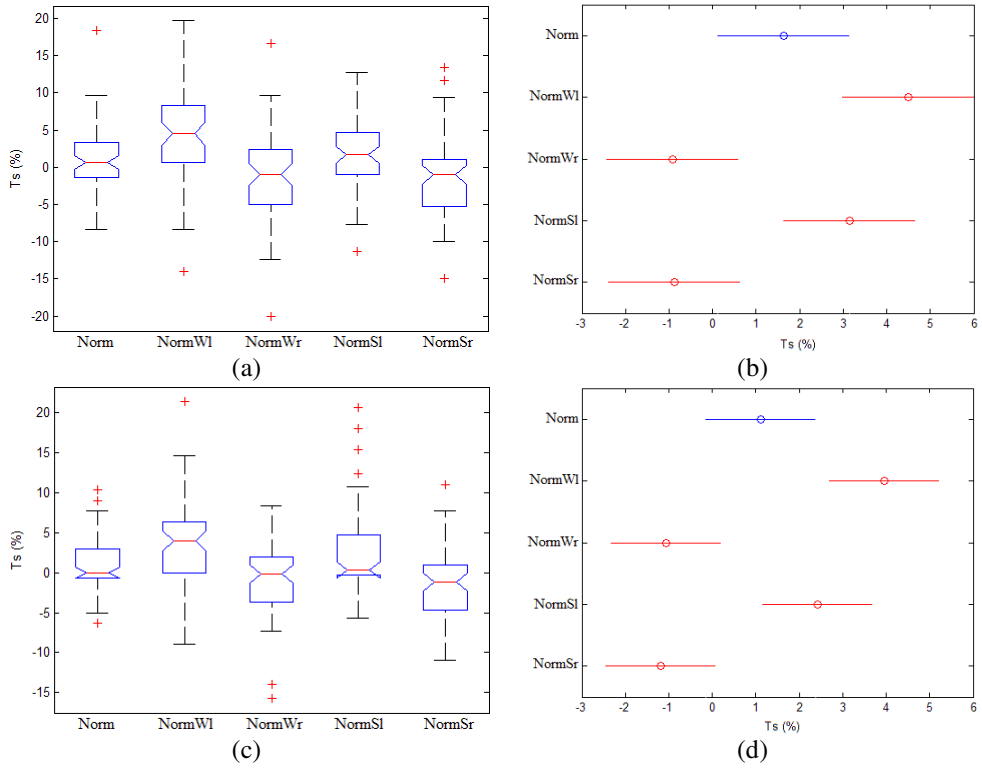

Figure 7.22 (a) Ts_{thigh} during different overground walking conditions with (b) Tukey-Kramer comparison test result; (c) Ts_{shank} during different overground walking conditions with (d) Tukey-Kramer comparison test result.

In contrast to Cc_{norm}, $|Ts|$ increased when the participants walked abnormally (Figure 7.22). In normal walking, Ts has average value of approximately 1.20% gait cycle for both thigh and shank. However, greater Ts was found in asymmetrical gait. This was predictable as timing differences existed in asymmetrical gait. ANOVA test result revealed that there was a significant difference in Ts_{thigh} (p<0.01) and Ts_{shank} (p<0.01). Tukey-Kramer comparison test indicated that Ts_{thigh} and Ts_{shank} in normal walking was statisically different from walking with a load placed on the left limb, as observed in Figure 7.22(b) and Figure 7.22(d). Furthermore, when left limb motion was

affected (a load was placed on the left limb or left foot wear a sandal), *Ts* was positive. On the contrary, *Ts* was negative when right limb motion was affected.

Similar observations of Cc_{norm} and *Ts* were found when the participants walked on a treadmill. Regardless of the walking speeds, Cc_{norm} was close to one (Figure 7.23) when participants walked with normal posture. However, when the participants walked with a load placed on one side of the limbs, Cc_{norm} decreased and it was found to be less than 0.93 and 0.96 on thigh and shank respectively. ANOVA test revealed that there were significant differences between symmetrical and asymmetrical gait ($p<0.01$). Tukey-Kramer test result indicated that $Cc_{norm\text{-}thigh}$ was greater than 0.93 and $Cc_{norm\text{-}shank}$ was greater than 0.965 in symmetrical gait. it also revealed that $Cc_{norm\text{-}thigh}$ was less than 0.93 and $Cc_{norm\text{-}shank}$ was greater than 0.96 in asymmetrical gait.

Significant difference was also found in *Ts* ($p<0.01$) when the participants walked on the treadmill with a load placed on one side of the limbs. When participants walked normally on a treadmill, *Ts* were found to be greater than -2% gait cycle and less than 2% gait cycle. On the contrary, when a load was placed on left limb, *Ts* were found to be ranging from 2% to 5% of the gait cycle. When the right limb was loaded, *Ts* varied between -2% to -5% of the gait cycle. Tukey-Kramer comparison test results revealed that when a load was placed on left limb, *Ts* should be greater than zero and when a load was place on the right limb, *Ts* should be less than zero.

The experimental results demonstrated the capability of Cc_{norm} and *Ts* in distinguishing symmetrical and asymmetrical gait. They also established normative data of Cc_{norm} and *Ts* for overground walking and treadmill walking. Lastly these results also showed that asymmetrical gait induced by placing a load on one limb and by wearing a sandal on one foot was reflected in Cc_{norm} and *Ts*.

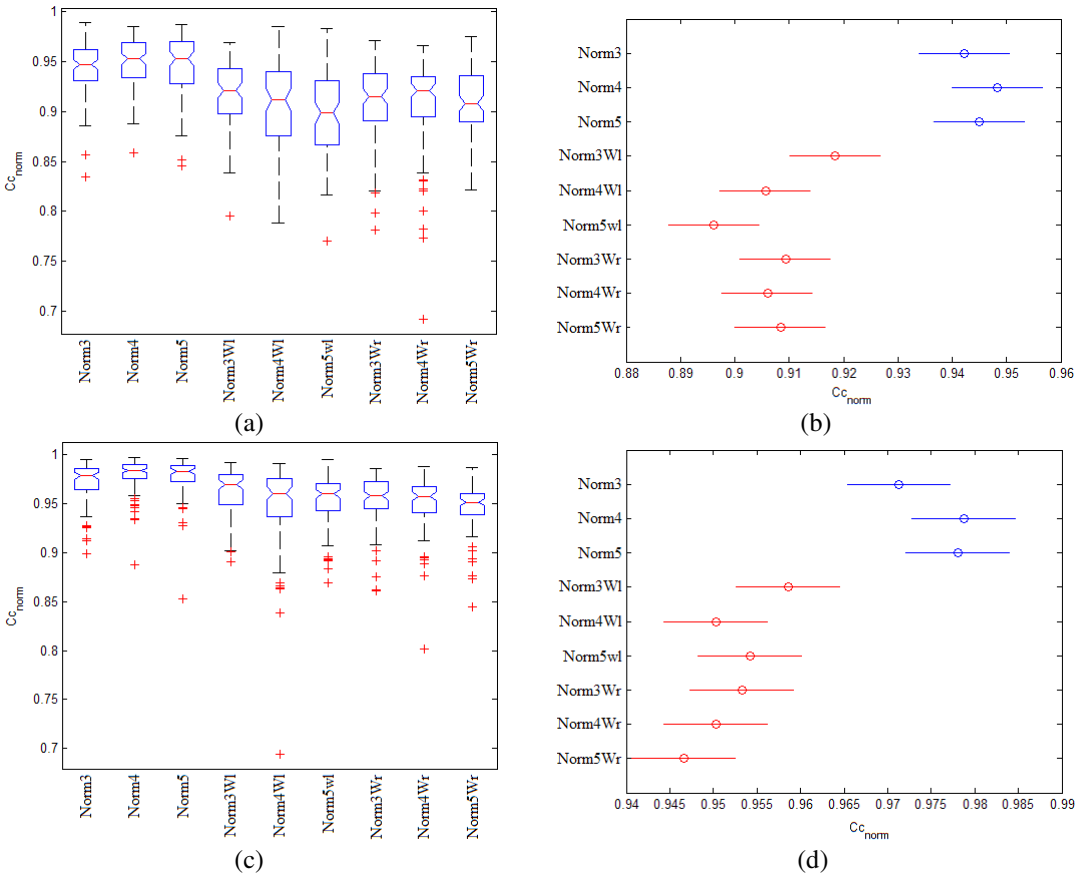

Figure 7.23 (a) $Cc_{norm\text{-}thigh}$ during different treadmill walking conditions with (b) Tukey-Kramer comparison test result; (c) $Cc_{norm\text{-}shank}$ during different treadmill walking conditions with (d) Tukey-Kramer comparison test result.

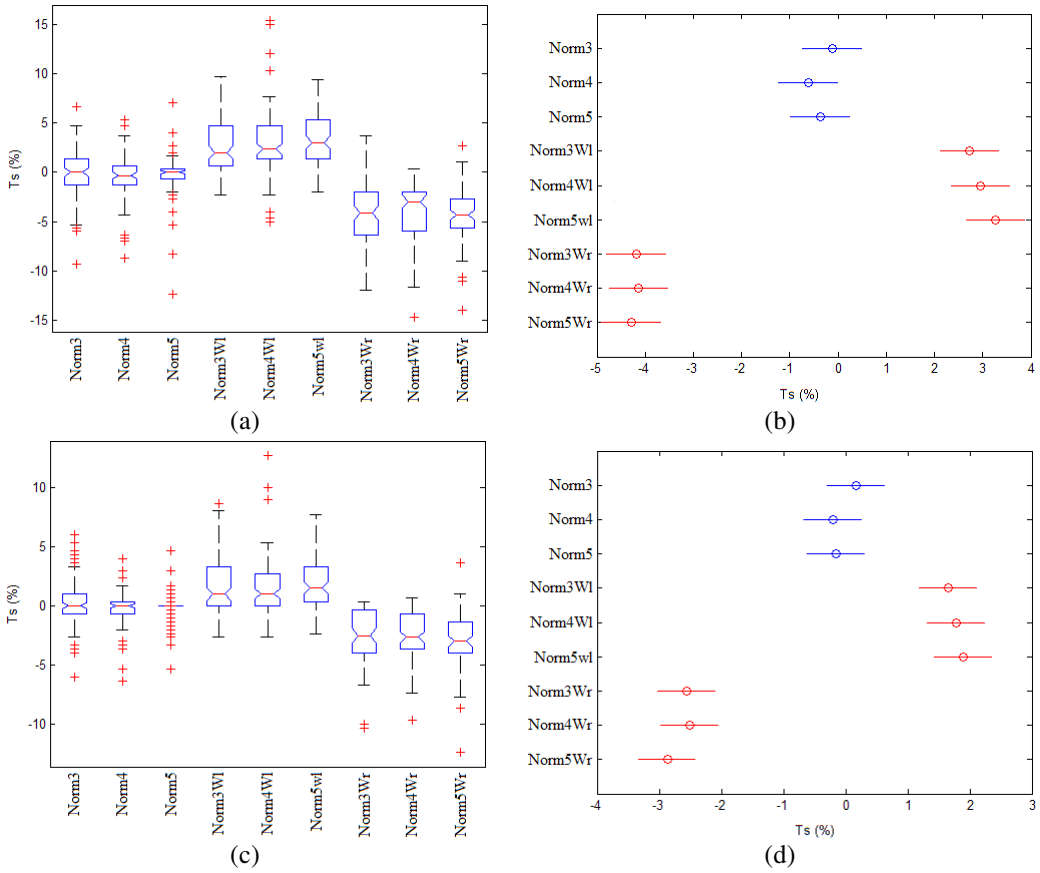

Figure 7.24 (a) Ts_{thigh} during different treadmill walking conditions with (b) Tukey-Kramer comparison test result; (c) Ts_{shank} during different treadmill walking conditions with (d) Tukey-Kramer comparison test result.

7.4.2 Symmetry Index for Duration of Stride (SI_{stride}), Stance Phase (SI_{stance}) and Swing Phase (SI_{swing})

Participants' SI_{stride}, SI_{stance} and SI_{swing} are presented in Figure 7.25 and Figure 7.26. Figure 7.25 shows that in average, SI_{stride} ranges between ±5% during normal overground walking. This was expected as there was no resistance encountered by the limb. These results agreed with findings presented in Table 7.1. On the contrary, when participants walked with a load placed on one side of the limbs or sandal on one side of the feet, $|SI_{stride}|$ was slightly larger than 5%.

Similar observations were found in SI_{stance} and SI_{swing}. When participants walked normally on the ground, SI_{stance} and SI_{swing} ranged between ±10%. These results were consistent with results compiled in Table 7.1. However, when there was a resistance encumbering thigh and shank movements, greater $|SI_{stance}|$ and $|SI_{swing}|$ were found. $|SI_{stance}|$ was found having maximum value of 35% whereas $|SI_{swing}|$ had a maximum value of 40%

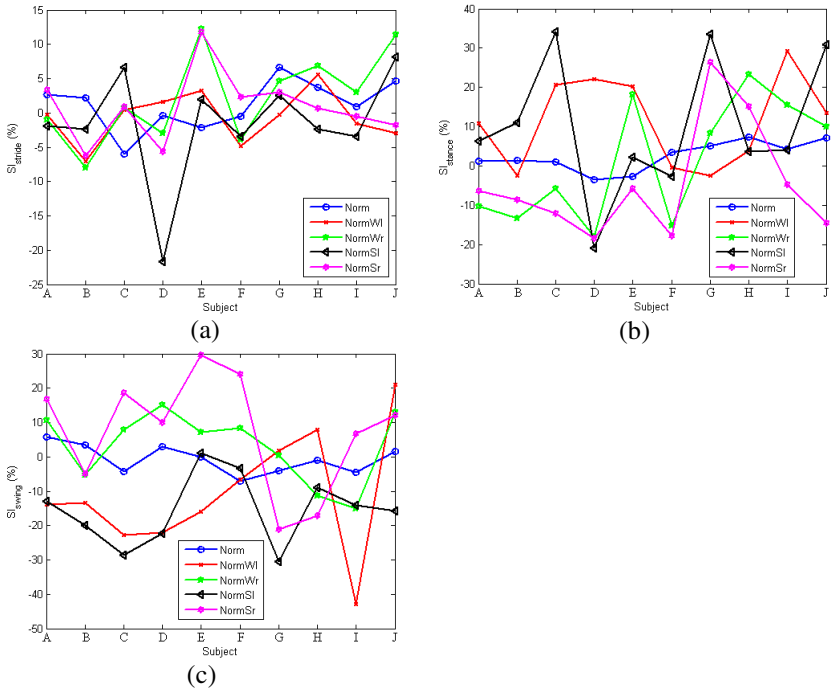

Figure 7.25 (a) SI_{stride} (b) SI_{stance} (c) SI_{swing} on different overground walking conditions.

For clarity of this thesis, only 4 Km/h treadmill walking experimental results are compiled and presented in Figure 7.26. Based on Figure 7.26(a), SI_{stride} was fairly consistent regardless of the walking conditions. It fluctuated between -1.2% and 0.6%.

These values were significantly smaller than SI_{stride} found in overground walking. Nevertheless, this was expected as the participants had to walk on a speed similar to the treadmill speed. Similar SI_{stride} were found when participants walked on the treadmill at speed of 3 Km/h and 5 Km/h.

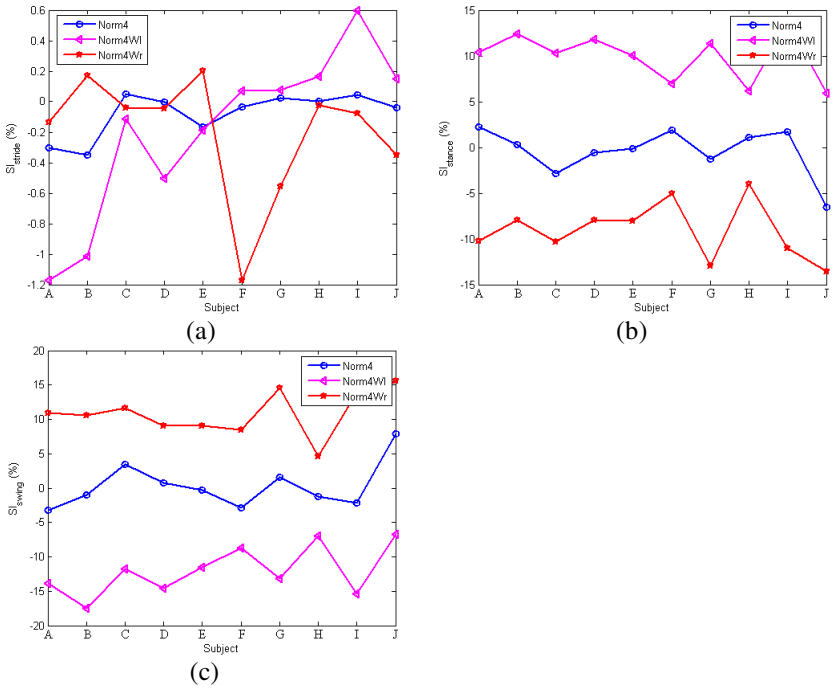

Figure 7.26 (a) SI_{stride} (b) SI_{stance} (c) SI_{swing} on different treadmill walking conditions.

Despite the consistency found in SI_{stride}, SI_{stance} and SI_{swing} generated greater magnitude when load was placed on one side of the limbs (Figure 7.26(b) and Figure 7.26(c)). SI_{stance} was found to be less than -5% and SI_{swing} was greater than 5% when load was placed on the right limb. When the load was placed on the left limb, SI_{stance} was greater than 5% and SI_{swing} was less than -5%. These results agreed with findings presented in Table 7.2, which reported that T_{stance} of the loaded limb were less than T_{stance} of the non-loaded limb and T_{swing} of the loaded limb were greater than T_{swing} of the non-loaded limb. These differences caused SI_{stance} to be less than zero and SI_{swing} to be greater than zero when a load was placed on the right limb. On the contrary, SI_{stance} were greater than zero and SI_{swing} were less than zero when a load was placed on the left limb. Similar SI_{stance} and SI_{swing} were found when participants walked at different walking speeds i.e. 3 Km/h and 5 Km/h.

7.4.3 Normalized Symmetry Index (SI_{norm}) in Different Walking Conditions

Figure 7.27 demonstrates the variation of SI_{norm} over one complete gait cycle in normal overground walking. It could be observed that $SI_{norm\text{-}thigh}$ and $SI_{norm\text{-}shank}$ exhibited different magnitudes at different gait phases. Maximum $SI_{norm\text{-}thigh}$ occurred during pre-swing (50% - 60% gait cycle) whereas maximum $SI_{norm\text{-}shank}$ occurred during initial swing (65% - 75% gait cycle). During the rest of the gait phases, SI_{norm} varied between ±15%.

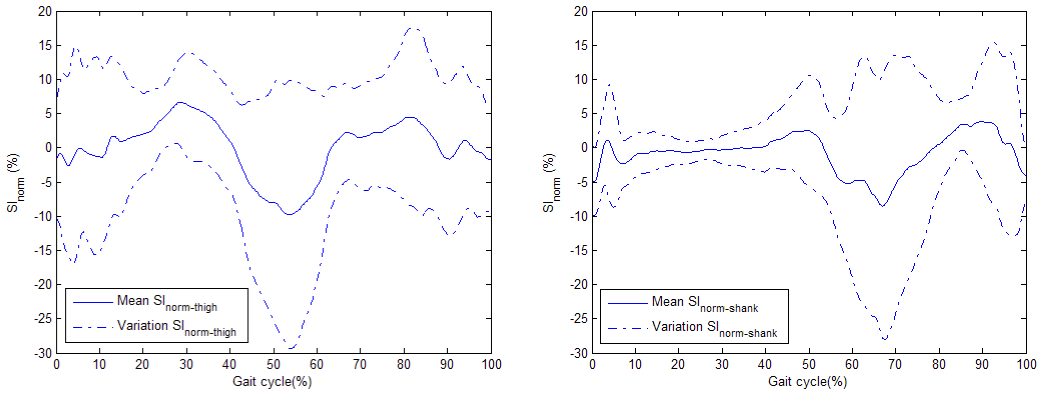

(a) (b)

Figure 7.27 SI_{norm} during normal overground walking: (a) $SI_{norm\text{-}thigh}$ (b) $SI_{norm\text{-}shank}$.

When asymmetrical gait was induced by placing a load on one side of the limbs, $SI_{norm\text{-}thigh}$ and $SI_{norm\text{-}shank}$ exhibited unique waveforms that were different from normal overground walking (Figure 7.28). When loading one side of the limbs, thigh exhibited greatest SI_{norm} during four different gait phases: loading response (0% - 10% gait cycle), pre-swing (45% - 55% gait cycle), mid-swing (75% - 85% gait cycle) and terminal swing (90% - 100% gait cycle). At the same time, shank exhibited greatest SI_{norm} during the initial swing (60% - 70% gait cycle). It is important to highlight that regardless of the loading side, SI_{norm} exhibited similar waveform but opposite in sign. This behavior is one of the merits possessed by SI_{norm}. Asymmetry found in healthy individuals (Figure 7.15 and Figure 7.18) is mainly caused by the difference in the left and right lower extremity motions during walking. Detailed descriptions of its merits are presented in Chapter 8.4.3. The location of the sensors on both legs will not create any asymmetry.

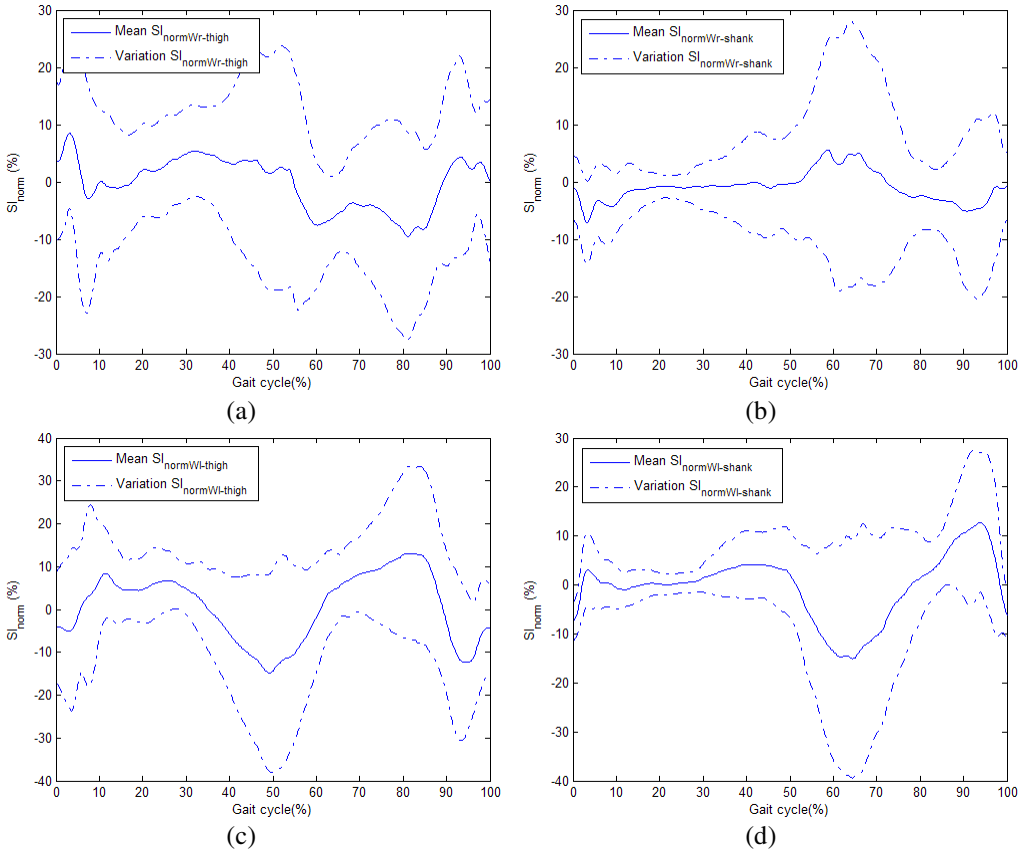

Figure 7.28 SI_{norm} during single limb loaded overground walking (a) $SI_{norm\text{-}thigh}$ while loading right limb (b) $SI_{norm\text{-}shank}$ while loading right limb (c) $SI_{norm\text{-}thigh}$ while loading left limb (d) $SI_{norm\text{-}shank}$ while loading left limb.

When asymmetrical gait was induced by wearing a sandal on one foot, thigh and shank also exhibited unique SI_{norm} (Figure 7.29). Thigh exhibited the greatest bilateral differences at two different gait phases: loading response (0% - 10% gait cycle) and pre-swing (45% - 55% gait cycle). Accordingly, shank exhibited the greatest bilateral differences during initial swing (60% - 70% gait cycle). Similar to previous findings, SI_{norm} exhibited similar waveform with opposite sign when sandal was worn on the opposite side.

Unlike overground walking, treadmill walking generated a more consistent $SI_{norm\text{-}thigh}$ (Figure 7.30). $SI_{norm\text{-}thigh}$ was ranging between ±5% throughout the gait cycle. However, $SI_{norm\text{-}shank}$ did not exhibit similar behaviour. $SI_{norm\text{-}shank}$ exhibited relatively larger magnitude during initial swing (65% - 75% gait cycle) and terminal swing (90% - 100% gait cycle). Similar waveforms were found in $SI_{norm\text{-}shank}$ regardless of the walking environments i.e. overground walking and treadmill walking.

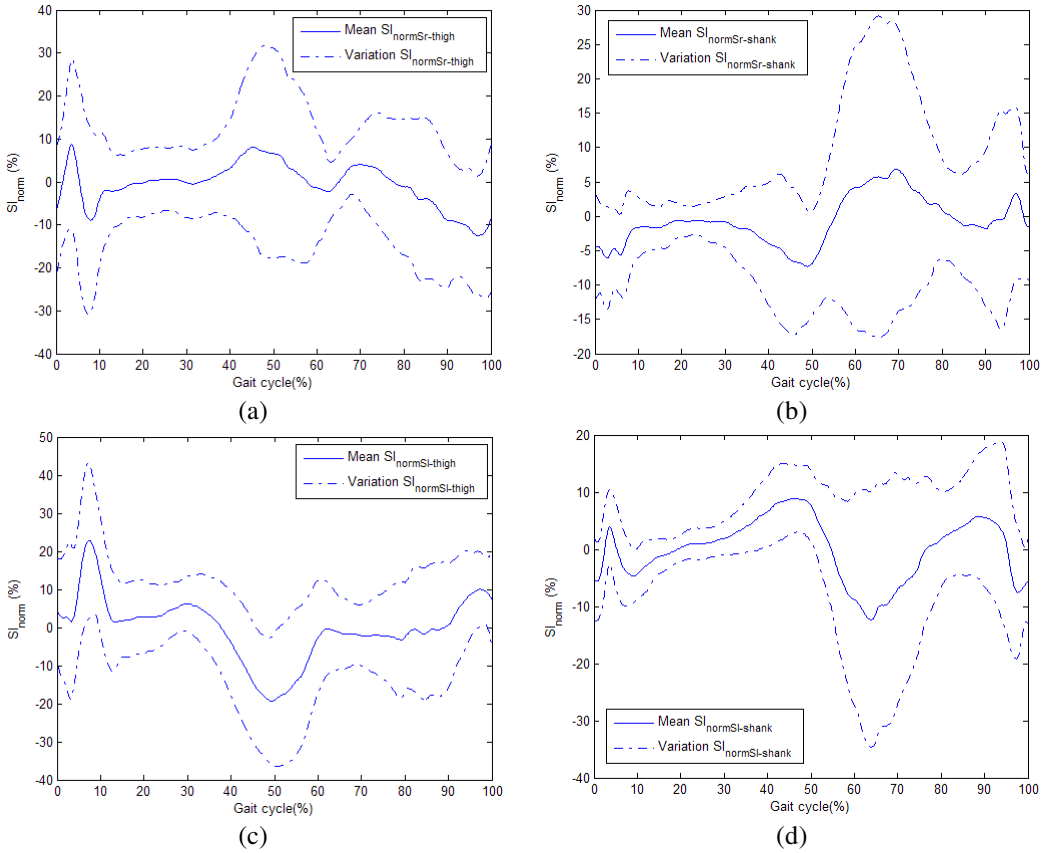

Figure 7.29 SI_{norm} during overground walking with sandal on one side of the feet: (a) $SI_{norm\text{-}thigh}$ with sandal on right foot (b) $SI_{norm\text{-}shank}$ with sandal on right foot (c) $SI_{norm\text{-}thigh}$ with sandal on left foot (d) $SI_{norm\text{-}shank}$ with sandal on left foot.

Walking on the treadmill with load placed on one side of the limbs generated unique waveform on $SI_{norm\text{-}thigh}$ and $SI_{norm\text{-}shank}$ (Figure 7.31). Participants experienced gait asymmetry during several gait phases. Thigh exhibited the largest asymmetry during mid-stance (10% gait cycle), pre-swing (45% - 55% gait cycle), mid-swing (75% - 85% gait cycle) and terminal swing (90% - 100% gait cycle). Shank exhibited the largest asymmetry during 60% - 70% of the gait cycle.

These experimental results demonstrated capability of SI_{norm} in defining gait asymmetry. These results also established normative data for overground walking and treadmill walking. More importantly, these results showed that SI_{norm} did not suffer from the artificial inflation and it was able to determine gait asymmetry throughout the gait cycle.

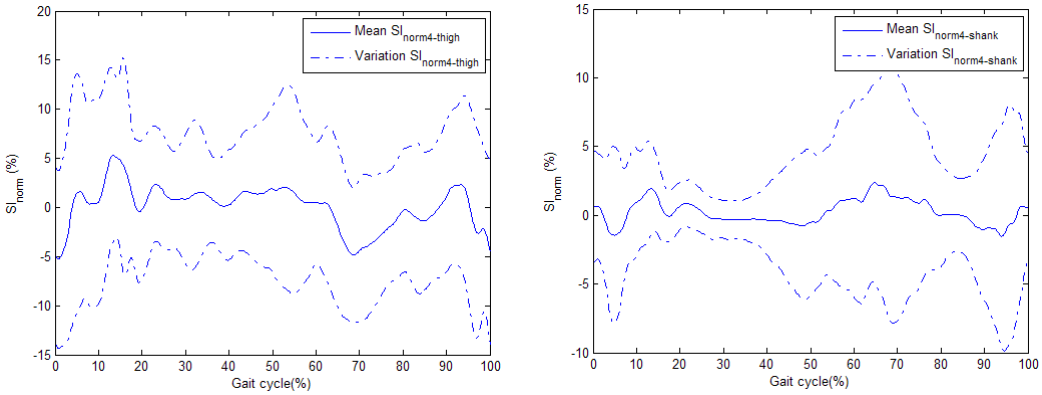

(a) (b)

Figure 7.30 SI_{norm} during normal treadmill walking: (a) $SI_{norm\text{-}thigh}$ (b) $SI_{norm\text{-}shank}$.

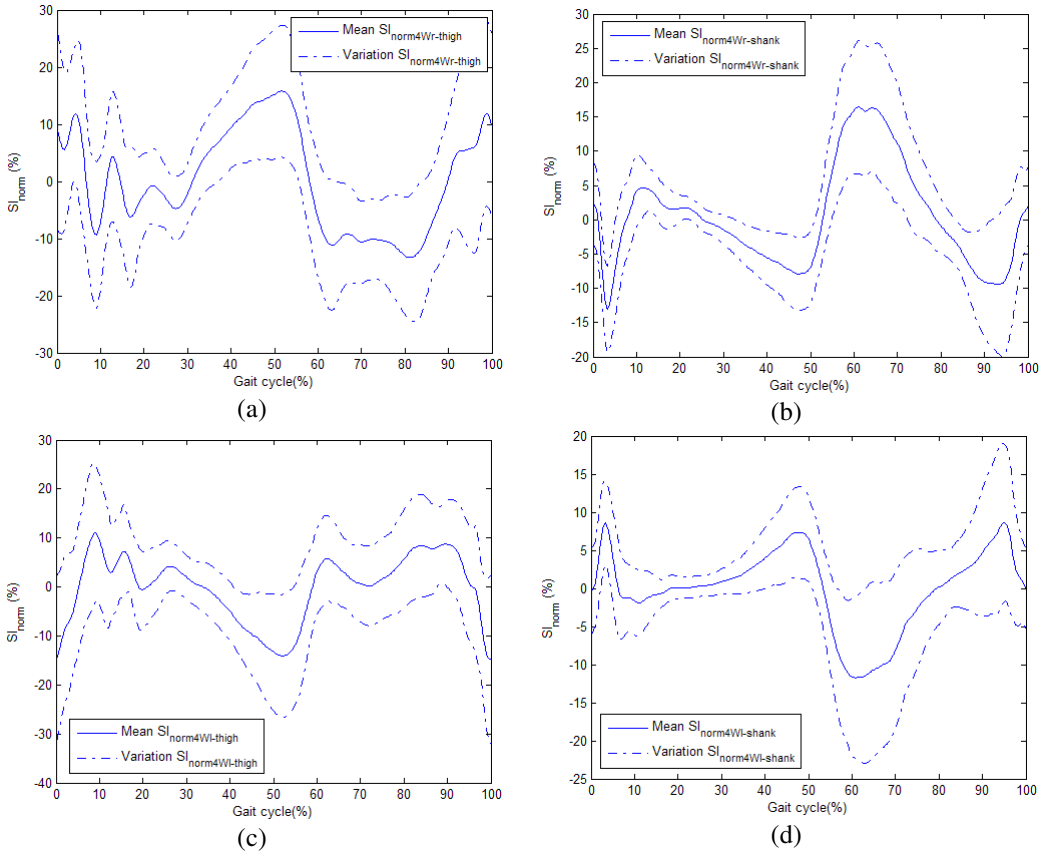

Figure 7.31 SI_{norm} during single limb loaded treadmill walking: (a) $SI_{norm\text{-}thigh}$ while loading right limb (b) $SI_{norm\text{-}shank}$ while loading right limb (c) $SI_{norm\text{-}thigh}$ while loading left limb (d) $SI_{norm\text{-}shank}$ while loading left limb.

7.5 Maximum Lyapunov Exponent (λ*) Experimental Results

Since 30 consecutive strides were required to estimate λ_S^* and λ_L^*, only experimental results carried out on the treadmill are presented in this thesis (Figure 7.32 and Figure 7.33). One of the significances of these experimental results is the linear relationship between walking speed and λ_S^*. When participants walked at speed of 3 km/h, λ_S^* for thigh and shank were ranging from ≈0.30 to ≈0.44 and from ≈0.63 to ≈0.74 respectively. When the participant walked at speed of 5 km/h, thigh λ_S^* increased and were found to be ranging from ≈0.30 to ≈0.45. Shank λ_S^* also increased and were calculated to be ranging from ≈0.75 to ≈0.87. Similar observations were found in other experimental results, particularly when

participants walked with a load placed on one side of the limbs. These findings were consistent with the results reported in [85],[98],[153].

However, when a load was placed on one side of the limbs, the loaded limb exhibited smaller λ_S^* whereas the non-loaded limb exhibited greater λ_S^*. These results were expected as over short period of time, particularly during the first few strides, participants' neuromuscular locomotor system tried to maintain walking stability despite the significant differences between left limb and right limb inertial properties. One way ANOVA test result revealed the statistical difference of λ_S^* in different walking conditions was less than 0.01.

In contrast to λ_S^*, λ_L^* exhibited different behavior. λ_L^* were similar in all treadmill walking experiments and no statistical differences were found in λ_L^* ($p>0.01$). These were anticipated as treadmill walking could reduce gait variability and improved gait dynamic stability [91]. More importantly, over long period of time, the participants' neuromuscular locomotor systems might have accustomed to the load placed on either side of the limb. Thus, they did not encounter much difficulty in maintaining walking stability. These results agreed with findings reported in [94],[99].

It is important to note that by comparing similar walking speeds, (Figure 7.32(a) and Figure 7.33(a)), one can notice that λ_S^* and λ_L^* found in thigh was smaller than λ_S^* and λ_L^* found in shank ($p<0.01$).These results were expected as the superior body segment i.e. thigh was less sensitive to small perturbations, thus its motion was more stable than the inferior body segment i.e. shank. These results were consistent with findings reported in [98]-[99].

From the experimental results, it can be deduced that instead of kinematic parameters collected from accelerometer [91],[94] and optical motion capture system[92]-[93],[97]-[102], gyroscope output i.e. angular rate can also be used as the main variable. Additionally, these results also established normative data to estimate dynamic stability using gyroscope outputs.

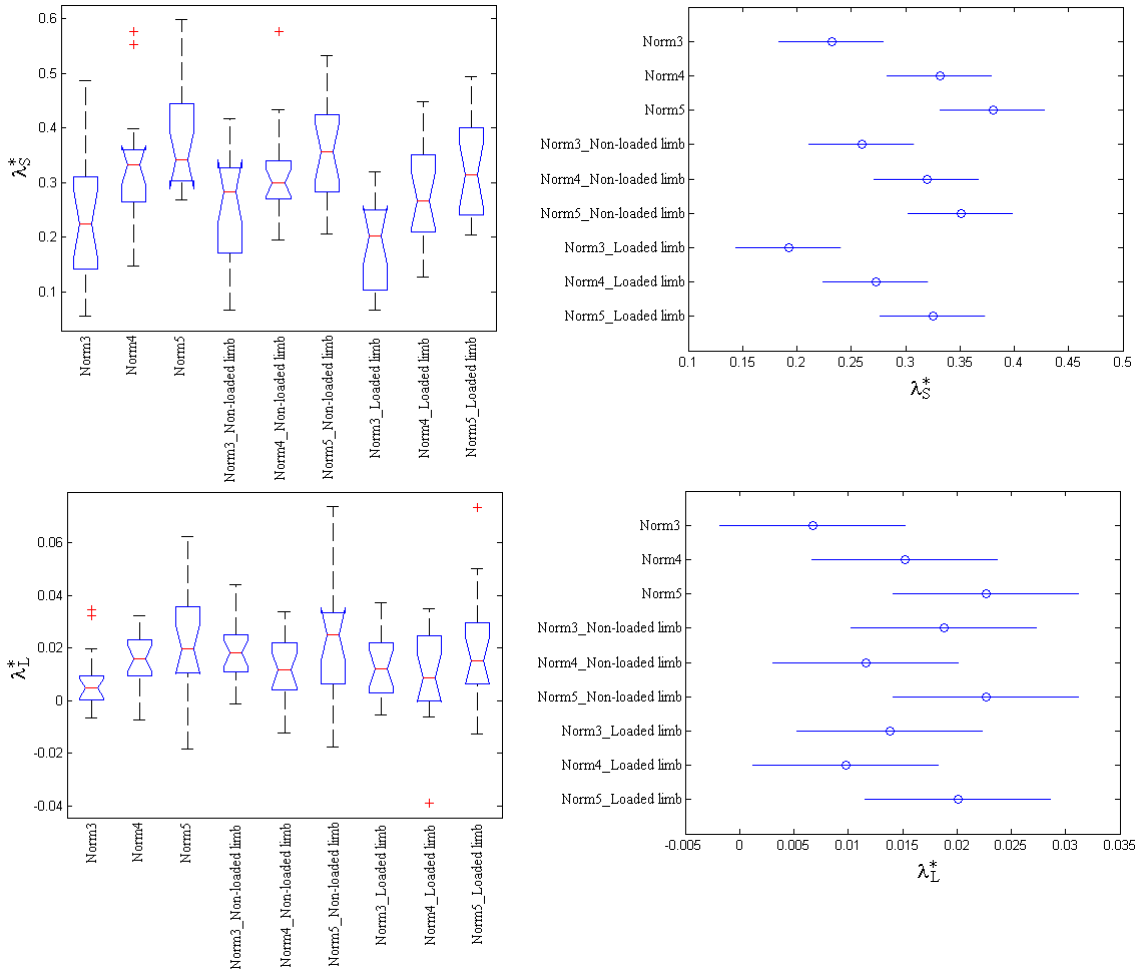

Figure 7.32 (a) Experimental results of thigh λ_S^* with (b) Tukey-Kramer comparison test result; (c) Experimental results of thigh λ_L^* with (d) Tukey-Kramer comparison test result.

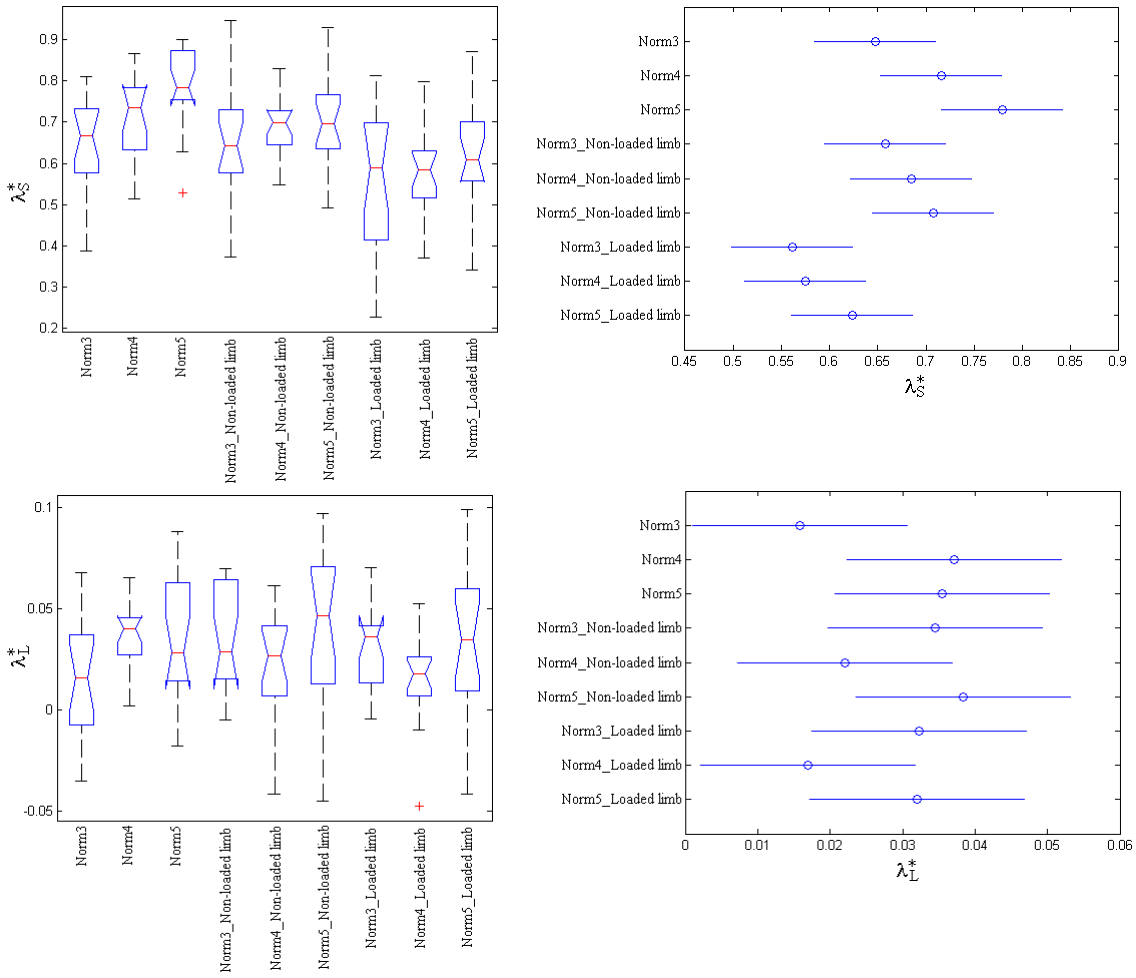

Figure 7.33 (a) Experimental results of shank λ_S^* with (b) Tukey-Kramer comparison test result; (c) Experimental results of shank λ_L^* with (d) Tukey-Kramer comparison test result.

Chapter 8

DISCUSSIONS

Experimental results showed that the wireless gait monitoring system performed well in capturing human lower extremity motion in both overground walking and treadmill walking. Gait data captured by the wireless inertial sensors were successfully transmitted to their respective wireless transceivers without any disturbances. Moreover, the periodical gait evaluation did not disrupt the real-time data acquisition and data visualization. The measurement data were also completely stored in the spreadsheet file without any data loss. These outcomes proved the viability of the system for various clinical applications and research in human gait analysis. Following sections highlight the significances of the methodologies used in this thesis to quantify and evaluate human walking condition.

8.1 Wireless Gyroscope as the Main Sensing Device

Optical motion capture system and force plates are the common methods to quantify human motion during walking. However, these approaches pose several limitations. Prior to each experiment, they have to be properly calibrated. Reflective markers have to be placed on the right locations to obtain accurate and reliable data. As one of the consequences, the time needed to set up the experiment is long. Moreover, the data processing is tedious and time-consuming. Hence, it is difficult to perform online data processing and provide immediate feedback to the clinician/researcher regarding the subject's walking condition.

Due to these limitations, wireless gyroscope was introduced to capture human lower extremity motion in real-time. Unlike the conventional instruments, gyroscope is

inexpensive, small, light-weight, and relatively easier to use. Other miniature inertial sensors, such as accelerometers, magnetometers and their variants also have similar features.

Nevertheless, accelerometer possesses several limitations when it is used to capture human motion. Firstly, accelerometer is sensitive to linear acceleration. Due to this characteristic, accelerometer may unintentionally measure the vibration of human body during walking. This vibration can vary greatly depending on the method used to place the accelerometer on human body and the accelerometer location on human body. Secondly, consistency of the measurement data collected using accelerometer greatly depends on the skills of assessor in placing the accelerometer in different body segments. Inconsistent location of the accelerometer on human body may lead to significant measurement error.

Other inertial sensor i.e. magnetometer also has its own drawback when it is used to capture human motion. Magnetometer is sensitive to nearby ferromagnetic materials that can distort the signal and lead to less accurate readings [1],[32],[49]. Bachmann et al. studied the capability of the inertial/magnetic sensor in measuring the angular displacement in the presence of ferromagnetic materials and electrical appliances such as computer monitor (CRT), electrical power supply, metal filing cabinet and small space heater with fan [125]. They reported that the direction of local magnetic field can be altered by the presence of surrounding ferromagnetic materials and electrical appliances hence it causes the sensor to be susceptible to errors (Figure 8.1). In an indoor environment i.e. gait laboratory which generally contains numerous sources of magnetic interference, it can be difficult to determine which objects are the major contributors to magnetic field deflections. This matter arises because magnetic field can vary greatly depending on the distances among ferromagnetic materials. Therefore, it can be deduced that magnetometer is not a suitable measuring device to capture human motion in clinical settings and rehabilitations.

Considering these limitations, gyroscope is a better option among the other miniature inertial sensors. Unlike accelerometer, gyroscope is less noisy and not affected by linear acceleration and/or gravity [51]. It produces similar results regardless of the minor differences in the attachment site on human body [21]. Moreover, it cannot be influenced by surrounding ferromagnetic materials and/or electrical appliances. Lastly, no calibration is required prior to every experiment.

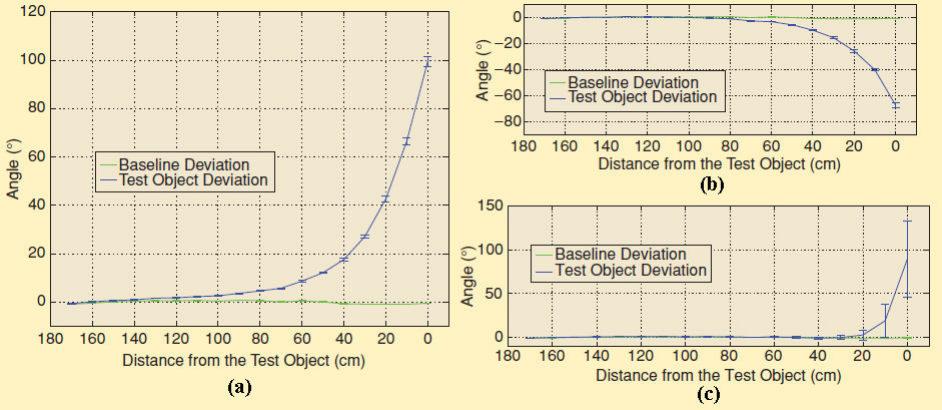

Figure 8.1 Deviation of the magnetic field vector in the horizontal plane versus distance from (a) CRT monitor (b) electrical power supply (c) small space heater with fan [125].

Gyroscope's output can be easily interpreted corresponding to different gait events [51]. Observing $\dot{\theta}_{thigh}$ and $\dot{\theta}_{shank}$ in each gait cycle (Figure 8.2), $\dot{\theta}_{shank}$ is negative during stance phase and it is rather positive during swing phase. Just before HS, $\dot{\theta}_{shank}$ becomes negative. During heel-strike, there is a change of slope sign of the $\dot{\theta}_{shank}$ from positive to negative. This is expected since the shank slows down to stop after the HS. Besides that, there is also a flexion of the knee which is marked by negative $\dot{\theta}_{shank}$ and negative $\dot{\theta}_{thigh}$. After HS, shank rotates clockwise around the ankle and generates negative $\dot{\theta}_{shank}$. During MS, knee becomes straight causing $\dot{\theta}_{shank}$ close to zero. Afterward, shank continues its clockwise rotation and accelerates its rotation at toe-off. This event causes positive slope at $\dot{\theta}_{thigh}$ and $\dot{\theta}_{shank}$. Knee then extends and moves the shank from backward to forward. This motion generates a maximum $\dot{\theta}_{shank}$ of approximately 5 rad/s. In this way, $\dot{\theta}_{thigh}$ and $\dot{\theta}_{shank}$ can provide comprehensive information regarding the thigh and shank flexion and extension throughout the gait cycle.

Gyroscope equipped with wireless technology also offers several advantages. It allows subject to move freely without being obstructed by wires that connect the sensors to the workstation. Subject's movement space is also not restricted by the length of the wires. This technology allows human motion to be captured in both indoor and outdoor environments.

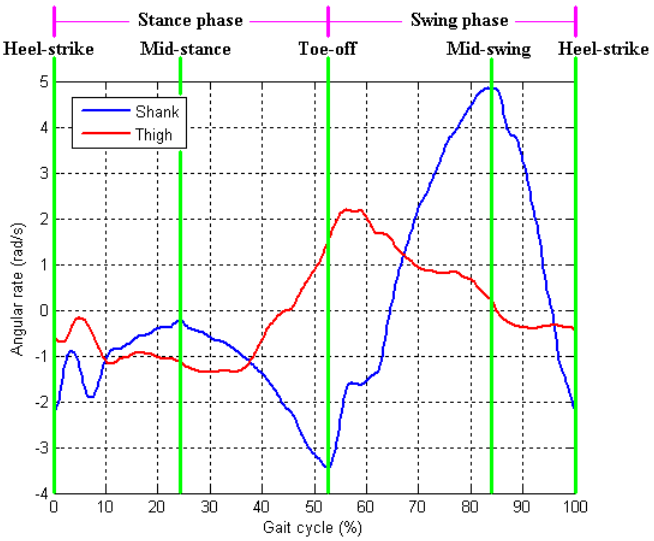

Figure 8.2 Typical thigh and shank angular rate at different gait events and gait phases.

Wireless gyroscopes were attached to a suit made of bulk straps and Velco^{TM} straps. The use of this suit considerably reduces the overall system setup time. In average, the overall setup time was less than two minutes. This suit also ensured the consistency of the gyroscopes placements on human body hence minimizing the measurement errors. In addition, this suit can be worn by a human subject regardless of his/her body height, weight, age and the circumferences of hip and lower limbs because it can be easily adjusted according to the his/her anthropometry properties.

8.2 Gait Event Identification

Identification of gait events is an important starting point for gait analysis [126]. As mentioned in Chapter 1.1, HS is generally considered as the start of a gait cycle and the beginning of the stance phase whereas TO is considered as the beginning of the swing phase. Definition of these events is widely used to estimate T_{stride}, T_{stance}, and T_{swing} to allow the time normalization of data per gait cycle hence facilitates comparison between different subjects and different walking conditions [126]-[127]. In practical, gait event is widely used to aid evaluation of treatments for pathological gait, particularly children with cerebral palsy [124] and the development of gait assistive devices such as prosthetic limb [128] and FES system [27]-[28],[52]-[54].

Identification of the gait event often relies on kinematic parameters derived from the optical motion capture system. However, this approach is only reliable when it is applied to a normal

and healthy individual [129]-[132]. To address this drawback, many researchers integrated additional instrument i.e. force platform to define the gait events. As mentioned in Chapter 2.1 and Chapter 8.1, optical motion capture system and force platform pose several limitations. Ghousssayni et al. also indicated that the use of optical motion capture system and force platform are subjected to the lack of automation, skills of the assessor in conducting the gait analysis, and encumbrance for the patient (The patient needs to control his walking speed or step length) [58]. More importantly, both systems are having difficulty in identifying consecutive gait cycles for long period of time because the optical motion capture system can only capture human motion in a laboratory and force platform can only capture one gait cycle at a time. Therefore, wireless gyroscope was used in this thesis to periodically identify the gait events during walking.

Knowing that $\dot{\theta}_{shank}$ can be used to identify gait events i.e. HS, TO and MS, this thesis developed HMWD to automate the identification of these events in both overground and treadmill walking. By automating this process, developed system can rapidly estimate T_{stride}, T_{stance}, and T_{swing}. Moreover, it is not susceptible to the assessor's skill in defining the gait events as gyroscope is not affected by minor differences in attachment locations. It is also not sensitive to any linear acceleration and/or gravity. Apart from these advantages, HMWD itself possesses several novelties. One of the novelties is the use of 2nd order Symmlet wavelet to decompose the angular rate of the shank as opposed to the 5th order Coiflet wavelet proposed in [51]. The other novelty is that HMWD only decomposes the angular rate into two scales rather than ten scales. Therefore, HMWD requires fewer calculations and consumes less computational time. These superiorities were justified, especially when HMWD periodically identified the gait events without disrupting the real-time data acquisition and data visualization (Figure 8.3).

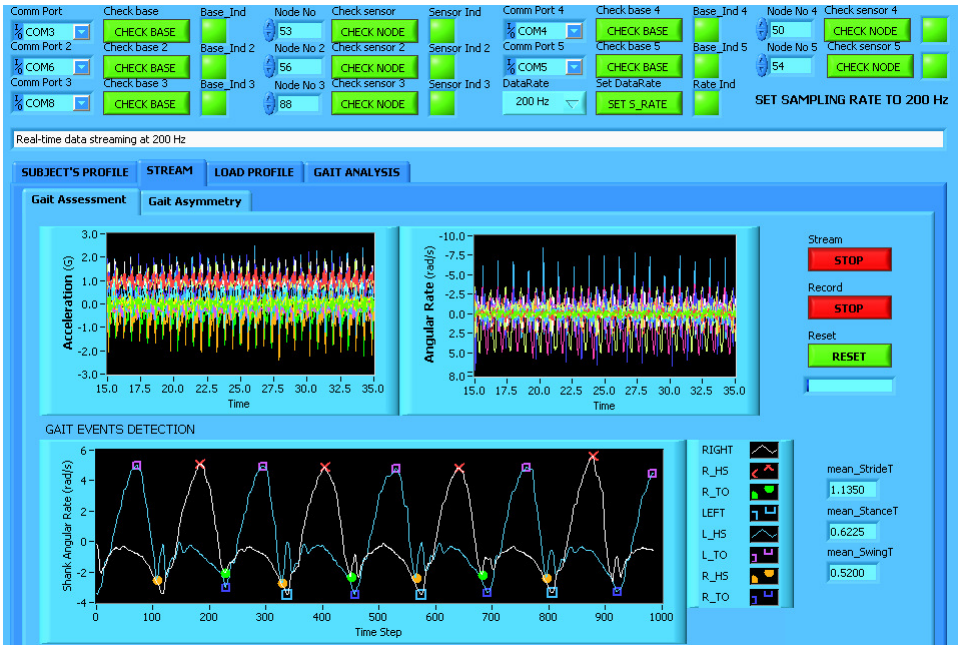

Figure 8.3 Periodical gait event identification during real-time data acquisition.

Another novelty of this method is that HMWD uses spatial-based local search to identify the local minima (HS and TO) within two successive MS.. This approach enables HMWD to be a time-independent method. Hence, it can facilitate the identification of gait events in various walking conditions regardless of the subject's walking speed and stride time. This was verified by the experimental results compiled in Chapter 7.1.

HMWD may suffer from slight systematic delay/error (approximately 10 ms) while defining HS and TO. This delay had been studied and reported in [51] thus no further study was conducted in this thesis to re-examine the systematic delay. However, it is necessary to mention this error is acceptable [51] considering the sampling rate of 200Hz (5ms per sample) and it can be compared favorably with other methods that use more expensive and complex instruments i.e. optical motion capture system and force platform. Using 50Hz optical motion capture system, Stanhope et al, reported that their algorithm suffered an error greater than 20 ms in more than 20% of the cases [134]. Mickelborough et al, reported that their method was only accurate within 30 ms [135]. Combining kinematic and kinetic parameters collected from optical motion capture system and force platform, Hansen et al found that their algorithm had an average error of 8.3 ms and 16.7 ms for HS and TO respectively [136].

8.3 Gait Normality Test

Temporal gait parameters i.e. duration T_{stride}, T_{stance}, and T_{swing} provide overall walking capability of a person. However, it is possible for certain patients with pathological conditions walk with right temporal gait parameters while having significantly abnormal joint motions. Therefore, there is a need for a motion capture system or a gait monitoring system to measure and record the human lower extremity movements, to provide sufficient information reflecting a person's walking conditions, and to determine whether his/her walking pattern is normal by comparing his/her movement patterns to the normative data.

Optical motion capture system has been commonly used in human gait analysis to quantify human lower extremity motion in walking. Optical motion capture system is a reflective marker based system that captures the movements of the markers placed on various parts of human body. However, this system suffers from several drawbacks as addressed in Chapter 2.1 and Chapter 8.1. To overcome these drawbacks, this thesis developed a gait monitoring system that uses wireless gyroscopes to capture human motion during walking. One of the merits of this system is that it can estimate the orientation of human lower extremity during walking. Hence, it allows these orientations to be compared with the ideal orientation of human lower extremity established in [2],[3], and [104]. More importantly, since its output is not as complicated as the output generated by an optical motion capture system, gyroscope based gait monitoring system can process the gait data and to present the gait analysis results periodically in every five seconds.

It is necessary to point out that a five second time frame is selected due to the optimal time required for the software to process the gait data and display the gait analysis results during the real-time data acquisition and data visualization. However, this time frame can be adjusted to cater for different needs of the gait analysis. It can also be adjusted according to the workstation computing capability. It is possible to be shortened if the workstation has higher computing capability than the workstation used in this thesis (CPU processor: Intel Core2 Duo E6750 @ 2.66 GHz; RAM: 4 GB). On the contrary, it can also be lengthened if the workstation has lower computing capability. A screenshot of the periodical gait normality test during real-time data streaming and data visualization is presented in Figure 8.4

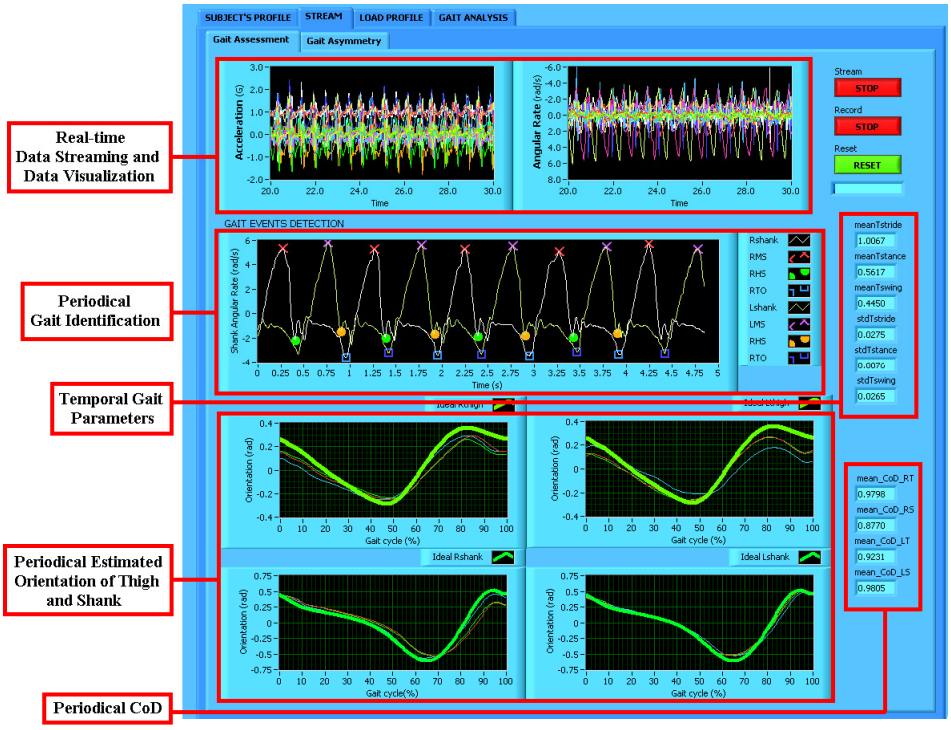

Figure 8.4 Periodical gait normality test during real-time data acquisition and data visualization.

Providing sufficient qualitative and quantitative feedbacks in a relatively short period of time allows clinician/researcher to understand his/her patient's walking condition and subsequently to advise appropriate treatment that can improve the patient's gait. This feature offers great benefits for patients who are under recovery process from hip or knee arthroplasty surgery, paraplegic patients who use FES system, and patients that have injury(s) that may disrupt their walking patterns.

In this system, qualitative feedback is obtained through visual comparison between the ideal and the actual orientations of the lower extremity, as illustrated in Figure 7.2, Figure 7.3, Figure 7.4, and Figure 7.5. This feedback offers clear and comprehensible information on the subject's gait relative to the gait of a normal and healthy individual. Through direct observation and comparison of each gait cycle to the reference profiles, researchers, clinicians and even someone who does not have good technical background, can identify the similarities and differences between the ideal and actual orientation of the thigh and shank.

Visual representation offered by the developed system may provide less accurate assessment concerning subject's walking condition therefore quantitative information is provided too. This information is computed and derived statistically, such as $\overline{T}_{stride}$, $\overline{T}_{stance}$,

and $\overline{T}_{swing}$ and CoD. The temporal gait parameters are taken into consideration as they hold crucial information closely related to pathological gait [72]-[73]. Normal and healthy gait has stance phase lasting approximately 60% of the gait cycle and swing phase lasting approximately 40% of the gait cycle during overground walking [2]-[3]. Stance phase is expected to be shorter (approximately 58%) and swing phase is expected to longer (approximately 42%) during treadmill walking [137]-[139]. Stolze et al. [140] explained that during walking on a treadmill or overground the timing of the stance and swing phase may be handled in a different way by the locomotor pattern generator. A variety of factors from afferent system could be involved including the differences in the behavioral context i.e. anxiety and caution during treadmill walking. Their experimental results was further justified by findings published in [139],[141]-[145], which elaborated that a sensory mismatch between the lack of optical flow and the information from the vestibular system and proprioceptive inputs from the limbs and trunk may play a role in the differences of the gait patterns between these two walking conditions. Regardless of the walking conditions, results compiled in Chapter 7.2 are similar to findings reported in [2]-[3],[137]-[139]. These results also demonstrated that developed system is capable of estimating various temporal gait parameters in both overground walking and treadmill walking.

On the contrary, abnormal gait may have shorter or longer T_{stance} and T_{swing} depending on the patient's pathological condition [12], [17],[70],[73],[146]. Yogev et al. found out patients with Parkinson's disease prolonged their stance phase (mean: 62%) hence shortened their swing phase (mean: 38%) [17]. Nolan et al. reported that trans-tibial amputees had longer stance phase up to 65% of the gait cycle and shorter swing phase [70]. On the other hand, trans-femoral amputees had shorter stance phase of approximately 56% of the gait cycle. While investigating vertical ground reaction force profile of stroke patients, Kim and Eng experimental results revealed that stroke patients exhibited longer stance phase (mean: 71%) and shorter swing phase (mean: 29%) on the nonparetic side of the limb [73].

Since no patients are involved in this thesis, abnormal gait was simulated by placing a load on one side of the limbs (lower shank) and by wearing a sandal on one side of the feet. The experimental results indicated that all participants tended to walk slower due to the resistance imposed to one side of the limbs. The affected limb exhibited shorter stance phase and longer swing phase than the non-affected limb. These incidents were expected as

the inertial property of the affected limb had been altered. Thus, apparent differences could be observed between the affected limb and the non-affected limb.

As mentioned earlier, other than temporal gait parameters, the developed system determines the *CoD* of the thigh and shank motion during walking. *CoD* compares the participant's movement pattern to the normative data. Unlike other gait analysis methods [64]-[68] (Characteristics of these approaches are discussed in Chapter 2.3), *CoD* is relatively simpler and does not require significant amount of time to examine the normality of a person's walking pattern. However, it is important to highlight that *CoD* cannot determine the underlying causes of the gait pathology. It was practically designed to be an initial clue that may assists clinicians, biomechanists or researchers to determine the normality of a person's gait.

Viability of *CoD* was tested on both normal and abnormal walking. The experimental results were satisfactory. They revealed that *CoD* was greater than 0.95 during normal walking whereas *CoD* was less than 0.95 during abnormal walking. The greater the differences between participant's lower extermity motion and the ideal lower extremity motion, the lower the *CoD* was. In addition, the experimental results also indicated that when the participants walked abnormally, only the affected limb i.e. thigh and shank exhibited lower *CoD* whereas the non-affected limb exhibited *CoD* was similar to *CoD* found in normal walking. These results were expected as the inertial properties of the lower limb had been altered and the affected limb experienced significant resistance hindering its movements to move forward and to maintain the overall body balance. It is worth noting that the statistical significance of *CoD* in discriminating abnormal gait is 0.01, which is relatively better than other approaches. More importantly, *CoD* can be implemented as one of the online processes without disrupting the real time data acquisition/data visualization (Figure 8.4). Schöllhorn who compiled all recent findings on the applications of artificial neural networks in clinical biomechanics reported that the discrimination rate between normal and abnormal gait can be as low as 40% [147]. Deluzio and Astephen who used PCA compare patients with end-stage knee osteoarthritis to asymptomatic control subjects reported that their method has misclassification rate of 8% [148]. Lafuente et al. applied Bayesian quadratic classifier to discriminate lower limb arthrosis patients and healthy subjects. Their experimental results indicated this classifier only has discrimination rate of 75% [14].

8.4 Gait Asymmetry

Gait asymmetry is typically found in amputee patients [12]-[13],[70], patients with limb length discrepancy [71], cerebral palsy [4],[69] and hemiplegic [8]-[9]. These pathological conditions generate significant differences in both spatial and temporal gait parameters. These differences include differences in T_{stride}, T_{stance} and T_{swing} [72]-[73], differences in ground reaction force profile [73]-[75] and differences in the range of motion [76]. Hence, gait asymmetry is commonly used as a strong indicator in rehabilitation and clinical settings.

So far, the research directions had been concentrated on the ground reaction force profiles, the orientation of the lower extremity and EMG (Electromyography) activities of the muscles while the use of angular rate of the lower extremity to identify gait symmetry has not been reported by any researcher yet. Therefore, this research introduces several new approaches i.e. SI_{norm} and Cc_{norm} that use $\dot{\theta}_{thigh}$ and $\dot{\theta}_{shank}$ to determine gait asymmetry. These approaches are relatively simpler and consume less computational time than other methods proposed in [76],[82]-[83]. Thus, these approaches can be implemented as one of the online processes without disrupting real-time data acquisition and data visualization of the system.

Since SI_{norm} and Cc_{norm} are new methods, this thesis also established a normative data that can be used to differentiate normal/symmetrical gait and abnormal/asymmetrical gait. The experimental study indicated that SI_{norm} and Cc_{norm} could give slightly different results when the participants walked on the ground and on a treadmill, therefore one must exercise great care when using these approaches to determine gait asymmetry. The normative data for both walking conditions are presented in Figure 7.21, Figure 7.23, Figure 7.27, and Figure 7.30

8.4.1 Normalized Cross-correlation (Cc_{norm})

In practice, human locomotory system may be regarded as a highly organized system. However, it is not a perfect one. Adjustments in human motion control system have to be continuously made to maintain speed, direction and body balance even though he/she is walking on an even surface [149]. Thus no identical movement pattern can be observed in every successive gait cycles. Similar concept is applicable to the left

and right limbs movement patterns. Gait asymmetry also exists in healthy individuals [77].

Experimental results compiled in Chapter 7.4.1 shows that Cc_{norm} in normal overground walking and treadmill walking was close to one. Cc_{norm} was greater than 0.9 and 0.95 on thigh and shank respectively when a person walked on the ground. Cc_{norm} was greater than 0.93 and 0.96 on thigh and shank respectively when he walked on a treadmill. In contrast, asymmetrical walking exhibited lower Cc_{norm} value due to large differences between left limb and right limb motions. The lower Cc_{norm} value, the greater the asymmetrical gait was. This was expected as there were significant differences between normal and abnormal gait simulated in this thesis. Loaded limb exhibited lower Cc_{norm} ($Cc_{norm\text{-}thigh} < 0.93$ and $Cc_{norm\text{-}shank} < 0.96$) than non-loaded limb. This finding correlates with results reported by Haddad et al. [120]. Even though they used different method to determine gait asymmetry, they did found out that placing a load on one side of the limbs could create asymmetrical gait. In the other experiments conducted in this thesis, participant's thigh and shank also exhibited lower Cc_{norm} ($Cc_{norm\text{-}thigh} < 0.86$ and $Cc_{norm\text{-}shank} < 0.94$) when they walked on the ground wearing sandal on one side of the feet. These results correlates with findings published by [71],[123],[150] which indicates that gait asymmetry can be clearly observed in patients with leg length discrepancy.

Cc byproduct, *Ts* indicates whether the motion of the left limb synchronize with the right limb. In normal walking *Ts* was ranging between -0.4% to 1.9% gait cycle while value greater than 1.9% or less than -0.4% was expected in asymmetrical walking. Positive *Ts* signifies that the left limb is leading ahead the right limb. Larger positive *Ts* also indicates that there is significant abnormality on the left limb, as indicated in Figure 7.22 and Figure 7.24. Vice versa, negative *Ts* indicates that the left limb is lagging behind the right limb and there is abnormality on the right limb. Hence, in practical, *Ts* can serve as an important indicator for many neurological diseases such as Parkinson disease and Huntington's disease.

8.4.2 Temporal Gait Asymmetry

The experimental results compiled in Chapter 7.4.2 indiated that SI_{stride}, SI_{stance} *and* SI_{swing} were ranging from -5% to 5% in normal walking. These results were anticipated as they were similar to findings reported in [70],[73],[149],[151]. However, when the participants walked abnormally, SI_{stance} *and* SI_{swing} were out of the normal range ($|SI_{stance}| > 5\%$ and $|SI_{swing}| > 5\%$). The main reason is that each limb has different T_{stance} and T_{swing}. The affected limb exhibited shorter T_{stance} and longer T_{swing} compared to the non-affected limb. Since right limb was the main reference, positive SI_{stance} was found when a load was placed on participant's right limb and when participant wore a sandal on his right foot.

In clinical settings, patients with pathologic gait experienced greater SI_{stance} *and* SI_{swing} as well. Nolan et al. reported that trans-tibial amputees exhibited SI_{stance} greater than 5.15% and SI_{swing} less than -10.30% [70]. They also discovered that trans-femoral amputees exhibited SI_{stance} greater than 23.92% and SI_{swing} less than -42.17%. While studying gait asymmetry in chronic stroke patients, Kim and Eng found that these patients had an average SI_{stance} of 13.6% and average SI_{swing} of 27.3% [73]. In one of the most recent publications, Patterson et al. reported that SI_{stance} *and* SI_{swing} had average value of 2.36% and 3.60% respectively in healthy individuals [152]. On the contrary, stroke patients exhibited larger SI_{stance} *and* SI_{swing} with average value of 18.61% and 31.58%

8.4.3 Normalized Symmetry Index (SI_{norm})

Providing single value indicator such as Cc_{norm} and Ts to define gait asymmetry in walking may not be sufficient, thus SI_{norm} is proposed to provide information regarding the timing and magnitude of movement deviations between the left and right limbs in each gait cycle. SI_{norm} is chosen instead of conventional SI because it can eliminates the artificial inflation that may lead to large SI value ($SI > 100\%$). A graphical illustration is presented in Figure 8.5 to describe this inflation. This effect generally occurs when one of the variables has positive value whereas the other has negative value and when the average of these values is very small or close to zero.

Proposed SI_{norm} bounds the index value to be less than ±100%. In normal walking SI_{norm} varies from -27% to 15% throughout the gait cycle during overground walking and varies between from -15% to 15% during treadmill walking. SI_{norm} collected from

these experiments can be regarded as the normative data of normal and healthy individuals.

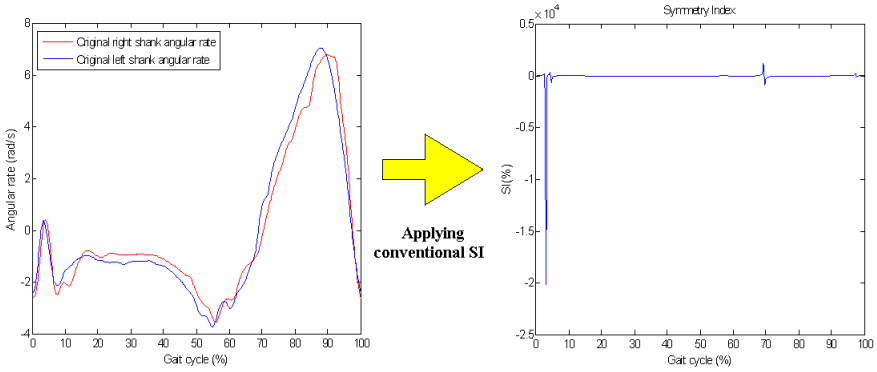

Figure 8.5 Artificial inflation when applying conventional SI to determine gait asymmetry.

Many authors argued that quantification of gait asymmetry using SI is greatly influenced by the side chosen as the reference value [80]. However, unlike conventional SI, SI_{norm} is not influenced by any side because choosing a different side as a reference still gives similar result but opposite in sign. Thus when it is interpreted correctly, SI_{norm} is still a valid indicator to determine gait asymmetry in walking. More importantly, SI_{norm} is not only applicable to the angular rate of the lower extremity; other kinematic and kinetic parameters can also be used as the main variables to determine gait asymmetry. Since it is adopted from conventional SI, it can be easily implement in various clinical applications, particularly those who had implemented SI to track patient's rehabilitation progress.

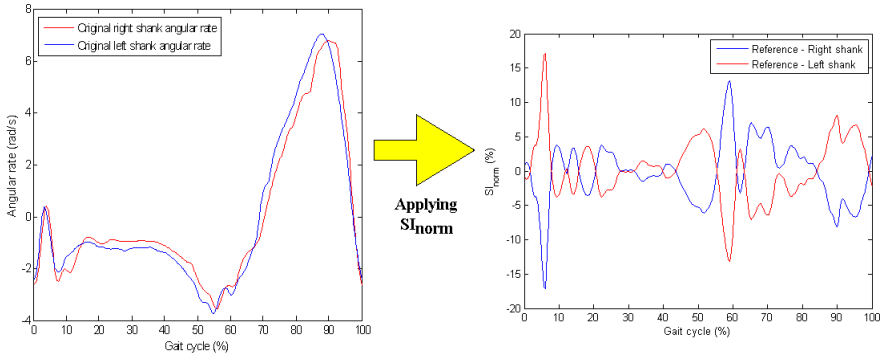

Figure 8.6 Applying SI_{norm} with different references.

8.5 Gait Dynamic Stability

Since human walking is not strictly periodic, traditional linear analysis may not be a suitable tool to examine human gait [95]. It can mask the true structure of motor variability if few strides are averaged to generate a mean picture of the subject's gait. Moreover, temporal variations of the gait may be lost. In contrast, nonlinear analysis focuses on how variations change in the human gait over the time [91],[94]-[95]. As one of the methods available in the nonlinear time analysis, λ* can estimate human dynamical stability during walking by measuring the local divergences of human motion in a state space. More importantly, λ* quantifies how the neuromuscular locomotor system responds to perturbations. Due to these reasons, many researchers have adopted this approach [91]-[99],[101],[153]. Their findings suggested that positive λ* is an indication of chaotic characteristic lying between completely periodic and completely random characteristics. Lower positive may indicate that human lower extremity has higher resistance to stride-to-stride variability and is less flexible and adaptable when variations from one stride to another occur [94]-[95],[99].

As mentioned in Chapter 5.10, two different time scales were used in this thesis to determine the dynamic stability of human walking: λ_S^* and λ_L^*. λ_S^* corresponds to short-term stability because it only examines the stability over first gait cycle. On the other hand, λ_L^* corresponds to long-term stability as it evaluates the stability over fourth to the tenth gait cycles.

Despite using different method to capture human motion during walking, the experimental results are similar to the findings reported in [85],[98],[153]. All participants exhibited lower λ_S^* for both thigh and shank when they walked slower. They exhibited larger λ_S^* when they walked faster. Thus, it can be deduced that the human neuromuscular locomotor systems can control kinematic disturbances better during slow walking than during fast walking [85]. These results agreed with basic clinical intuition that patients with higher risk of falling walk slower to improve their stability [153]. However, λ_L^* exhibited different behavior, λ_L^* had the lowest values when the participants walked at speed of 4 km/h. These results signified that over the long period of time, participants controlled their neuromuscular locomotor system better when they walked at this speed. These results were consistent with findings reported in [94],[99]. When asymmetrical gait is simulated during

the experimental study, loaded limb exhibited lower λ_S^* and λ_L^* than the non-loaded limb. These results suggested that due to changes in the loaded limb inertial properties, non-loaded limb neuromuscular system was challenged to balance perturbations induced on the other limb, which in turn increased both λ_S^* and λ_L^* of the non-loaded limb. Apart from these observations, the experimental results also revealed that thigh exhibited lower λ_S^* and λ_L^* than the shank during walking. These findings are consistent with results published [85],[94],[98].

The experimental study demonstrated the capability of the developed system in estimating gait dynamic stability. This study also indicated that human walking is not strictly periodic, thus non-linear time analysis is necessary to assess walking stability. Moreover, it demonstrates that angular rate of human lower extremity is a valid kinematic parameter to estimate λ*. Lastly, this study also established normative baseline of normal and healthy individuals walking in different conditions i.e. on the ground and on the treadmill, and at different walking speed i.e. 3 km/h, 4km/h and 5 km/h. With satisfactory outcomes, this system is expected to be employed in clinical research to assist clinicians and biomechanists to further study the influences of λ_S^* and λ_L^* in walking stability, particularly on which neuromuscular locomotor system is responsible for changes in λ_S^* and λ_L^* thus allows clinicians and biomechanists to devise appropriate strategies that can improve human walking stability and reduce the risk of falls in elderly.

Chapter 9

CONCLUSION

Human gait analysis is an effective tool in determining patients' pathological conditions, particularly patients with celebral palsy, hemiplegic, osteoarthritis and Parkinson disease. It also holds significant role in the design and development of many gait assistive devices such as prosthetic limb and FES system. Until recent years, optical motion capture system and force platform were the most common tools to capture human gait. However, these tools are expensive, bulky and can only capture human motion in a dedicated environment i.e. laboratory. With recent advancements in MEMS technology and wireless data communication, inertial sensors, such as accelerometer, gyroscope and magnetometer gain tremendous popularity among clinicians and researchers. Hence, this thesis developed a gait monitoring system that used wireless gyroscopes to capture human motion in real-time. It also used several computational methods to periodically evaluate a person's gait when he/she is walking on the ground or on a treadmill.

Several evaluation methods were introduced in this thesis to examine three different aspects of human gait. These evaluations include gait normality test, analysis of gait asymmetry and estimation of gait dynamic stability. First evaluation, 'Gait normality test' produces a series of results such as T_{stride}, T_{stance}, T_{swing}, and *CoD*. Temporal gait parameters are taken into account because they hold crucial information closely related to pathological gait. *CoD* is a new method used to distinguish the normal and abnormal gait. *CoD* is close to one when the gait is normal. Second evaluation, 'Gait asymmetry analysis' examines whether there is a significant difference between the left and right limbs motions in each gait cycle. It uses angular rates measured by

the wireless gyroscopes to determine Cc_{norm}, *Ts* and SI_{norm}. Cc_{norm} is a dimensionless parameter that evaluates the waveforms generated by human lower extremity motions. *Ts* denotes the synchronization between the left and right limbs. SI_{norm} determines the timing and magnitudes of the bilateral differences in each gait cycle. Last evaluation, 'Estimation of gait dynamic stability' examines a person's walking stability using nonlinear time series analysis. It uses λ* to determine the ability of human neuromuscular locomotor system in maintaining body balance during walking.

An experimental study was conducted to examine the capability of the system. Since no patient with any pathological condition was involved in this study, abnormal gait was simulated on healthy individual by altering the inertial property of the lower limb. This was done by placing a load on one side of the limbs and by wearing a sandal on one side of the feet. As expected, artificially simulated abnormal gait produced results that were significantly different from normal gait. These results demonstrated the viability of this system to be deployed in various clinical settings and rehabilitations. More importantly, they also validated the computational methods i.e. *CoD*, Cc_{norm}, *Ts,* SI_{norm}, and λ*, *CoD*, Cc_{norm}, *Ts,* SI_{norm}, and λ* to examine different aspects of human gait. Lastly, these results also established normative data of *CoD*, Cc_{norm}, *Ts,* SI_{norm}, and λ*, which could be used as references to determine a person's walking condition.

As one of future research directions, developed system is expected to be deployed in a hospital and/or a health institution to quantify patient's lower extremity motion during walking and to examine patient's walking conditions. Having this system in a health institution will be beneficial for clinicians and researchers. Clinicians can use this system to determine the severity of patient's condition and to examine the effectiveness of the patient's rehabilitation program. Researchers can use this system to characterize different pathologic gaits and to study their underlying causes. They can also use this system to devise appropriate treatments that can improve a person's gait to be more adaptive, consumes less energy and minimizes the risk of fall. Lastly, this system can be used to design and develop better assistive devices for amputees, stroke patients and other patients who require the use of FES systems.

REFERENCE

[1] Best R. Begg R. Overview of Movement Analysis and Gait Features. In: Begg, R., Palaniswami, M., editors. Computational Intelligence for Movement Science: Neural Networks and Other Emerging Techniques. London: Idea Group Inc; 2006. p. 1-69.

[2] Perry J. Gait cycle. In: Gait Analysis: Normal and Pathological Function. New Jersey: Slack; 1992. p. 3-7.

[3] Whittle MW. Normal gait. In: Gait Analysis: An Introduction. China: Elsevier; 2008, p. 47-100.

[4] Seeger BR, Caudrey DJ, Scholes JR. Biofeedback therapy to achieve symmetrical gait in hemiplegic cerebral palsied children. Archives of Physical Medicine and Rehabilitation. 1981;62:364-368.

[5] Desailly E, Daniel Y, Sardain P, Lacouture P. Foot contact event detection using kinematic data in cerebral palsy children and normal adults gait. Gait and Posture. 2009;29:76–80.

[6] Romei M, Galli M, Motta F, Schwartz M, Crivellini M. Use of the normalcy index for the evaluation of gait pathology. Gait and Posture. 2004;19:85-90.

[7] Schwartz MH, Novacheck TF, Trost J. A tool for quantifying hip flexor function during gait. Gait and Posture. 2000;12:122-127.

[8] Balasubramanian CK, Bowden MG, Neptune RR, Kautz SA. Relationship between step length asymmetry and walking performance in subjects in chronic hemaparesis. Archives of Physical Medicine and Rehabilitation. 2007;88:43-49.

[9] Brandstater ME, de Bruin H, Gowland C, Clark BM. Hemiplegic gait: analysis of temporal variables. Archives of Physical Medicine and Rehabilitation. 1983;64:583-587

[10] Griffin MP, Olney SJ, McBride ID. Role of symmetry in gait performance of stroke subjects with hemiplegia. Gait and Posture. 1995;3:132-142

[11] Schutte LM, Narayanan U, Stout JL, Selber P, Gage JR, Schwartz MH. An index for quantifying deviations from normal gait. Gait and Posture. 2000;11:25-31

[12] Andres RO, Stimmel SK. Prosthetic alignment effects on gait symmetry: a case study. Clinical Biomechanics. 1990;5:88-96.

[13] Prince F, Allard P, Therrien RG, McFadyen BJ. Running gait impulse asymmetries in below-knee amputees. Prosthetics and Orthotics International. 1992;16:19-24.

[14] Lafuente R, Belda JM, Sanchez-Lacuesta J, Soler C, Poveda R, Prat J. Quantitative assessment of gait deviation: contribution to the objective measurement of disability. Gait and Posture. 2000;11:191-198.

[15] Deluzio KJ, Wyss UP, Zee B, Costigan PA, Sorbie C. Principal component models of knee kinematics and kinetics: normal vs pathological gait patterns. Human Movement Science. 1997;16:201-217.

[16] Plotnik M, Giladi N, Hausdorff JM. Bilateral coordination of walking and freezing of gait in Parkinson's disease. European Journal of Neuroscience. 2008;27:1999-2006.

[17] Yogev G, Plotnik M, Peretz C, Giladi N, Hausdorff JM. Gait asymmetry in patients with Parkinson's disease and elderly fallers: when does the bilateral coordination of gait require attention?. Experimental Brain Research. 2007;177:336-346

[18] Miki H, Sugano N, Hagio K, Nishii T, Kawakami H, Kakimoto A, Nakamura N, Yoshikawa H. Recovery of walking speed and symmetrical movement of the pelvis and lower extremity joints after unilateral THA. Journal of Biomechanics. 2004;37:443-455

[19] McCrory JL, White SC, Lifeso RM. Vertical ground reaction force: objective measures of gait following hip arthoplasty. Gait and Posture. 2001;14:104-109

[20] Lakany H. Extracting a diagnostic gait signature. Pattern Recognition. 2008;41:1627-1637

[21] Tong K, Granat MH. A practical gait analysis system using gyroscope. *Medical Engineering and Physics*. 1999;21:87-94

[22] Esquenazi A, Talaty M. Gait analysis: technology and clinical applications. In. Braddom RL, editor. *Physical Medicine and Rehabilitation*. 2nd ed. Philadelphia: WB Saunders; 2000. p. 93-108

[23] Sabatini AM, Martelloni C, Scapellato S, Cavallo F. Assessment of walking features from foot inertial sensing. *IEEE Transactions on Biomedical Engineering*. 2005;52(3):486-494.

[24] Aminian K, Najafi B. Capturing human motion using body-fixed sensors: outdoor measurement and clinical applications. *Computer Animation and Virtual Worlds*. 2004;15:79-94.

[25] Gouwanda D, Senanayake SMNA. Emerging trends of body-mounted sensors in sports and human gait analysis. *IFMBE Proceedings of 4th Kuala Lumpur International Conference on Biomedical Engineering*. 2008;21:715-718.

[26] Ohtaki Y, Sagawa K, Inooka H. A method for gait analysis in daily living environment by body-mounted instrument. *JSME International Journal*. 2001;44(4):1125-1132.

[27] Pappas IPI, Popovic MR, Keller T, Dietz V, Morari M. A reliable gait phase detection system. *IEEE Transactions on Neural Systems and Rehabilitation Engineering*. 2001;9(2):113-125.

[28] Veltink PH, Bussman HBJ, de Vries W, Martens WLJ, Van Lummel, RC. Detection of static dynamic activities using inertial accelerometers. *IEEE Transaction on Rehabilitation Engineering*. 1996;4(4):375-385

[29] Bouten CVC, Koekkoek KTM, Verduin M, Kodde R, Janssen, JD. A triaxial accelerometer and portable data processing unit for the assessment of daily physical activity. *IEEE Transaction on Biomedical Engineering*. 1997;44(3):136-147.

[30] Bussmann JBJ, Veltink, PH, Koelma F, Van Lummel RC, Stam HJ. Ambulatory monitoring of mobility-related activities: the initial phase of the development of an activity monitor. *European Journal of Physiology and Medical Rehabilitation*. 1995;5(1):2-7.

[31] Sabatini AM. Inertial sensing in biomechanics: a survey of computation techniques bridging motion analysis and personal navigation. In: Begg, R., Palaniswami, M., editors. *Computational Intelligence for Movement Science: Neural Networks and Other Emerging Techniques*. London: Idea Group Inc; 2006. p. 70-100.

[32] Aminian K. Monitoring human movement with body-fixed sensors and its clinical application. In: Begg, R., Palaniswami, M., editors. *Computational Intelligence for Movement Science: Neural Networks and Other Emerging Techniques*. London: Idea Group Inc; 2006. p. 101-138

[33] Boulgouris NK, Hatzinakos D, Plataniotis N. Gait recognition: a challenging signal processing technology for biometric identification. *IEEE Signal Processing Magazine* 2005;22(6):78-90.

[34] Wang L, Hu W, Tan T. Recent developments in human motion analysis. *Pattern Recognition*. 2006;36:585-601

[35] Gavrila DM. The visual analysis of human movement: a survey. *Computer Vision and Image Understanding*. 1999;73(1):82-98

[36] O' Donovan KJ, Kamnik R, O' Keeffe DT, Lyons GM. An inertial and magnetic sensor based technique for joint angle measurement. *Journal of Biomechanics*. 2007;40:2604-2611.

[37] Williamson R, Andrews BJ. Detecting absolute human knee angle and angular velocity using accelerometers and rate gyroscopes. *Medical and Biological Engineering and Computing*. 2001;39:294-302.

[38] Plamondon A, Delisle A, Larue C, Brouilette D, McFadden D, Desjardins P, Lariviere C. Evaluation of a hybrid system for three dimensional measurement of trunk posture in motion. *Applied Ergonomics*. 2007;38: 697-712.

[39] Kaufman KR. Future direction in gait analysis. *RRDS Gait Analysis in the Science of Rehabilitation*. 1998;4:85-112

[40] Jasiewicz JM, Allum JHJ, Middleton JW, Barriskill A, Condie P, Purcell B, Che RTL. Gait event detection using linear accelerometers or angular velocity transducers in able-bodied and spinal cord injured individuals. *Gait and Posture*. 2006;24:502-509.

[41] Mamizuka N, Sakane M, Kaneoka K, Hori N, Ochiai N. Kinematic quantitation of the patellar tendon reflex using a tri-axial accelerometer. *Journal of Biomechanics*. 2007;40: 2107-2111

[42] Watanabe K, Hokari M. Kinematical analysis and measurement of sports form. *IEEE Transaction on Systems Man and Cybernetics – Part A: Systems and Humans.* 2006;36(3):549-557

[43] Davey NP, James DA, Anderson ME. Signal analysis of accelerometry data using gravity based modeling. *Proceedings of SPIE Microelectronics: Design, Technology, and Packaging*. 2004;5274: 362-370

[44] Ohgi Y. Microcomputer-based acceleration sensor device for sports biomechanics – stroke evaluation using swimmer's wrist acceleration. *Proceedings of IEEE Sensors* 2002;1:699-704

[45] Doo YK, Gross M. Combining Body Sensors and Visual Sensors for Motion Training, *ACM Proceedings of SIGCHI International Conference on Advances in Computer Entertainment Technology*. 2005. p. 94-101

[46] Brunetti F, Moreno JC, Ruiz AF, Rocon E, Pons JL. A new platform based on IEEE802.15.4 wireless inertial sensors for motion caption and assessment. *28th Annual International Conference of the IEEE*. 2006. p. 6497-6500

[47] Mayagoita RE, Nene VA, Veltink PH. Accelerometer and rate gyroscope measurement of kinematics: an inexpensive alternative to motion analysis system. *Journal of Biomechanics*. 2002;35:537-542

[48] Vicon Motion Systems and Peak Performance Inc. Available: http://www.vicon.com

[49] Roetenberg D, Slycke PJ, Vetlink PH. Ambulatory Position and Orientation Tracking fusing Magnetic and Inertial Sensing. *IEEE Transcations on Biomedical Engineering*. 2007;54(5):883-890

[50] Ascension Technology Corporation, Available: http://www.ascension-tech.com

[51] Aminian K, Najafi B, Bula C, Leyvraz PF, Robert Ph. Spatio-temporal parameters of gait measured by an ambulatory system using miniature gyroscopes. *Journal of Biomechanics*. 2002;35:689-699.

[52] Willemsen ATM, Bloemhof F, Boom HBK. Automatic stance-swing phase detection from accelerometer data from peroneal nerve stimulation. *IEEE Transaction on Biomedical Engineering*. 1990;37(12):1201-1208

[53] Dai R, Stein RB, Andrew BJ, James KB, Wieler M. Application of tilt sensors in functional electrical stimulation. *IEEE Transaction of Rehabilitation Engineering*. 1996;4(2):63-71

[54] Mansfield A, Lyons GM. The use of accelerometry to detect heel contact events for use as a sensor in FES assisted walking. *Medical Engineering and Physics*. 2003;25:879-885

[55] Winter DA, Greenlaw RK, Hobson DA. A microswitch shoe for use in locomotion studies. *Journal of Biomechanics*. 1972;5:553-554

[56] Veltink PH, Liedtke CB, Droog E, van der Kooij H. Ambulatory measurement of ground reaction forces. *IEEE Transaction on Rehabilitation Engineering*. 2005;13(3):423-427

[57] Catalfamo P, Moser D, Ghoussayni S, Ewins D. Detection of gait events using an F-Scan in-shoe pressure measurement system. *Gait and Posture*. 2008;28:420-426

[58] Ghoussayni S, Stevens C, Durham S, Ewins D. Assessment and validation of a simple automated method for the detection of gait events and intervals. *Gait and Posture*. 2004;20:266-272

[59] Mansfield A, Lyons GM. The use of accelerometry to detect heel contact events for use as a sensor in FES assisted walking. *Medical Engineering and Physics*. 2003;25:879-885

[60] Baker R. Gait Analysis Methods in Rehabilitation. *Journal of NeuroEngineering and Rehabilitation*. 2006;3(4).

[61] Lai DTH, Begg RK, Palaniswami M. Computational intelligence in gait research: A perspective on current applications and future challenges. IEEE Transaction Information Technology in Biomedicine. 2009;13(5):687-702.

[62] Chau T. A review of analytical techniques for gait data Part I: fuzzy, statistical and fractal methods. Gait and Posture. 2001;13:49-66

[63] Chester VL, Tingley M, Biden EN. An extended index to quantify normality of gait in children. Gait and Posture. 2007;25:594-554

[64] Barton G, Lisboa P, Lees A, Attfield S. Gait quality assessment using self-organising artificial neural networks. Gait and Posture. 2007;25:374 – 379

[65] Tingley M, Wilson C, Biden E, Knight WR. An index to quantify normality of gait in young children. Gait and Posture. 2002;16:149-158.

[66] Holzreiter SH, Kohle ME. Assessment of gait patterns using neural networks. Journal of Biomechanics. 1993;26:645-651.

[67] Xu S, Zhou X, Sun Y. A novel gait analysis system based on adaptive neuro-fuzzy inference system. Expert Systems with Applications. 2010;37:1265-1269.

[68] Schwartz MH, Rozumalski A. The gait deviation index: A new comprehensive index of gait pathology. Gait and Posture. 2008;28:351-357.

[69] Descatoire A, Femery V, Potdevin F, Moretto P. Step-to-step reproducibility and asymmetry to study gait auto-optimization in healthy and celebral palsied subjects. Annals of Physical and Rehabilitation Medicine. 2009;52:319-329

[70] Nolan L, Wit A, Dudzinski K, Lees A, Lake M, Wychowanski M. Adjustments in gait symmetry with walking speed in trans-femoral and trans-tibial amputees. Gait and Posture. 2003;17:142-151

[71] Perttunen JR, Anttila E, Sodergard J, Merikanto J, Komi PV. Gait asymmetry in patients with limb length discrepancy. Scandinavian Journal of Medicine and Science in Sports. 2004;14:49-56

[72] Dewar ME, Judge G. Temporal asymmetry as a gait quality indicator. Medical and Biological Engineering and Computing. 1980;18:689-693

[73] Kim CM, Eng JJ. Symmetry in vertical ground reaction force is accompanied by symmetry in temporal but not distance variables of gait in persons with stroke. Gait and Posture. 2003;18:23-28

[74] Morita S, Yamamoto H, Furuya K. Gait analysis of hemiplegic patients by measurement of ground reaction force. Scandinavian Journal of Rehabilitation Medicine. 1995;27:37-42

[75] Herzog W, Nigg BM, Read LJ, Olsson E. Asymmetries in ground reaction force patterns in normal human gait. Medicine Science Sports and Exercise. 1989;21(1):110-114

[76] Shorter KA, Polk JD, Rosengren KS, Hsiao-Wecksler ET. A new approach to detecting asymmetries in gait. Clinical Biomechanics. 2008;23:459-67

[77] Sadeghi H, Allard P, Prince F, Labelle H. Symmetry and limb dominance in able-bodied gait: A review. Gait Posture. 2000;12:34–45

[78] Robinson RO, Herzog W, Nigg BM. Use of force platform variables to quantify the effects of chiropractic manipulation on gait symmetry. Journal of Manipulative Physiology Therapy. 1987;10:172-176

[79] Becker HP, Rosenbaum D, Kriese T, Gerngrob H, Claes L. Gait asymmetry following successful surgical treatment of ankle fracture in young adults. Clinical Orthopaedics and Related Research. 1995;311:262-269

[80] Zifchock RA, Davis I, Higginson J, Royer T. The symmetry angle: A novel, robust method of quantifying asymmetry. Gait and Posture. 2008;27:622-627.

[81] Crenshaw SJ, Richards JG. A method for analyzing joint symmetry and normalcy with an application to analyzing gait. Gait and Posture. 2006;24:515–521

[82] Sadeghi H. Local or global asymmetry in gait of people without impairments. Gait and Posture. 2003;17:197-204

[83] Allard P, Lachance R, Aissaoui R, Duhaime M. Simultaneous bilateral 3-D able-bodied gait. Human Movement Science .1996;15:327–346

[84] Hurmuzlu Y, Basdogan C. On the measurement of dynamic stability of human locomotion. Journal of Biomechanical Engineering. 1994;116:30-36

[85] England SA, Granata KP. Influence of gait speed on local dynamic stability of walking. Gait and Posture. 2007;25:172-178

[86] Hausdorff JM, Zemany L, Peng CK, Goldberger AL. Maturation of gait dynamics: stride-to-stride variability and its temporal organization in children. Journal of Applied Physiology. 1999;86:1040-1047

[87] Hausdorff JM, Ashkenazy Y, Peng CK, Ivanov PC, Stanley HE, Goldberger AL. When human walking becomes random walking: Fractal analysis and modeling of gait rhythm fluctuations. Physica A: Statistical Mechanics and its Applications. 2001;302(1-4):138-147

[88] Hausdorff JM, Rios DA, Edelberg HK. Gait variability and fall risk in community-living older adults: a 1-year prospective study. Archives of Physical Medicine and Rehabilitation. 2001;82(8):1050-1056

[89] Maki BE. Gait changes in older adults: Predictors of falls or indicators of fear?. Journal of American Geriatric Society. 1997;45(3):313-320

[90] Winter DA. Biomechanics of normal and pathological gait:implication for understanding human locomotor control. Journal of Motor Behavior. 1989;21:337-355

[91] Dingwell JB, Cusumano JP, Cavanagh PR, Sternad D. Local dynamic stability versus kinematic variability of continuous overground and treadmill walking. Journal of Biomechanical Engineering, 2001;123;17-32

[92] Kang HG, Dingwell JB. Effects of walking speed, strength and range of motion on gait stability in healthy older adults. Journal of Biomechanics. 2008;41:2899-2905

[93] Buzzi UH, Ulrich BD. Dynamic stability of gait cycles as a function of speed and system constraints. Motor Control. 2004;8(3):241-254

[94] Dingwell JB, Cusumano JP. Nonlinear time analysis of normal and pathological human walking. Chaos. 2000;10:848-863

[95] Rosenstein MT, Collins JJ, DeLuca CJ. A practical method for calculating largest Lyapunov exponents from small data sets. Physica D. 1997;65:117-134

[96] Kantz H, Schreiber S. Nonlinear time series analysis. Cambridge: Cambridge University Press; 1997

[97] Stergiou N, Moraiti C, Giakas G, Ristanis S, Georgoulis AD. The effect of the walking speed on the stability of the anterior cruciate ligament deficient knee. Clinical Biomechanics. 2009;19:957-963

[98] Kang HG, Dingwell JB. Dynamic stability of superior vs inferior segments during walking in young and older adults. Gait and Posture. 2009;30:260-263

[99] Son K, Park J, Park S. Variability analysis of lower extremity joint kinematics during walking in healthy young adults. Medical Engineering and Physics. 2009;31:784-792

[100] Kang HG, Dingwell JB. A direct comparison of local dynamic stability during unperturbed standing and walking. Experimental Brain Research. 2006;172:35-48

[101] Schablowski M, Gerner HJ. Comparison of two measures of dynamic stability during treadmill walking. Lecture Notes in Control and Information Sciences. 2006;340:345-360

[102] Miller DJ, Stergiou N, Kurz MJ. An improved surrogate method for detecting the presence of chaos in gait. Journal of Biomechanics. 2006;39:2873-2876

[103] MicroStrain Inc. Available: www.microstrain.com

[104] Winter DA. Biomechanics and Motor Control of Human Movement. 3rd ed. New Jersey:John Wiley & Sons; 2004

[105] McGinley JL, Barker R, Wolfe R, Morris ME. The reliability of three-dimensional kinematic gait measurements: a systematic review. Gait and Posture. 2009;29:360-369

[106] MicroStrain, Inc. 3DM-GX2 Data Communications Protocol for Inertia-Link and 3DM-GX2 Orientation Sensors Version 1.13, Available: www.microstrain.com

[107] Gouwanda D, Senanayake SMNA. Application of hybrid multi-resolution wavelet decomposition method in detecting human walking gait events. Proceedings of Soft Computing and Pattern Recognition 2009. 2009. p. 580-585

[108] Hegger R, Kantz H, Schreiber T. Practical implementation of nonlinear time series methods: the tisean package. Chaos. 1999;9:413-435

[109] Wu G, Siegler S, Allard P, Leardini A, Rosenbaum D, Whittle M, D'Lima DD, Cristofolini L, Witte H, Schmid O, Stokes I. ISB recommendation on definitions of joint coordinate system of various joints for the reporting of human joint motion-part I: ankle, hip, and spine. Journal of Biomechanics. 2002;35:543-548

[110] Wu G, van der Helm FCT, Veeger HEJ, Makhsous M, Roy PV, Anglin C, et al. ISB recommendation on definitions of joint coordinate system of various joints for the reporting of human joint motion-part II: shoulder, elbow, wrist and hand. Journal of Biomechanics. 2005;38:981-992

[111] Addison PS. The Illustrated Wavelet Transform Handbook – Introductory Theory and Applications in Science, Engineering, Medicine and Finance. London: Institute of Physics Publishing; 2002

[112] Mallat SG. A theory for multi-resolution signal decomposition (the wavelet representation). IEEE Transaction on Pattern Analysis and Machine Intelligence. 1989;11:674-693

[113] Proakis JG, Manolakis DG. Digital Signal Processing: Principles, Algorithms and Applications. 3rd ed. New Jersey: Prentice Hall; 1996

[114] Perc M. The dynamic of human gait. European Journal of Physics. 2005;26:525-534

[115] Abarbanel HDI. Analysis of Observed Chaotic Data. New York: Springer-Verlag; 1996

[116] Baker GL, Gollub JP. Chaotic Dynamics. New York: Cambridge University Press;1996

[117] Fraser AM, Swinney HL. Independent coordinates for strange attractors from mutual information. Physical Review A. 1986;33:1134-1140

[118] Kennel MB, Brown R, Abarbanel HD. Determining embedding dimension for phase-space reconstruction using a geometrical construction. Physical Review A. 1992;45:3403-3411

[119] Theiler J. Spurious dimensions from correlation algorithms applied to limited time-series data. Physical Reviews A. 1986;34:2427-2432

[120] Haddad JM, van Emmerik REA, Whittlesey SN, Hamill J. Adaptations in interlimb and intralimb coordination to asymmetrical loading in human walking. Gait Posture. 2006;23:429-434

[121] Whittlesey SN, Ward T, Van Emmerik REA, Hamill J. Roles of leg inertial properties in human walking. Proceeding of 3rd NACOB, 1998. p. 87-88

[122] Mattes SJ, Martin PE, Royer TD. Walking symmetry and energy cost in persons with unilateral transtibial amputations: matching prosthetic and intact limb inertial properties. Archives of Physical Medicine and Rehabilitation. 2000;81(5):561-568

[123] Gurney B. Leg length discrepancy. Gait and Posture. 2002;15:195-206

[124] Kirtley C, Whittle MW, Jefferson RJ. Influence of walking speed on gait parameters. Journal of Biomechanical Engineering. 1985;7:282-288

[125] Bachmann ER, Yun X, Brumfield A. Investigating the effects of magnetic variations on inertial/magnetic orientation sensor: limitations of attitude estimation algorithms for inertial/magnetic sensor modules. IEEE Robotics & Automation Magazine. 2007;14(3):76-87

[126] O'Connor CM, Thorpe SK, O'Malley MJ, Vaughan CL. Automatic detection of gait events using kinematic data. Gait and Posture. 2007;25:469-474

[127] Desailly E, Daniel Y, Sardain P, Lacouture P. Foot contact event detection using kinematic data in celebral palsy children and normal adult gait. Gait and Posture. 2009;29:76 – 80.

[128] Czerniecki JM, Gitter AJ. Gait analysis in the amputee; has it helped the amputee or contributed to the development of improved prosthetic components?. Gait and Posture. 1996;4:258-268

[129] Zeni JA, Richards JG, Higginson JS. Two simple methods for determining gait events during treadmill and overground walking using kinematic data. Gait and Posture. 2008;27:710-714

[130] Hreljac A, Marshall RN. Algorithms to determine event timing during normal walking using kinematic data. Journal of Biomechanics. 2000;33:783-786

[131] Ghoussaynni S, Stevens C, Durham S, Ewins D. Assessment and validation of a simple automated method for the detection of gait events and intervals. Gait and Posture. 2004;20:266-272

[132] Hreljac A, Stergiou N. Phase determination during normal running using kinematic data. Medical and Biological Engineering and Computing. 2002;38:503-506

[133] Sabatini AM, Martelloni C, Scapellato S, Cavallo F. Assessment of walking features from foot inertial sensing. IEEE Transactions on Biomedical Engineering. 2005;52(3):486-494

[134] Stanhope SJ, Kepple TM, McGuire DA, Roman NL. Kinematic-based technique for event time determination during gait. Medical and Biological Engineering and Computing. 1990;28:355-360

[135] Mickelborough J, van der Linden ML, Richard J, Ennos AR. Validity and reliability of a kinematic protocol for determining foot contact events. Gait and Posture. 2000;11:32-37

[136] Hansen AH, Childress DS, Meier MR. A simple method for determination of gait events. Journal of Biomechanics. 2002;35:135-138

[137] Kawamura K, Tokuhiro A, Takechi H. Gait analysis of slope walking: a study on step length, stride width, time factors and deviation in the center of pressure. Acta Medicine Okayama. 1991;45(3):170-184

[138] Leroux A, Fung J, Barbeau H. Postural adaption to walking on inclined surfaces: I. Normal Strategies. Gait and Posture. 2002;15:64-74

[139] Pearce ME, Cunningham DA, Donner AP, Rechnitzer PA, Fullerton GM, Howard JH. Energy cost of treadmill and floor walking at self selected paces. European Journal of Applied Physiology. 1983;52:115-119

[140] Stolze H, Kuhtz-Buschbeck JP, Mondwurf C, Boczek-Funcke A, Johnk K, Deuschl G, Illert M. Gait analysis during treadmill and overground locomotion in children and adults. Electroencephalography and clinical Neurophysiology. 1997;105:490-497

[141] Strathy GM, Chao EY, Laughman RK. Changes in knee function associated with treadmill ambulation. Biomechanics. 1983;16:517-522

[142] Wall JC, Charteris JA. A kinematic study of long-term habituation to treadmill walking. Ergonomics, 1981;24:543-555

[143] Murray MP, Spurr GB, Sepic SB, Gardner GM, Mollinger LA. Treadmill vs. floor walking: kinematics, electromyogram and heart rate. Journal of Applied Physiology. 1985;59:87-91

[144] Prokop T, Schubert M, Berger W. Visual influence on human locomotion: modulation to changes in optic flow. Experimental Brain Research. 1997;114:63-70

[145] Pelah, A, Barlow HB. Visual illusion from running. Nature. 1996;38:283

[146] Cheung C, Wall JC, Zelin S. A microcomputer-based system for measuring temporal asymmetry in amputee gait. Prosthetics and Orthotics International. 1983;7:131-140

[147] Schöllhorn WI. Applications of artificial neural nets in clinical biomechanics. Clinical Biomechanics. 2004;19:876-898

[148] Deluzio KJ, Astephen JL. Biomechanical features of gait waveform data associated with knee osteoarthritis: an application of principal component analysis. Gait and Posture. 2007;1:86-93

[149] Crowe A, Samson MM, Hoitsma MJ, van Ginkel AA. The influence of walking speed on parameters of gait symmetry determined from ground reaction force. Human Movement Science. 1996;15:347-367

[150] Kaufman KR, Miller LS, Suttherland DH. Gait asymmetry in patients with limb-length inequality. Journal of Pediatric Orthopaedic. 1996;16:144-150

[151] Giakas G, Baltzopoulos V. Time and frequency domain of ground reaction forces during walking: an investigation of variability and symmetry. Gait Posture. 1997:5:187-197

[152] Patterson KK, Gage WH, Brooks D, Black SE, McIlroy WE. Evaluation of gait symmetry after stroke: a comparison of current methods and recommendations for standardization. Gait and Posture. 2010;31:241-246

[153] Dingwell JB, Marin LC. Kinematic variability and local dynamic stability of upper body motions when walking at different speeds. Journal of Biomechanics. 2006;39:444-452